EFFECT OF CORRELATION AND DISORDER ON THE PROPERTIES OF URANIUM BASED COMPOUNDS: FIRST PRINCIPLES CALCULATIONS

By

GURPREET KAUR
Enrolment No. PHYS02201004015

Indira Gandhi Centre for Atomic Research, Kalpakkam, India.

A thesis submitted to the
Board of Studies in Physical Sciences
In partial fulfillment of requirements
For the Degree of

DOCTOR OF PHILOSOPHY

of

HOMI BHABHA NATIONAL INSTITUTE

February, 2018

Homi Bhabha National Institute

Recommendations of the Viva Voce Board

As members of the Viva Voce Committee, we certify that we have read the dissertation prepared by **Gurpreet Kaur** entitled **"Effects of correlation and disorder on the properties of Uranium based compounds: first principles calculations"** and recommend that it may be accepted as fulfilling the thesis requirement for the award of Degree of Doctor of Philosophy.

For. Dean, Physics 26/10/18

Chairman: **Dr. C. S. Sundar** **Date:**

26/10/18

Guide/Convener: **Dr. B. K. Panigrahi** **Date:**

26/10/2018

External Examiner: **Prof. Rita John** **Date:**

26/10/2018

Member 1: **Dr. Sharat Chandra** **Date:**

Member 2: **Dr. S. Mathi Jaya** **Date:** 26/10/18

Final approval and acceptance of this thesis is contingent upon the candidate's submission of the final copies of the thesis to HBNI.

I hereby certify that, I have read this thesis prepared under my direction and recommend that it may be accepted as fulfilling the thesis requirement

Date: 26/10/18

Place: Kalpakkam

Dr. B. K. Panigrahi

(Guide)

STATEMENT BY AUTHOR

This dissertation has been submitted in partial fulfillment of requirements for an advanced degree at Homi Bhabha National Institute (HBNI) and is deposited in the Library to be made available to borrowers under rules of the HBNI.

Brief quotations from this dissertation are allowable without special permission, provided that accurate acknowledgment of source is made. Requests for permission for extended quotation from or reproduction of this manuscript in whole or in part may be granted by the Competent Authority of HBNI when in his or her judgment the proposed use of the material is in the interests of scholarship. In all other instances, however, permission must be obtained from the author.

Date: 26/10/2018
Place: Kalpakkam

Gurpreet Kaur
(Gurpreet Kaur)

DECLARATION

I, hereby declare that the investigation presented in the thesis has been carried out by me. The work is original and has not been submitted earlier as a whole or in part for a degree/diploma at this or any other Institution/University.

Gurpreet Kaur

(Gurpreet Kaur)

List of Publications

(a) Journal papers

1. Thermal properties of UO_2 with a nonlocal exchange-correlation pressure correction: A systematic first principles DFT+U study. **Gurpreet Kaur**, Puspamitra Panigrahi and M. C. Valsakumar, Modeling and Simulations in Materials Science and Engineering **21**, 065014 (2014).

2. Phonon instability and charge density wave in U_2Ti. **Gurpreet Kaur**, S. Mathijaya and B. K. Panigrahi, Journal of Alloys and Compounds **730**, 36 (2018).

3. First principles study of lattice stability and thermal properties of delta-UZr_2. **Gurpreet Kaur**, Ravi Chinnappan and B.K. Panigrahi. (to be submitted).

(b) Conference Papers

1. First principles study of lattice stability and thermal properties of delta-UZr_2. **Gurpreet Kaur**, Ravi Chinnappan and B.K. Panigrahi. Indo-UK Workshop on Modelling and Simulation of Safety and Materials for Nuclear Application (MSMNA), December 2015, Kalpakkam, India.

2. Nonlocal exchange correlation pressure corrected thermal properties of UO_2 within LDA+U approach, Puspamitra Panigrahi, **Gurpreet Kaur** and M. C. Valsakumar, AIP Conf. Proc. **1447**, 139 (2012).

3. Thermal properties of UO_2 from density functional theory: Role of strong correlations, Puspamitra Panigrah, **Gurpreet Kaur** and M. C. Valsakumar, Second International Conference on Advances in Nuclear Materials (ANM), February 2011, Mumbai, India.

(c) Publications not included in the thesis

1. Simulating radiation damage in a bcc Fe system with embedded yttria nanoparticle, T Lazauskas, S. D. Kenny, R. Smith, **Gurpreet Kaur**, Manan Dholakia, M. C. Valsakumar, Journal of Nuclear Materials **437**, 317-325 (2013).

2. Linear Compressibility and thermal expansion of $KMn[Ag(CN)_2]_3$ studied by Raman spectroscopy and first principle calculations. K. Kamali, T.R. Ravindran, C. Ravi, R.M. Sraguna, T.N. Sairam and **Gurpreet Kaur**, Journal of Phys. Chem. C **117**, 25704 (2013).
3. Characterization of M-O bonds in Y_2Ti_2 O_7 and Y_2TiO_5 with EELS. P. Jegadeesan, S.Amrithapandian, **Gurpreet Kaur**, Sharat Chandra and B.K. Panigrahi, Physica Status Solidi B **252**, 206 (2015).
4. Formation of Y-Ti-O nanoclusters in fcc Fe from Density Functional Theory, **Gurpreet Kaur**, D. Murali, B. K. Panigrahi, M. C. Valsakumar, AIP Conf. Proc. **1447**, 853 (2012).
5. Molecular Dynamics Studies of Radiation Damage in Yttria, Manan Dholakia, **Gurpreet Kaur** and MC Valsakumar, AIP Conf. Proc. **1512**, 1288 (2013).
6. Hybrid functional study of alpha-uranium. **Gurpreet Kaur**, Ravi Chinnappan and B. K. Panigrahi, AIP Conf. Proc. **1731**, 090030 (2016).

Gurpreet Kaur

(Gurpreet Kaur)

I dedicate this thesis to my parents.

Acknowledgements

First and foremost, I take this opportunity to thank my guide Dr. B. K. Panigrahi for his motivation, constant support and encouragement. I want to convey my heartfelt thanks to Shri. M. C. Valsakumar, for introducing me to the field of computational physics and being a source of constant motivation.

I sincerely thank Dr. S. Mathi Jaya and Dr. Sharat Chandra for their constant support, valuable suggestions for my research work and providing feedback on thesis manuscript. I thank my doctoral committee chairman, Dr. C. S. Sundar for sharing his valuable time and for his suggestions during my Ph.D. tenure. I thank Dr. N. V. Chandrashekhar, Dean, Physical Sciences, HBNI, for his help and encouragement. I sincerely thank the present Director IGCAR, Dr. A. K. Bhaduri for his support and encouragement.

I would like to thank colleagues from my section and friends, for their cooperation, constant help and support. I express my gratitude to my family for their unconditional love and support.

Contents

Synopsis

Studies on the properties of uranium compounds and its alloys have been an active area of research for many decades as they are extensively used as nuclear fuels. Inside a nuclear reactor the fuel materials are exposed to high temperature and irradiation damage by fission products and intense neutron flux. The fuel behaviour is predicted by fuel performance codes which incorporate models of material properties that are based on empirical correlations. The applicability of such models is limited to the regime, for which experimental data is available. To reliably extrapolate to a regime where experimental data is not available and to design new and better fuel materials for which experimental data on material properties is not available, physics based models and atomistic informed fuel performance codes are required. This involve the generation of models for the fuel materials from atomic scale through the mesoscale, to the macroscopic scale. At the smallest scale, first principles density functional theory (DFT) calculations can accurately determine the physical and chemical properties of materials like elastic properties, relative phase stability, energetics of formation and migration of defects like vacancies, solute atoms, fission gas atoms, and their clusters etc. DFT can also provide data for the adjustment of parameters (or potentials) at higher level computational techniques like molecular dynamics simulations, cluster expansion methods, kinetic Monte Carlo methods etc. DFT has been applied to determine the structural and dynamical properties of a variety of solids but the limitation of the DFT modelling of the nuclear fuels is the strong correlations in 5f electrons of uranium which cannot be satisfactorily described by mean field based theories. Based on the structure and bonding environment the strong Coulomb correlations can be of varying importance. In uranium metal the 5f electrons participate in bonding and strong correlations are not that important but in many uranium compounds like UO_2, UC, UI_2, UAl_3, UPt_3, USe, UTe etc the strong correlations in 5f electrons are very important and give rise to many interesting phenomena like Mott insulating behaviour, heavy fermionic behaviour, existence of superconductivity, magnetism and charge density wave modulations . On one side our aim is to get reliable data on the properties of nuclear fuel materials and on other side the complexity of the electronic structure makes the description of material characteristics very challenging. In this thesis work, different uranium compounds are studied using DFT based methods and their modifications to access their applicability and their prediction capabilities for different properties.

UO_2 , UZr_2 and U_2 Ti are important oxide and metallic nuclear fuels, the oxide being used in commercial reactors and the metallic alloy based fuels are proposed fuel material for future metal fuel fast reactors. The extent of correlations of 5f electrons in the above mentioned compounds and their effect on various properties are reported in this thesis. The effect of disorder on the stability and properties of these intermetallic compounds is also reported. This thesis consist of six chapters and the brief outline of these six chapters is given below:

CHAPTER-1: Introduction

This chapter gives an overview of different choices of uranium based nuclear fuel materials and the role of first principles calculations in understanding, predicting and designing the material properties. Challenges of the first principles based calculations in describing the material characteristics of the uranium compounds and alloys are also listed . Presence of different extents of correlations in 5f electrons of Uranium in different compounds is discussed along with the 'Hill' plot. Review and applications of different techniques to handle strong Coulomb correlations in uranium compounds are given in detail . The choice of compounds studied in this thesis viz UO_2 , UZr_2 and U_2Ti and the importance of their electronic, structural, elastic, lattice dynamical and thermal properties is also discussed along with the scope of thesis.

CHAPTER-2: Theoretical and computational methods

The theoretical and computational methods employed in this thesis are discussed in this chapter. Various approximations used to solve the many body problem using the density functional theory based methods are given in detail. Numerical techniques for implementing density functional theory in Vienna ab-initio Simulation Package (VASP) and WIEN2k are also mentioned. DFT+U method to incorporate strong

Coulomb correlations is also discussed. Methods to calculate phonon spectrum and elastic constants, as well as quasi harmonic approximation (QHA) used to obtain high temperature properties are explained in detail. The importance and generation of special quasi random structures to represent the disordered structures is also given in this chapter.

CHAPTER-3: Electron correlations and thermal properties of $\mathbf{UO_2}$

UO_2 is most commonly used nuclear fuel material because of its higher melting point, phase stability and better radiation resistance. UO_2 is a Mott insulator and DFT based on local density approximation and generalized gradient approximation for exchange correlational functional wrongly predict it to be a metal. The strong Coulomb correlations of 5f electrons in uranium atom are responsible for this. DFT+U is a method based on Hubbard model to introduce strong onsite Coulomb correlations and it is applied successfully to reproduce the anti-ferromagnetic ground state of UO_2 . The studies on the effect of strong Coulomb correlations on other properties like phonon dispersion, equilibrium volume and bulk modulus are presented in this chapter. Quasi harmonic approximation was used to get thermal expansion, bulk modulus and specific heat as a function of temperature and the results of these studies are also presented in this chapter. The effect of applying non- analytical term correction to longitudinal optical phonon frequencies is also reported. The non-local exchange correlation pressure correction to correct the over prediction of lattice parameter by the DFT+U calculations and its effect on bulk modulus and thermal expansion coefficient are also discussed in this chapter.

CHAPTER-4: Structural stability and disorder in $\mathbf{UZr_2}$

Zirconium is added to the uranium metal fuel to improve the phase stability in harsh conditions existing in the nuclear reactor . The constituent redistribution and the thermal gradient in these conditions leads to formation of different zones having different phases, central high temperature region in bcc phase and peripheral lower temperature zone is a mixture of orthorhombic phase and delta phase. Delta UZr_2 phase is the only intermetallic in U-Zr phase diagram. It is having a stoichiometry range of 63 to 86% Zr. This phase can also have a substantial effect on the fission gas behaviour in the fuel . This chapter discusses the structure, elastic and dynamic stability of stoichiometric UZr_2 and explores the role played by disorder in site occupancy by U and Zr atoms. The first principles calculations reveal that the site occupation disorder on the 2b site of the C32 hexagonal structure is energetically favourable. The elastic and dynamical stability of both ordered and disordered structure is studied by calculating elastic constants and phonon spectrum which shows that the disorder in the site occupation provide the dynamical stability to UZr_2 . Further the bulk modulus, thermal expansion and specific heat for the disordered structure are calculated as a function of temperature using quasi harmonic approximation. The results are discussed in this chapter.

CHAPTER-5: Structural stability and evidence of charge density wave in U_2Ti

U-Ti alloy is not only a potential candidate for nuclear fuel materials but also for storage of radioactive tritium to be used as fuel in nuclear fusion reactors. Specially U_2Ti has been studied as a safe and heavy metal based storage material for radioactive hydrogen in nuclear fusion reactor because of high durability of its hydride against powdering. In contrast to UZr_2 which is having a stoichiometry range as mentioned earlier, U_2Ti is a line compound and have ordered structure. This chapter presents the studies on the electronic structure, elastic constants and phonon spectrum of the known hexagonal ground state of U_2Ti. The structural instability found through the phonon spectrum is analysed in detail which suggests the distortion of the structure is due to the dimerization of U atoms. Further the charge density analysis is done and compared with that of the CDW in alpha uranium. It suggests the possibility of similar transition in U_2Ti. The behaviour of this possible CDW transition under pressure is also given in this chapter. The existence of CDW transition is further verified using the all electron based electronic structure calculations. These results are described in this chapter.

CHAPTER-6: Conclusions and future outlook

The overview of the results obtained in this thesis work and a brief discussion of the important findings are described in this chapter. The role of 5f electrons as well as the importance of Coulomb correlations in UO_2, UZr_2 and U_2Ti are discussed. A brief discussion of the strong correlations present in the 5f electrons of UO_2 and their effect on bonding, structure, elastic constants and phonons is also given. The dynamical instability of UZr_2 and U_2Ti and role played by disorder and distortion is briefly discussed. The requirement of further studies for better understanding the properties these systems is also discussed.

List of Figures

List of Tables

Chapter 1

Introduction

This chapter gives a brief overview of properties and applications of uranium compounds used as nuclear fuel materials. The need for modelling and prediction of nuclear fuel behaviour is given in detail. The different extents of the strong electron correlations present in uranium compounds and their effect on various properties are discussed. The difficulties and challenges associated with strongly correlated compounds and various techniques to handle strong correlations are also outlined. Finally a brief outline and the scope of the thesis is presented in this chapter.

Uranium is an important element for nuclear industry. It is used as a nuclear fuel in the form of oxide, alloy, nitride or carbide. Uranium and its alloys are potential candidates for tritium storage in nuclear fusion reactor [1, 2] and depleted uranium has applications in ammunition and armour. Uranium compounds also exhibit a particularly rich variety of properties and phenomena in solid state physics [3, 4]. The origin of these properties is the behaviour of partially filled 5f electronic states of uranium, which are on the verge of delocalisation. The complex physical and chemical properties of uranium compounds, make them challenging systems to characterize both experimentally and theoretically. Based on the structure and the bonding environment, 5f electrons in the uranium compounds exhibit different strengths of correlations [5] and particularly strong correlations are difficult to capture with computationally tractable methods. So they are not only important from technological point of view as nuclear fuel but are also a subject for the check of various condensed matter theories and advancement of the understanding of solid state physics. Density Functional theory provide a useful tool for the first principles based calculations of material properties and it has been proved to be successful in a wide range of materials for calculation and prediction of material behaviour [6, 7]. But the use of this tool, in general for actinides, in particular for uranium compounds is not straightforward. Uranium or in general actinide compounds are challenges for DFT based calculations because of the nature of f-electrons. In this thesis, the structural, elastic, dynamical and thermal properties of three uranium compounds: UO_2, UZr_2 and U_2Ti are studied using DFT based first principles techniques. The role of f electrons and importance of the structural disorder is discussed with respect to stability of these uranium compounds. In this chapter a brief survey of use of uranium compounds as nuclear material is provided along with the need for modelling and simulation of their properties and the vital role of DFT based calculations. The general behaviour and the properties of Uranium compounds, with emphasis on nature of 5f electrons and the importance of structural disorder, is given along with the different DFT based techniques to handle strong electron correlations in f electrons. The chapter is organized as

- Overview of nuclear fuel materials and need for modelling.

- 5f electrons and different properties of uranium compounds.
- Strong electron correlations and density functional theory.
- Choice of uranium compounds for study: Literature survey for UO_2, UZr_2 and U_2Ti.
- Objective and overview of thesis.

1.1 Overview of nuclear fuel materials

Fuel material in the nuclear reactor is the most important component as it is the place where actual energy is produced by fission reaction. This fission energy is dissipated as heat in the fuel material which is transferred to coolant and ultimately used to produce steam and generate electricity. The properties of fuel material such as structural and chemical stability, thermal expansion and thermal conductivity are very important for both safety and efficiency of the nuclear reactor. For different types of reactors because of different requirements, there are different choices of fuel materials. Metallic fuels give higher fissile atom density and are ideal for research reactors and also for fast breeder reactors where fuel breeding is important, whereas oxide fuels are supposed to be more safe because of high melting point and radiation stability and are used in most commercial reactors. Nitride and carbide fuels are seen as alternative fuel materials because of their better thermal conductivity than oxide fuel material and higher melting point as compared to metallic fuel.

U-235 is the fissile isotope of uranium but naturally occurring uranium has only 0.72 % of this fissile isotope (U-235) rest 99.3 % is U-238. Enrichment is done to increase the concentration of U-235 in uranium for use as fuel in nuclear reactors except for heavy water based nuclear reactors where no enrichment is required and natural uranium can be used as oxide fuel. As enrichment is a costly process, apart from enrichment fissile content in fuel material is also increased by adding plutonium. In those cases fuel is U-Pu mixed compound e.g. (U, Pu) mixed oxide or carbide. For metallic fuel along with U-Pu other elements (Zr, Mo, Ti) are also added to increase melting point and to enhance phase stability. U-Zr alloy is being tested as a fuel material for fast reactors and U-Mo and U-Ti are also studied as potential candidates.

1.1.1 Need for modelling nuclear fuel materials

Fuel performance code and multiscale materials modelling

Evaluating the properties of the fuel and predicting the change in properties caused by the reactor environment is a challenging task. A fuel performance code is a set of computer codes that includes models of fuel properties and are able to simulate phenomena in the nuclear fuel during operation, or in general during fuel manufacturing and storage. In the fuel performance codes along with the description of heat and mass transport phenomena, the models of materials properties are also very important. Mostly the models of material properties in use, are based on the empirical correlations deduced from the experiments. The applicability of such models is limited to the regime, for which experimental data is available. The extrapolation to the regime where experimental data is not available may lead to errors. Also to design new and better fuel materials (e.g. the concept of accident tolerant fuel (ATF)) for which experimental data on material properties is either not available or only limited data is available, physics based models and atomistic informed fuel performance codes are required [8, 9]. This involves the generation of models for the fuel materials from atomic scale through the mesoscale, to the macroscopic scale. The theoretical approach to model the properties of materials at different scales use techniques like ab-initio, molecular dynamics, kinetic Monte Carlo, dislocation dynamics and finite elements calculations etc. This multi-physics approach to developing a fundamental understanding of the properties of complex nuclear fuel materials in the reactor environment, will lead to improved tools for predicting phenomena such as heat transfer, phase stability, species diffusion, and fission product retention. Some efforts done in this area are discussed in the next paragraph.

In spirit of advancing towards atomistically informed fuel performance code, thermal properties of the fuel (thermal temperature gradient) is simulated using FRAPCON and molecular dynamics simulation [10]. Thermal conductivity and thermal expansion data for UO_2 is fed into the fuel performance code FRAPCON from the Molecular dynamics simulations. This study indicates that one of the puzzles in developing a predictive atomistically informed fuel performance code is the development of higher fidelity interatomic potentials.

Another example of atomistic modelling as input to fuel performance code is BaCo code [11], which has the feature of providing the unavailable data needed for development of new fuel or clad materials through multiscale modelling. Marino et al [11] have discussed the example case of fcc Th to check the accuracy of this methodology to describe their thermal and elastic properties.

Stan et al [8] has also developed multi-scale and multi-physics approach for a better understanding of heat transfer and oxygen diffusion in UO_2. The method involves a theoretical framework to allow for prediction of phenomena such as phase stability, heat transfer, species diffusion, and fission products retention. The calculations of point defect concentration, helium bubbles formation, oxygen diffusivity, and simulations of heat and mass transport in hyper stoichiometric UO_2 are done in a multiscale approach. By studying the coupled heat and oxygen transport in fuel material using finite element simulations, they have demonstrated that including the dependence of thermal conductivity and density on non-stoichiometry, can lead to changes in the calculated centreline temperature and thermal expansion displacements exceeding by 5%.

These examples are just the beginning in order to have atomistically informed fuel performance code which will use the models of material properties and behaviour calculated using multiscale modelling methods and lot need to be yet done on both individual scales and in linking the different scales of materials modelling.

1.1.2 Role of Density Functional Theory based calculations for nuclear fuel materials

In the multiscale based materials modelling of nuclear fuels, the electronic structure calculations stand at the lowest scale. These are quantum mechanical calculations aimed at describing properties such as energy bands, cohesive energy, lattice parameters and phonon spectra. They provide invaluable information about structures for which there is no experimental data. It also provides the input to higher scale models. The technique used for electronic structure calculations is based on density functional theory (DFT). The main idea of DFT is to express the energy as a functional of electron density of the system. The Hohenberg-Kohn theorems [12] proves that it is formally possible. DFT has proven to be a very powerful tool for the quantitative prediction of materials properties in both chemistry and solid state physics [6, 7]. DFT has made possible the quantitative prediction of materials from the first principles. It does not need any experimental inputs. In the scheme of multi-scale modelling of material properties, DFT provides the valuable input to higher level techniques like molecular dynamics, cluster expansion and kinetic Monte Carlo simulations etc. DFT has made possible the first principles based calculations of the properties of point defects and fission products in nuclear materials. Energetics, interaction and migration of point defects and fission products can be studied using DFT. It can also give equation of state for different phases, their mechanical stability as well as their relative phase stability along with the phonon based properties. Even though DFT is applicable to ground state that is at 0 K, it can also be used to calculate properties as a function of temperature using quasi harmonic approximation [13]. Also DFT can provide input in form of inter atomic potential to molecular dynamics which can directly incorporate temperature effects and can give thermophysical properties (like thermal conductivity, thermal expansion and specific heat etc) as a function of temperature.

Yun et al [14] and Liu et al [15] have reviewed the first principles DFT modelling of nuclear fuel materials for better understanding of current nuclear fuel materials and finding favourable properties in candidate fuel materials in terms of stability and properties. DFT has been used to investigate the fundamental properties of the standard nuclear material UO_2, where it fails to reproduce its Mott insulating behaviour. The advanced DFT-based methods like DFT+U, self interaction correction (SIC), hybrid functionals (HF) and dynamical mean field theory (DMFT) has been used to correctly capture the strong correlations of 5f electrons in UO_2 responsible for its insulating nature [16–20]. The DFT calculations have been used to calculate the formation and migration of point defects and fission gas Xe in UO_2 and ThO_2 [21] and have shown that Xe diffusion is slower in ThO_2 than in UO_2 which corroborate with the experiments showing that Xe release is slower in UO_2 mixed with ThO_2 than in UO_2 [22]. There are studies on thermodynamical properties of nuclear fuel UO_2 and PuO_2 using DFT+DMFT [17] which suggest that an improved thermal conductivity could be achieved through dedicated materials design based on the fact that longitudinal optical modes are not contributing to thermal conductivity. Phonon and elastic moduli for these materials are calculated using DFT [23, 24].

UN and UC are also studied using DFT as alternative fuel materials because of their better thermal conductivities and high melting points. Studies of defect formation and migration energies, thermodynamical properties and phase diagram are also done [25]. The electron correlation and transport properties of UN and UC fuel are studied by Yin et al [26]. Metallic fuels are also investigated using DFT. Landa et al [27] studied thermodynamics of U-Zr and U-Mo solid solutions using DFT, whereas the diffusion of interstitials and vacancies in alpha U-Zr alloys are done by Huang et al [28]. Importance of relativistic effects and electron correlation effects in U-Zr system are studied by Xie et al [29].

Even though there were many studies of nuclear fuel materials using DFT, but to explore the full potential of DFT more systematic investigations and data generation is required. Along with the present capabilities, improvements in terms of better description of strong correlations and use of temperature dependent DFT are very much desirable.

Strong correlations which exist in 5f electrons of uranium are important to understand the properties and behaviour of uranium compounds which are discussed in next section.

1.2 5f electrons and different properties of Uranium compounds

Uranium which belongs to actinide series of Periodic table, has partially filled 5f orbitals. These 5f electrons are on the verge of delocalisation and exhibit an enigmatic array of magnetic and electronic properties. Depending on the bonding environment, these 5f electrons can be localized or itinerant [5]. In localized limit, there is strong Coulomb correlations between the 5f electrons. There is a relation between the U-U spacing and the nature of uranium system. If U-U spacing is shorter than a critical value then 5f electrons are participating in bonding and are itinerant and system is mostly non magnetic [4]. If the U-U spacing is more than that critical value, the 5f electrons will be localized and show magnetic moment. This critical value is called Hill limit and its value is 3.4-3.6 Å.

The degree of f electron localization is widely recognized as a dominant factor in determining the structural, magnetic and electronic properties of actinides. There are also some examples of dual nature of 5f orbitals, where some fraction of the f-electrons contribute to de-localized behaviour and the rest contribute to the more localized local moment behaviour [30].

The behaviour of 5f electrons give rise to many interesting properties like Mott insulating behaviour, heavy fermionic behaviour, existence of superconductivity, magnetism and charge density wave modulations [5, 31, 32]. UO_2 lies above the hill limit and is known to be a Mott insulator where the strong correlations among the 5f electrons give rise to both insulating behaviour and anti-ferromagnetism. UN is close to the limit and show heavy fermionic character along with anti-ferromagnetism below tem-

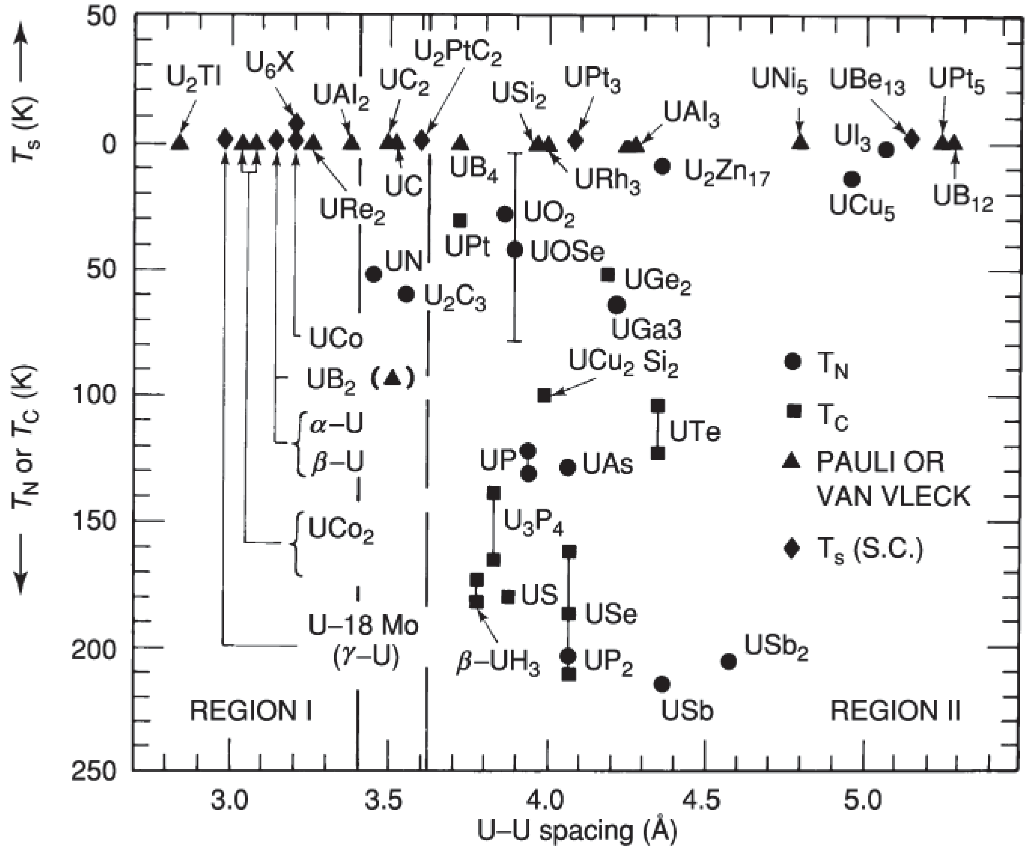

Figure 1.1 – Hill plot [5] showing U-U spacing vs the transition temperature (magnetic or superconducting). Magnetism is generally favoured with U-U spacing above 3.4 Å, while non-magnetic ground states are common below this separation. (Original Hill plot[4] shows fewer compounds than the present one). This distance roughly defines the localized/itinerant boundary for 5f states in uranium compounds.

perature of 53 K [26]. UC is also close to limit and a Fermi liquid [26]. Pure uranium lies much below the limit and is weakly correlated metal. U_2Ti is non magnetic and the U-U separation lies far below the Hill limit. Uranium intermetallics, in general, span from weakly correlated to heavy fermions to strongly correlated depending on the U-U distance and hybridisation with the ligand atoms [33, 34].

Hill plot correlates U-U distance with degree of localization, but it ignores the role of ligands. Uranium 5f states interact with ligand states (d states in case of intermetallics with transition metal), that also have an effect on the localization of uranium 5f states

[34].

Some of the different behaviours shown by uranium compounds are Mott insulating behaviour, heavy fermionic nature, and instabilities like charge density waves and spin density waves etc. A brief introduction to some of these is given below.

1.2.1 Mott insulator

In a Mott insulator, the insulating behaviour stems from the strong interaction of electrons rather than a filled Bloch band. Classical examples of Mott insulators are NiO, MnO, V_2O_3 and UO_2. Band theories fail to explain their insulating nature. It is because of absence of explicit electron-electron interactions. Physics of Mott insulators is well captured by Hubbard model [35] which is widely used to describe strongly interacting electrons in a solid. Physics of strongly correlated systems is still far from being fully understood using various theories and models in condensed matter.

1.2.2 Heavy fermions

There are many uranium compounds like UPt_3 , UBe_3 , UAl_3 , UCd_{11} , U_2Zn_{17}, UCu_5 etc which show heavy fermionic behaviour [5, 36]. These are very narrow band materials on the verge of localization and conduction 5f electrons behave as if they have an extremely heavy effective mass. The hallmark of heavy fermions is the enormous low temperature electronic specific heat coefficient γ (typically larger than 100 mJ /mol-UK^2). They blur the distinction between itinerant and localized states. Fully localized electrons can be thought of as belonging to an infinitely narrow band and having an infinite effective mass since they are unable to travel beyond the bounds of their atomic sites. The effective mass of heavy fermion materials range from tens to hundreds of times the mass of a typical itinerant electron in normal metals, indicating a very low but finite velocity through the crystal. Heavy fermions consist of superconductors, magnets and systems with no magnetic ordering [36].

1.2.3 Charge density waves

Charge density waves (CDWs) are periodic modulations of conduction electron densities and the associated lattice distortions in solids. Alpha-U is the only element showing charge density waves. It shows three charge density waves below 43 K [37]. The origin of charge density waves in general can be electron-electron interaction or electron-phonon interaction resulting in Fermi surface nesting and electron-phonon couplings [38]. In alpha-U strong electron-phonon coupling is shown to be the origin of charge density wave [39]. Losada et al has predicted charge density wave in U_2Mo by first principles based DFT calculations [40].

1.2.4 Disorder effects

Moderate crystallographic disorder has been found to substantially alter and even control the ground state properties of strongly correlated electron materials [41]. In particular, pronounced disorder effects have been observed in heavy fermion related uranium compounds like $UCu_{5\text{-}x}Pd_x$, URh_2Ge_2, UGa_2 derivatives [42–44]. The delta phase in U-Zr system is also shown to have partially disordered AlB_2 structure[45, 46] where U and Zr atoms are randomly occupying one of the sub-lattice sites. Partial disorder is mainly driven by entropy effects and is stable only at higher temperatures. But the stability of partial disorder at lower temperatures without entropy contribution in d and f-electron compounds suggest itinerant electrons play a key role in stabilizing the partial disorder. The existence of so many heavy fermion spin glasses compared to other classes of crystalline dense magnetic metals reflects the interplay of crystallographic disorder and strong correlations which both in a complicated and interdependent fashion control the ground state properties of these materials. Thus, the bonding characteristics and the behaviour of 5f electron are complicatedly related to the crystallographic disorder.

1.3 Strong electron correlations and density functional theory

Even though the band description for the strongly correlated f-band materials is still questionable but modern DFT approaches go far beyond a naive band description of f systems providing a unique frame for the theoretical description of this fascinating class of materials. Whenever strong Coulomb correlations in these 5f electrons dominate in the so called strongly correlated systems, simple minded DFT in standard local density approximation (LDA) and generalized gradient approximation (GGA) generally fails to represent these systems. But there are methods developed over DFT to account for these strong correlations.

According to DFT, energy is a functional of density. But the exact form of the functional is not known. Thus even though DFT is an exact theory, its implementation relies on the approximations used for exchange correlation functional. Typical approximations for exchange correlation functional are semi local in nature, exchange-correlation energy density depend only on local density in LDA, and on its derivative in GGA and the local kinetic energy in meta-GGA. But these approximations are incapable of describing the strongly correlated materials. Typical examples include the compounds of the elements of the first transition metal series, and the lanthanide and the actinide rows, where orbitals participating in bonding are compact and there is weak overlapping with their neighbours. For example, the LDA predicts UO_2 to be a ferromagnetic metal [47] but it is an anti-ferromagnetic Mott insulator [48]. Problem is not solved by subsequent generation of semilocal approximations (GGA and meta-GGA). The major deficiency of these approximations is the self-interaction error [49], which is severe for the systems with partially filled d or f states because of their compact size.

One-electron self-interaction error can be understood as inexactness for one-electron systems. In practice, the origin lies in the form used for the Coulomb repulsion between electrons. This Coulomb repulsion does not vanish for one-electron system. In a wave-function based theory such as Hartree-Fock approximation, it is exactly cancelled by self-exchange. But with approximate exchange-correlation functionals, however, the cancellation of self-Coulomb repulsion and self-exchange is incomplete. This error leads semi local functionals to artificially delocalize electrons in order to mitigate the self-interaction. In addition this error causes the potential at long range to be different from the Coulombic 1/r. Some approaches to overcome these difficulties are self-interaction correction (SIC) [50], DFT+U [51], hybrid functionals [52] and dynamical mean field theory (DMFT) [53, 54] based methods.

1.3.1 Self interaction correction

Conceptually, the simplest approach to overcome these difficulties is to explicitly eliminate self-interaction energy by applying self-interaction correction. Self interaction correction is proposed by Perdew-Zunger [50]. This correction exactly eliminates the self-interaction error in one-electron systems and is assumed to reduce or eliminate the self-interaction error in many electron systems. There is no unique definition of the self-interaction error for a many electron system treated with a conventional semilocal exchange-correlation functional. It is also not trivial to apply and implement as the self-interaction correction is not invariant to unitary transformation among the occupied levels. SIC has been quite successful in treating strongly correlated systems. However, the SIC vanishes for a metal, so when it is applied to an LDA or GGA metallic solution for an oxide, special approach must be taken to transform the delocalized states of metallic LDA/GGA solutions to the localized orbital space to which the correction is applied. This requires a priori knowledge of which orbitals should be singled out for special treatment [49].

1.3.2 DFT+U approach

Another approach of handling the strongly correlated systems is by applying models that empirically address the self-interaction error by modifying the electron repulsion directly via Hubbard U parameter [51] in DFT+U. In this method electrons are divided into two classes: delocalized s and p electrons, that are well described by LDA/GGA and localized d or f electrons, for which an orbital dependent term is added to describe Coulomb d-d or f-f interactions. The original LDA+U functional proposed [51] is

$$E^{LDA+U}([\rho_\sigma(r),\{n_\sigma\}] = E^{LDA}[\rho] + E^{U}[\{n_\sigma\}] - E^{dc}[\{n_\sigma\}] \tag{1.1}$$

where σ denotes the spin index, $\rho_\sigma(r)$ is the electron density for spin-σ electron and $\{n_\sigma\}$ is the density matrix of d or f electrons for spin-σ. Details are explained in chapter 2. This approach shifts atomic orbital spaces in energy, thereby adjusting their occupations so as to counter-balance the effects of self-interaction and typically, also introducing a gap. The empirical parameter U is material dependent and must be carefully chosen so as to counter-balance self-interaction without introducing errors in the opposite direction. At most basic level, LDA+U correction tends to drive the occupation number of correlated orbital to integer values of 0 or 1. This in turn produces, under appropriate conditions, insulating states out of conducting LDA states, and the Mott insulating state of several systems is regarded as being well described by LDA+U at band theory level. However, the most important correlation effects in metals, fluctuation induced mass renormalization are missing from LDA/GGA+U methods [55].

1.3.3 Dynamical mean field theory

Dynamical mean field theory (DMFT) [53, 54] typically build on DFT+U approaches, which when applied to a specific atomic orbital space in the metallic DFT solution define an orbital subspace for an embedding treatment. DMFT adds important new physics by mapping this orbital space onto an impurity Hamiltonian model, which is then solved using established many-body techniques. Its great strength is that it can handle the atomic multiplets which arise from partially filled localized orbitals. In practice, the localized orbital space is assumed to be in a spherical environment, so that the localized problem may be solved using the Coulomb integrals familiar from Slater's theory of atomic structure. But the Coulomb parameters must be screened and this is typically done by simply scaling the atomic values by an additional empirical constant.

1.3.4 Hybrid functionals

Hybrid density functional theory [52] is a particularly promising method for correcting the description of strongly correlated systems. In hybrid DFT, the self-interaction error is partly corrected by incorporating a fixed portion of exact Hartree-Fock exchange into the exchange-correlation functional. By solid arguments [56] this fraction is found to be 25% which is applied in PBE0 hybrid functional. Hybrid DFT significantly improves the description of d or f electron systems, generally predicting the correct insulating and magnetic behaviour in Mott insulating cases. But calculating the non local exchange energy and exchange potential can be very expensive in extended systems, particularly as the gap narrows. Also the fraction of HF exchange should ideally be a dynamic variable not static as in the simple hybrid functionals. For typical semiconducting systems, hybrid functionals tend to over correct semilocal approximations.

Screened hybrid functionals [57, 58] are specially developed for solids, where the long range portion of HF exchange is eliminated. Screened functionals are still static in the amount of HF exchange present in the energy expression. It does not incorporate dynamic screening. It uses the concept of range separation of the inter-electronic Coulomb potential. At short range the screened hybrid functional are equivalent to unscreened hybrid functional and at long range they reduce to semilocal functional. These can be viewed as an interpolation between these two limits and are proven to be very useful for studies of semiconductors and insulators, specially for reliable band gaps [59]. One of the major advantages of screened hybrid functionals is their drastically reduced computational cost for both localized basis sets and plane-waves compared with unscreened calculations in periodic systems and large molecules.

1.4 Literature survey for UO_2, UZr_2 and U_2Ti

In this thesis, the structural, elastic, dynamical and thermal properties of three uranium compounds: UO_2, UZr_2 and U_2Ti are studied using DFT based first principles techniques. A brief review of literature regarding the DFT calculations of these compounds is discussed in these forthcoming subsections:

1.4.1 UO_2

UO_2 is most commonly used nuclear fuel material in the commercial nuclear reactors. It has attracted lot of attention not only for its role in nuclear industry but also as an interesting material from solid state physics point of view. It is one of the classic examples of Mott insulators [60] where insulating nature originates from the strong electron-electron correlations among the localized f electrons. Ground state for UO_2 is anti-ferromagnetic insulator with Neel's temperature of 30.8 K [61]. Above Neel's temperature also it continues to be insulator. UO_2 has been explored extensively in last several decades by experimental techniques. It is having a fluorite structure with space group $Fm\bar{3}m$ (#225). The thermophysical properties are studied by various experimental techniques and a consistent database [62] is proposed over the entire temperature range by careful examination of the available data. At higher temperatures UO_2 shows the behaviour of a super-ionic conductor.

The DFT based calculations have failed to give the correct ground state of UO_2 and predicted its ground state as ferromagnetic conductor [47]. Dudarev et al [18–20] have used DFT+U formalism to incorporate the strong correlations in 5f electrons and get the insulating ground state of UO_2. They studied the effect of correlations on electronic structure and structural stability. Hybrid functional [16] and DMFT [17] are also applied to account for the strong correlation in 5f electrons. There are also some DFT studies on the defect and fission product energetics and diffusion in UO_2 [21, 63]. Molecular dynamics is also used extensively to study various thermophysical properties of UO_2 [64–66]. A number of empirical interatomic potentials are developed for UO_2, to be used in molecular dynamics simulations and their relative performance for various thermophysical properties is evaluated [65, 67]. Even though a large number of experimental and theoretical studied exist for UO_2, still the current understanding is far from complete. There are recent efforts to both calculate the thermal and elastic properties from first principles [23, 24, 68] and also experimental investigations to get more insight into the material behaviour [60]. The first principles studies have shown that including the strong correlations is a must for reproducing the insulating state of UO_2, but there are no studies on how the incorporation of strong electron correlations affect the other properties like phonon and thermal properties. A systematic study of the structure, electronic, mechanical and thermal properties for the insulating state of UO_2 reproduced by incorporation of strong electron correlations will give insight to the effect of strong correlations on these properties.

1.4.2 UZr_2

U-Zr based metallic fuel are material for future fast reactors. They have better thermal conductivity and higher fissile atom density. Their harder neutron spectrum combined with higher density gives higher breeding ratio [69]. Zr is added to metallic uranium to improve the phase stability and increase its melting point. Zr forms a completely miscible bcc phase with uranium at higher temperatures and also stabilizes the high temperature bcc phase to comparatively lower temperatures. In the optimally designed alloy composition, Zr content varies from 6 to 10 percent [70]. U with 6-10% Zr at normal temperature and pressure conditions have an orthorhombic structure but in reactor conditions of high temperature, pressure and irradiation, the U-Zr alloy fuel has different regions in different phases, central high temperature region in bcc phase whereas peripheral lower temperature zone is a mixture of orthorhombic phase and delta phase. U-Zr phase diagram is extensively studied by Kaity et al [71], which is

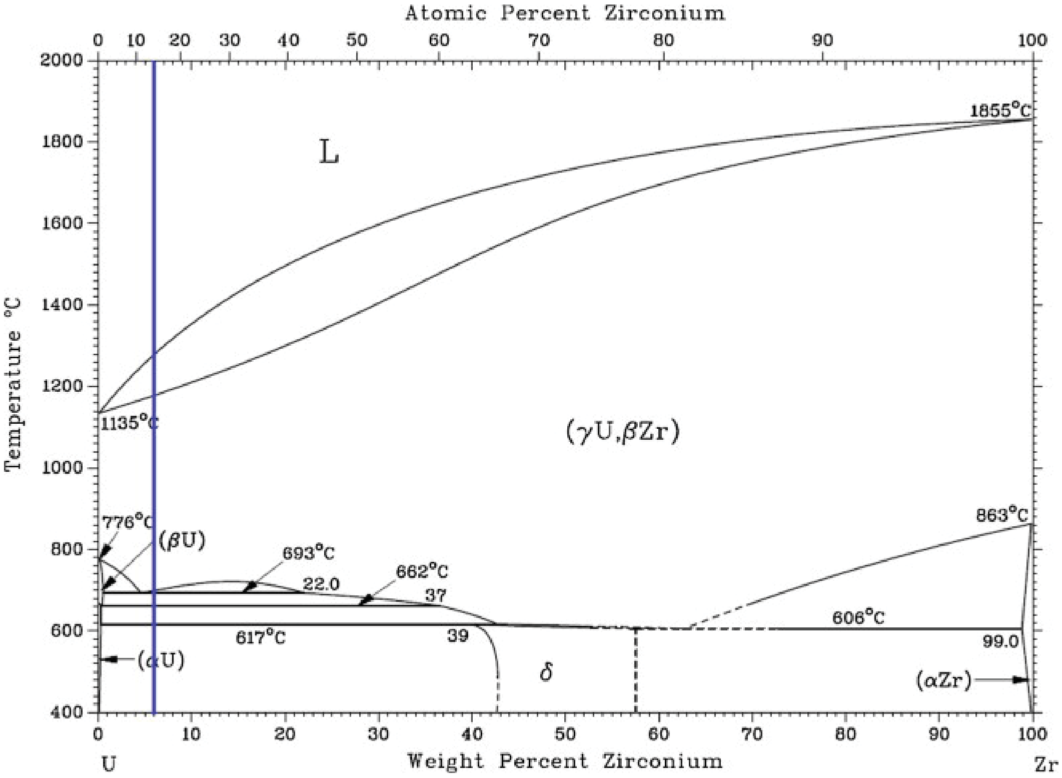

Figure 1.2 – U-Zr Phase diagram [71].

shown in figure 1.2.

Pure uranium stabilizes in orthorhombic phase up to 941 K (668 °C), in tetragonal phase up to 1049 K (776 °C) and in bcc phase at temperatures from 1049 K (776 °C) to the melting temperature of 1408 K (1135 °C). Pure zirconium is in hcp phase up to 1136 K (863 °C) and in bcc phase from 1136 K (863 °C) up to the melting point 2128 K (1855 °C). Delta-UZr_2 is the only intermetallic phase in U-Zr phase diagram. The crystal structure and stability of the UZr_2 phase have been studied by Akabori et al using electron probe microanalysis, X-ray diffraction and differential thermal analysis[45, 46]. This study establishes that the UZr_2 phase form below 885 K in a modified AlB_2-type structure with a homogeneity range of 63 to 82 at.% Zr. Basak et al [70] have also confirmed that UZr_2 is having a stoichiometry range over varying zirconium concentration. Landa et al have computed the formation enthalpy of the bcc (U, Zr) and UZr_2 phases, estimated the decomposition temperature of the γ-(U, Zr) and established the partial ordering in UZr_2 using Korringa-Kohn-Rostoker (KKR), exact muffin-tin orbital (EMTO) and full potential linear muffin-tin orbital (FPLMTO) methods of density functional theory (DFT) calculations [72, 73]. However, studies on the phonon spectrum and thermal properties such as specific heat and thermal expansion coefficients are lacking in the literature. The role played by the partial disorder on the stability of UZr_2 is also not clear. Ab-initio calculations can be used to study electronic structure, phonon and mechanical stability and the role played by crystallographic disorder.

1.4.3 U_2Ti

U-Ti system is not only a possible metallic fuel for nuclear fission reactor, but also seen as potential candidate for hydrogen storage in nuclear fusion reactor [74, 75]. U-Ti is an isoelectronic system with U-Zr system as Ti is second member of 3d transition metal series just above the Zr which is the second member of 4d transition metal series and both makes completely solid solution with U in high temperature bcc phase. Pure titanium is having hcp phase up to 1156 K (883 °C) and bcc phase from 1156 K (883 °C) to the melting point 1943 K (1670 °C). The intermetallic phase in U-Ti phase diagram is U_2Ti having a hexagonal structure similar to UZr_2 . But U_2Ti, in contrast to UZr_2 which is having a stoichiometry range, is a line compound having perfect stoichiometry as shown in phase diagram 1.3.

Chattaraj et al [77] studied its structure and electronic properties and inferred that electronic density of states at Fermi level is mostly because of uranium f electrons and Ti atoms contribution is at higher binding energies. They also show that spin orbital coupling is having a small effect below Fermi level and predominantly effects

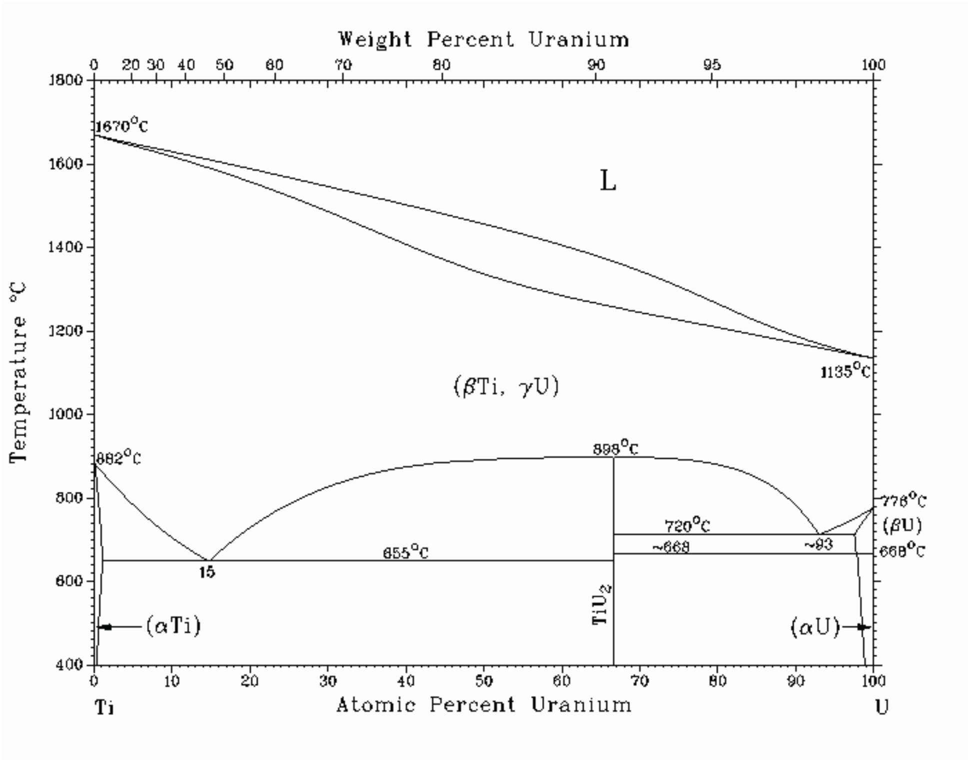

Figure 1.3 – U-Ti Phase diagram [76]

the states above Fermi level. Hasan et al [78] calculated the thermodynamical and optical properties showing that the material will be an excellent reflector between 8 eV to 12.45 eV. Elastic anisotropy, vibrational and thermal properties of U_2Ti are studied by Yang et al [79], who showed that this compound possesses slight elastic anisotropy at zero pressure, however the anisotropy becomes more and more significant with the increasing pressure. They also showed that U_2Ti will be mechanically stable up to 100 GPa.

A detailed study of the structure and stability will be important in understanding of the thermodynamic, elastic and cohesive properties of the system.

1.5 Objective and overview of the thesis

This thesis deals with three uranium compounds: UO_2 , UZr_2 and U_2Ti. UO_2 is standard fuel material in most commercial nuclear reactors, UZr_2 and U_2Ti are components in metallic alloy based fuels proposed for future metal-fuelled fast reactors. An insight of the ground state and thermophysical properties of these compounds is essential for understanding their behaviour inside the nuclear reactor and for the bigger goal of atomistic informed fuel performance codes. The behaviour of 5f electrons which play a major role in the overall properties of uranium compounds, will be evaluated in these uranium compounds along with the extent of strong correlation among these electrons. Density functional theory based first principles simulations are done to study the electronic, structural, elastic, lattice dynamical and thermal properties of these uranium compounds.

Specifically, the following objectives are addressed in this thesis:

- The effect of strong correlation in 5f electrons of UO_2 which is known to be important for band gap opening and making it insulating, on structure, bulk modulus, phonons and thermal properties.

- The correlations present in 5f electrons and the structure and stability of UZr_2 with respect to phonon induced distortion and the presence of site occupancy disorder.

- The correlations present in 5f electrons and the structure and stability of U_2Ti with respect to phonon induced distortion and the presence of site occupancy disorder.

The thesis consist of six chapters and a brief outline of these chapters is given below:

In chapter 2, the theoretical and computational methods employed in this thesis are discussed. Various approximations used to solve the many body problem using the density functional theory based methods are given in detail [80]. Numerical techniques for implementing density functional theory in Vienna ab-initio Simulation Package (VASP) [81, 82] and WIEN2k [83] are also mentioned. DFT+U [55] method to incorporate strong Coulomb correlations is also discussed. Methods to calculate phonon spectrum and elastic constants, as well as quasi harmonic approximation (QHA) [84] used to obtain high temperature properties are explained in detail. The importance and generation of special quasi random structures to represent the disordered structures is also given in this chapter.

In chapter 3, the Mott insulating nature of UO_2 is discussed. Performance of DFT and DFT+U in reproducing the insulating anti-ferromagnetic state of UO_2 is evaluated. The strength of Coulomb correlations in 5f electrons of uranium atom is varied by varying the value of Hubbard U parameter (U_{eff}) and its effects on band gap, magnetic moment and bulk modulus are studied. The optimized value of U_{eff} is found to be 4 eV which reproduce the band gap correctly. The study of the effect of strong Coulomb correlations on other properties like bonding, phonon dispersion, equilibrium volume and bulk modulus is done, which shows that inclusion of strong correlations lead to increase in bulk modulus but an over prediction of lattice parameter. Quasi harmonic approximation is used to get thermal expansion, bulk modulus and specific heat as a function of temperature which shows an under prediction of bulk modulus and over prediction of thermal expansion coefficient. This discrepancy is corrected by applying a non-local exchange correlation pressure correction to correct the over prediction of lattice parameter by the DFT+U calculations and its effect on bulk modulus and thermal expansion coefficient is also discussed.

In chapter 4, along with role of 5f electrons and type of bonding, the role of site occupancy disorder in the elastic and dynamic stability of UZr_2 is studied. The partially ordered structure is not only found to be energetically stable but also is the only dynamically stable structure. The ordered structure even though elastically stable, is dynamically unstable and the unstable phonon mode leads to distortion of U atoms along Z direction leading to dimerization of the unit cell. The distorted dimerized structure is dynamically stable but found to be energetically less stable than disordered structure. Study of thermal properties (thermal expansion, bulk modulus and specific heat) using quasi harmonic approximation leads to the under prediction of thermal expansion even though the equilibrium volume is predicted correctly indicating the presence of strong anharmonicity.

In chapter 5, the nature of uranium 5f electrons, band structure, structural, lattice vibrational and elastic properties of U_2Ti are studied. In contrary to the case of UZr_2, site occupancy disorder is not found to be energetically favourable corroborating with the fact that U_2Ti is a line compound. The elastic and the dynamical stability is analysed through calculated elastic constants and phonon dispersion. U_2Ti is found to be elastically stable but dynamically unstable with phonon instability corresponding to 'A' point in Brillouin zone. This predicted phonon instability was not seen in any of the earlier studies and is verified by increasing the accuracy of the calculations. The nature of instability is analysed and a structural distortion in the system is found from this analysis. The charge density distribution becomes unsymmetrical around the uranium atoms along Z direction showing the possibility of charge density wave. Further, study as a function of pressure shows that this charge density wave will be stable up to a pressure of 4 GPa.

In the concluding chapter, the summary of results and the scope of future work are given briefly.

Chapter 2

Theoretical and computational methods

This chapter discusses the theoretical and computational methods employed in this thesis. The various approximations involved in deducing many body problem to Kohn-Sham equations are explained. A brief introduction to the techniques for solving Kohn-Sham equations is also given. Methods to calculate phonon dispersion and elastic constants are also explained along with quasi harmonic approximation for calculating thermal properties as a function of temperature.

2.1 The many body problem

Solids can be considered as a collection of interacting nuclei and electrons. The ground state properties of any solid can thus be obtained by solving time independent Schrödinger equation

$$H\Phi\left(\mathbf{R},\mathbf{r}\right)=\mathbb{E}\Phi\left(\mathbf{R},\mathbf{r}\right) \tag{2.1}$$

where $\Phi\left(\mathbf{R},\mathbf{r}\right)$ is the total wavefunction of the system, $\mathbb{E}$ is the energy eigenvalue and H is the Hamiltonian for system of interacting nuclei and electrons which can be written as

$$H=\sum_{I=1}^{N}\frac{-\mathrm{h}^2}{2M_I}\nabla_I^2+\sum_{i=1}^{n}\frac{-\mathrm{h}^2}{2m_i}\nabla_i^2+\frac{e^2}{2}\sum_{I=1}^{N}\sum_{J\neq I}^{N}\frac{Z_IZ_J}{|R_I-R_J|}+\frac{e^2}{2}\sum_{i=1}^{n}\sum_{j\neq i}^{n}\frac{1}{|r_i-r_j|}-e^2\sum_{I=1}^{N}\sum_{j=1}^{n}\frac{Z_I}{|R_I-r_j|} \quad (2.2)$$

where I=1,2...N represent N nuclei and i=1,2,....n represent n electrons. R_I and M_I are positions and masses of the nuclei, r_i and m_i are positions and masses of the electrons and Z_I is the atomic number of nucleus I. The first and the second term are the kinetic energies of the nuclei and the electrons respectively, the third and the fourth terms are the potential energies of nucleus-nucleus Coulomb interaction and the electron-electron Coulomb interaction, and the last term is the potential energy of nucleus-electron Coulomb interaction.

In principle, if one solves this equation, everything about the system will be known. But this is a multi-component many body problem and is impossible to solve within a full quantum mechanical framework (except for single atoms and small molecules). A number of approximations are done to make this equation solvable.

2.1.1 Born-Oppenheimer approximation

The masses of the nuclei and the electrons are different by an order of magnitude (the mass of a proton is about 1836 times the mass of an electron). Nuclei being heavier in mass move much slower as compared to electrons. For time scale on which nuclei move electrons can be assumed to be following them instantaneously. As a result we can assume nuclei to be stationary on the time scale of electron movement. This is the Born-Oppenheimer approximation[85]. The total wavefunction of the system can then be written as

$$\Phi\left(\mathbf{R},\mathbf{r}\right)=\Theta\left(\mathbf{R}\right)\Psi\left(\mathbf{R},\mathbf{r}\right) \tag{2.3}$$

where $\Theta\left(\mathbf{R}\right)$ describes the nuclei and $\Psi\left(\mathbf{R},\mathbf{r}\right)$ describes the electrons (depending parametrically on $\mathbf{R}$). Thus with Born-Oppenheimer approximation equation 2.1 can be written as two separate equations:

$$H_e\Psi\left(\mathbf{R},\mathbf{r}\right)=E\left(\mathbf{R}\right)\Psi\left(\mathbf{R},\mathbf{r}\right) \tag{2.4}$$

where

$$H_e=\sum_{i=1}^{n}\frac{-\mathrm{h}^2}{2m_e}\nabla_i^2+\frac{e^2}{2}\sum_{I=1}^{N}\sum_{J=1}^{N}\frac{Z_IZ_J}{\left|R_I-R_J\right|}+\frac{e^2}{2}\sum_{i=1}^{n}\sum_{j=1}^{n}\frac{1}{\left|r_i-r_j\right|}-e^2\sum_{I=1}^{N}\sum_{j=1}^{n}\frac{Z_I}{\left|R_I-r_j\right|} \tag{2.5}$$

and

$$\left(\sum_{I=1}^{N}\frac{-h^2}{2M_I}\nabla_I^2+E\left(\mathbf{R}\right)\right)\Theta\left(\mathbf{R}\right)=\mathbb{E}\Theta\left(\mathbf{R}\right) \tag{2.6}$$

Equation 2.4 is the equation for the electrons with nuclei position fixed. The eigenvalue $E\left(\mathbf{R}\right)$ depend parametrically on nuclei positions $\mathbf{R}$. After solving equation 2.4, $E\left(\mathbf{R}\right)$ will be known and then from equation 2.6 motion of nuclei can be obtained. Equation 2.6 is sometimes replaced by Newton's equation of motion and nuclei are moved classically with forces ∇E.

The significance of Born-Oppenheimer approximation is the simplicity obtained by the separation of the movement of electrons and nuclei. The problem is reduced to electrons moving in the static external field $\mathrm{V}_{\mathrm{ion}}(\mathrm{r})$ formed by nuclei whose positions are fixed,

$$\left(\sum_{i=1}^{n}\frac{-\mathrm{h}^2}{2m_e}\nabla_i^2+\frac{e^2}{2}\sum_{i=1}^{n}\sum_{j=1}^{n}\frac{1}{|r_i-r_j|}-\sum_{i=1}^{n}V_{ext}(r_i)\right)\Psi\left(\mathbf{r}\right)=\mathrm{E}\Psi\left(\mathbf{r}\right) \tag{2.7}$$

Solving this equation is called electronic structure calculation. Note that second term in equation 2.5 is just a constant as far as electron degree of freedom is concerned.

2.1.2 Hartree-Fock approximation

The task is to solve the many electron Schrödinger equation 2.7. It is not possible to solve this equation when number of electrons is large. Hence approximations are inevitable. The first one is the Hartree approximation. In the Hartree approximation many-electron wave function is written as a product of one-electron wavefunctions (orbitals) as

$$\Psi_H(\mathbf{r})=\prod_{i=1}^{n}\psi_i\left(\mathbf{r}_i\right) \tag{2.8}$$

where $\psi_i\left(\mathbf{r}_i\right)$ represent the orbital for i^{th} electron. Total energy of the system will be

$$E^H=\left\langle\Psi_H\left|H_e\right|\Psi_H\right\rangle \tag{2.9}$$

Applying the variational principle with respect to one electron orbitals we get n single particle equations called Hartree equations:

$$\left(\frac{-h^2}{2m_e}\nabla^2+V_{ion}(\mathbf{r})+e^2\sum_{j\neq i}^{n}\langle\psi_j(\mathbf{r}')|\frac{1}{|\mathbf{r}-\mathbf{r}'|}|\psi_j(\mathbf{r}')\rangle\right)\psi_i(\mathbf{r})=\epsilon_i\psi_i(\mathbf{r}) \tag{2.10}$$

where ϵ_i are Lagrange multipliers introduced to take into account the normalization of the single-particle states ψ_i. $\psi_i's$ can be determined by solving above equations self consistently.

Equation 2.10 represent an electron moving in the mean field $\mathrm{V}^{\mathrm{H}}(\mathbf{r})$ created by all other electrons.

$$V_i^H(\mathbf{r}) = e^2 \sum_{j\neq i}^{n} \langle\psi_j(\mathbf{r}')| \frac{1}{|\mathbf{r}-\mathbf{r}'|} |\psi_j(\mathbf{r}')\rangle \tag{2.11}$$

This is Hartree potential and includes only Coulomb repulsion between electrons. The potential is different for each particle. It is a mean field approximation to electron-electron interaction, taking into account only the electronic charge.

Electrons being Fermionic in nature, their wavefunction should be antisymmetric with respect to the exchange of any two electrons. But the product of one-electron wavefunctions as given in equation 2.8 is not antisymmetric. Anti-symmetry can be included by writing many-electron wave function as a Slater determinant of one-electron orbitals as

$$\Psi_{HF}(\mathbf{r}) = \frac{1}{\sqrt{n!}} \begin{vmatrix} \psi_1(\mathbf{r}_1) & \psi_2(\mathbf{r}_1) & ... & \psi_n(\mathbf{r}_1) \\ \psi_1(\mathbf{r}_2) & \psi_2(\mathbf{r}_2) & ... & \psi_n(\mathbf{r}_2) \\ ... & ... & ... & ... \\ \psi_1(\mathbf{r}_n) & \psi_2(\mathbf{r}_n) & ... & \psi_n(\mathbf{r}_n) \end{vmatrix} \tag{2.12}$$

Using this wavefunction in equation 2.7 total energy E is

$$\begin{aligned} E^{HF} = \langle\Psi_{HF}| H_e |\Psi_{HF}\rangle = \sum_i \langle\psi_i| \frac{-h^2\nabla^2}{2m_e} + V_{ion}(\mathbf{r}) |\psi_i\rangle + \frac{e^2}{2} \sum_{i,j(j\neq i)}^{n} \langle\psi_i\psi_j| \frac{1}{|\mathbf{r}-\mathbf{r}'|} |\psi_i\psi_j\rangle \\ - \frac{e^2}{2} \sum_{i,j(j\neq i)}^{n} \langle\psi_i\psi_j| \frac{1}{|\mathbf{r}-\mathbf{r}'|} |\psi_j\psi_i\rangle \end{aligned} \tag{2.13}$$

The single particle Hartree-Fock equation, obtained by variational principle is:

$$\left[\frac{-h^2}{2m_e}\nabla^2 + V_{ion}(\mathbf{r}) + V_i^H(\mathbf{r})\right] \psi_i(\mathbf{r}) - e^2 \sum_{j\neq i}^{n} \langle\psi_j| \frac{1}{|\mathbf{r}-\mathbf{r}'|} |\psi_i\rangle \psi_j(\mathbf{r}) = \epsilon_i \psi_i(\mathbf{r}) \tag{2.14}$$

This equation has one extra term compared to Hartree equation, which is called the exchange term. This term describes the effect of exchange between electrons.

The Hartree-Fock equations look the same as the Hartree equations, except for the very important non local exchange which depend on the location of other electrons. Basically due to Pauli exclusion principle, electrons with the same spin do not like to be too close to each other. Even if we solve the HF equations exactly, method turns out to be theoretically incomplete. Even though there is exact exchange but correlation is completely missing. Many body wavefunction is not necessarily well represented by a single Slater determinant.

2.1.3 Beyond Hartree-Fock approximation

Electron-electron correlation is completely missing in HF approximation. The difference in actual total energy and HF total energy in HF based methods is called correlation energy. Møller-Plesset (MP) perturbation theory , configuration interaction and coupled cluster are the methods to include electron correlations. Configuration interaction and coupled cluster methods use multi determinant wavefunction in place of single determinant. In Møller-Plesset method the difference between the exact Hamiltonian and sum of one electron operators is introduced as a perturbation to the unperturbed HF solution. But these methods are computationally very demanding and practically solvable for small number of atoms only. A different approach to solve many-body problem is using Density Functional Theory which is discussed in next section.

2.2 Density functional theory

Wave function based approaches become very difficult to solve when the particle number becomes very large. Wave function for a system depends on the position coordinates of all the electrons. Alternative approach using electron density simplifies the problem as it depends on only three position coordinates. The idea of describing a system of many electrons in terms of single particle density was introduced by Thomas and Fermi. They suggested that the calculation of the ground state properties of a system can be done knowing the ground state density without requiring the full many body wave function. Modern density functional theory is based on the fundamental theorems of Hohenberg and Kohn [12] and a practical way of using this is given by Kohn and Sham [86].

2.2.1 Hohenberg Kohn theorems

First theorem: *For any system of interacting particles in an external potential* $V_{ext}(\mathbf{r})$*, the potential* $V_{ext}(\mathbf{r})$ *is determined uniquely, except for a constant, by the ground-state particle density* $n_0(\mathbf{r})$*.*

Since the Hamiltonian is thus fully determined, except for a constant shift of the energy, it follows that the many-body wave functions for all states (ground and excited) are determined. Therefore all properties of the system are completely determined given only the ground-state density $n_0(\mathbf{r})$.

Second theorem: *A universal functional of the energy* $E[n]$ *in terms of the density* $n(\mathbf{r})$ *can be defined, valid for any external potential* $V_{ext}(\mathbf{r})$*. For any particular* $V_{ext}(\mathbf{r})$*, the exact ground-state energy of the system is the global minimum value of this functional, and the density* $n(\mathbf{r})$ *that minimizes the functional is the exact ground-state density*

$n_0(\mathbf{r})$.

Thus total energy can be written as :

$$E[n(\mathbf{r})] = F[n(\mathbf{r})] + \int V_{ext}(\mathbf{r})n(\mathbf{r})d\mathbf{r} = T[n(\mathbf{r})] + E_{int}[n(\mathbf{r})] + \int V_{ext}(\mathbf{r})n(\mathbf{r})d\mathbf{r} \quad (2.15)$$

where $F[n(\mathbf{r})]$ represents the universal functional of electron density n(r), $T[n(\mathbf{r})]$ kinetic energy and $E_{int}[n(\mathbf{r})]$ represent the potential energy.

Although Hohenberg-Kohn theorems put particle density n(r) as the basic variable, it is still impossible to calculate any property of a system because the universal functional $F[n(\mathbf{r})]$ is unknown. This difficulty was overcome by Kohn and Sham, who proposed the well known Kohn-Sham ansatz.

2.2.2 Kohn Sham equations

The practical tools to determine ground state density is given by the Kohn-Sham ansatz. They replace the interacting many body problem by auxiliary problem of non interacting electrons having same density as that of original interacting system. Total energy functional can be expressed as

$$E_{KS}[n(\mathbf{r})] = T_0[n(\mathbf{r})] + \frac{1}{2}\int\int \frac{n(\mathbf{r})n(\mathbf{r}')}{|\mathbf{r}-\mathbf{r}'|}d\mathbf{r}d\mathbf{r}' + E_{xc}[n(\mathbf{r})] + \int V_{ext}(\mathbf{r})n(\mathbf{r})d\mathbf{r} \quad (2.16)$$

where the first term is the kinetic energy functional of the system of non-interacting electrons with the same density, the second term is the classical Coulomb energy for the electron-electron interaction, the third term is energy functional incorporating all the many-body effects of exchange and correlation and the last term is the attractive Coulomb potential provided by the fixed nuclei (external potential).

The solution of the auxiliary system can be viewed as the minimization problem of the Kohn-Sham functional with respect to the density. This leads to Kohn-Sham equations :

$$\left(-\frac{1}{2}\nabla^2 + V_{eff}(\mathbf{r})\right)\psi_i(\mathbf{r}) = \varepsilon_i\psi_i(\mathbf{r}) \tag{2.17}$$

where density is $n(\mathbf{r}) = \sum_i |\psi_i(\mathbf{r})|^2$.

Here ε_i are eigenvalues, ψ_i are Kohn-Sham orbitals and $\mathrm{V}_{\mathrm{eff}}$ is the effective potential given by

$$V_{eff}(\mathbf{r}) = V_{ext}(\mathbf{r}) + \int \frac{n(\mathbf{r}')}{|\mathbf{r}-\mathbf{r}'|}d\mathbf{r}' + V_{xc}(\mathbf{r}) \tag{2.18}$$

that is the sum of potential from the nuclei, Hartree potential and the potential for exchange and correlation. Exchange correlation potential is

$$V_{xc}(\mathbf{r}) = \frac{\partial E_{xc}[n(\mathbf{r})]}{\partial n(\mathbf{r})} \tag{2.19}$$

Equation 2.17 and equation 2.18 are solved self consistently to solve the Kohn-Sham equations. Beginning with a guess electron density n($\mathbf{r}$), V_{eff} is calculated and equation 2.17 is solved to get $\psi_i(\mathbf{r})$'s and new n($\mathbf{r}$) is calculated and used to get $V_{eff}(\mathbf{r})$ for equation 2.17. This process is repeated until self-consistency is achieved.

The most important term in these calculations is exchange correlation term, which contain all the many body effect. This term is explained in detail in next section.

2.2.3 Exchange-correlation functional

The reduction of the many body problem into single electron Kohn Sham equation has introduced an unknown functional E_{XC} of charge density. The main problem is how to obtain this functional for a given problem. For homogeneous(uniform) electron density this functional is known exactly. For non uniform electron densities approximations are used. Two most widely used approximations being Local Density Approximation (LDA) and Generalized Gradient Approximation (GGA). In LDA the exchange-correlation energy at each point of the real space is assumed to be equal to that of a uniform electron gas with same density and total exchange-correlation energy is written as

$$E_{xc}^{LDA}[n] = \int n(\mathbf{r})\epsilon_{xc}^{heg}(n(\mathbf{r}))d\mathbf{r} \tag{2.20}$$

where $\epsilon_{xc}^{heg}(n(\mathbf{r}))$ is exchange-correlation energy per electron in a homogenous electron gas having density n(r). This equation is exact for homogeneous electron gas and can be assumed to work well for slowly varying electron densities. But the applicability of LDA has been found to be much beyond nearly homogeneous electron density systems to atoms and molecules. But it was failure for many systems mostly insulators and semiconductors.

An important improvement in exchange correlation functional is to include dependence on gradient of electron density in GGA. The exchange correlation energy is written as

$$E_{xc}^{GGA}[n] = \int n(\mathbf{r})F[n(\mathbf{r}), \nabla n(\mathbf{r})]d\mathbf{r} \tag{2.21}$$

This approximation is found to successfully describe many properties in finite and extended systems. Two widely used GGA exchange-correlation functional are parametrized by Perdew and Wang (PW91) [87], and Perdew, Burke and Ernzerhof (PBE) [88].

The next successful development to the approximation of exchange-correlation functional is the inclusion of HF exact exchange. These functionals are known as Hybrid functionals. In these functionals a fraction of exact Hartree-Fock exchange is added to the approximate functional. The PBE0 [89] hybrid functional based on the PBE exchange–correlation functional can be written as

$$E_{xc}^{PBE0} = aE_x^{HF} + (1-a)E_x^{PBE} + E_c^{PBE} \tag{2.22}$$

where mixing fraction $'a'$ comes out to be 0.25 by perturbation theory calculations. This functional is shown to be very successful in describing a wide range of molecular properties [90]. However the long-range nature of the Hartree-Fock exchange results in the large computational requirements. This factor is improved by Heyd, Scuseria and Ernzerhof (HSE) [91] by introducing a screened Coulomb potential for Hartree–Fock exchange enables. These screened Coulomb hybrid functionals because of their accuracy combined with computational advantage are widely applicable to large molecules and periodic systems.

2.2.4 LDA+U Method

Systems containing transition metal or rare-earth metal ions with partially filled d or f shells usually show strong correlation effects. These are not properly described by the orbital-independent potentials in LDA and GGA. For example, LDA predicts Mott insulators to be metallic because of the partially filled d or f shells. Instead, these d or f electrons are well localized. In order to properly describe these strongly correlated systems, orbital-dependent potentials should be used. A number of approaches have been developed to describe the electronic structure of strongly correlated systems. These include the self-interaction correction(SIC) [92], Hybrid functionals, DFT+U formalism [51, 55] and Dynamical Mean Field theory (DMFT) based models. DFT+U formalism is used in this thesis in coming chapters.

DFT+U formalism is the most popular and efficient method for systems with strong electron-electron correlations. The idea is to separate the electrons in two subsystems:

the delocalized s and p electrons, which can be described well by LDA or GGA and the more localized (d or f) electrons for which an orbital dependent term is used to describe the electron-electron interactions. The interaction between electrons is added using term:

$$\frac{1}{2}U\sum_{i\neq j} n_i n_j \tag{2.23}$$

where U is the effective Coulomb repulsion between the localized electron. The energy functional for DFT+U (in particular for LDA+U) can be written as:

$$E^{LDA+U}([\rho_\sigma(r), \{n_\sigma\}] = E^{LDA}[\rho] + E^{U}[\{n_\sigma\}] - E^{dc}[\{n_\sigma\}] \tag{2.24}$$

where σ is the spin index, $\rho_\sigma(r)$ is the electron density for spin-σ electrons and $\{n_\sigma\}$ is the density matrix of d or f electrons for spin σ. The first term is the standard LDA energy functional, the second term is the electron-electron Coulomb interaction energy and the third term is the double counting term which removes averaged LDA energy contribution of these d or f electrons.

2.2.5 Solving Kohn-Sham equations

Kohn-Sham equations 2.17 provide a way to obtain the exact density and energy of the ground state of a condensed matter system. These single particle equations must be solved consistently as V_{eff} is a functional of density n(r).

2.2.5.1 Periodic boundary condition

A bulk system contains infinitely large number of electrons. Solving single particle KS equations for these electrons will be impossible. But the problem can be simplified if the system is periodic. For a periodic system the wave function can be calculated for the electrons in the unit cell and the wave function in all other periodic images of that cell can be obtained by multiplying by a phase factor. This is the statement of Bloch's theorem [93]. According to Bloch's theorem, for an electron in a periodic system (potential V(r), which can be Kohn-Sham potential, being invariant under translation by a lattice vector (R)) the wave function can be written as product of a periodic function and a phase factor as:

$$\psi_{\mathbf{k}}(\mathbf{r}) = u(\mathbf{r})e^{i\mathbf{k}.\mathbf{r}} \tag{2.25}$$

where k is the wave vector in the first Brillouin zone of the reciprocal lattice and u(r) is a periodic function of r. Thus due to periodicity of the crystal, instead of solving the wave function over the infinite space, one requires solution of the wave function only within the unitcell. In the reciprocal space within the first Brillouin zone of the supercell, there are infinite number of possible k points at which the wave functions need to be calculated, as the occupied states at each k point contributes to the electronic potential of the system. But the electronic wave function and the eigenvalues vary smoothly over a particular region of the Brillouin zone. Hence the wave function over a region of k-space can be represented by a wave function at single k-point. Thus finite number of k-points in the first Brillouin zone are only needed to calculate the potential as well as total energy of the system. Monkhorst-Pack [94] and Chadi-Cohen [95] are special methods to generate k point mesh that increases the computational efficiency.

Plane wave basis set

For solving the KS equations, electronic wave function at each k-point needs to be expressed in terms of basis vectors. Most convenient basis vector set is plane waves. The wave function can be written as a summation over infinite plane waves as

$$\psi_{i,\mathbf{k}} = \frac{1}{\sqrt{\mathit{\Omega}}} \sum_{\mathbf{G}=0}^{\infty} C_{i\mathbf{k}}(\mathbf{G}) e^{i(\mathbf{k}+\mathbf{G}).\mathbf{r}} \tag{2.26}$$

where $\mathit{\Omega}$ is unitcell volume, G is reciprocal lattice vector and k is the wave vector in first Brillouin zone. Practically, infinite plane waves are truncated to finite number of plane waves. But the contribution (importance) decreases as the energy of plane waves increases. A finite set of plane waves is defined by using an energy cut off and selecting the plane waves which satisfy

$$\frac{\hbar^2 \left|\mathbf{k}+\mathbf{G}\right|^2}{2m} \leq E_{cut} \tag{2.27}$$

i.e. all those plane waves having kinetic energy less than cut-off energy are only used as basis set. The error in calculation of total energy with the truncated finite basis set can always be reduced by increasing the value of the cut-off energy.

2.2.5.2 Pseudopotential method

The eigen states of an atomic Hamiltonian should be mutually orthogonal to each other. The core states are localized in the vicinity of the nucleus. The valence electron wave function oscillates rapidly in the core region to maintain orthogonality with the core states. To represent these oscillations in wave function a very large number of plane waves will be required. Most of the physical properties of solids have a greater dependence on valence electron than the core electrons. In the pseudopotential approach[96, 97] the external potential of the nuclei are represented using an effective potential which include effects from core electrons. The pseudopotential is constructed in such a way that the pseudo wave function (ψ_{pseudo}) for the valence electron and the atomic wave function (ψ) should match outside a cut-off radius $'r_c'$. ψ_{pseudo} as well as its first and second derivative should be continuous at $'r_c'$. The pseudopotential should match the true ionic potential outside $'r_c'$. In the core region the pseudopotential should be a softer potential and the pseudo wavefunction for the valence electron should be smoother inside the core region. The pseudo wave function being smoother in the core region also will require lesser number of plane waves and will improve the computational efficiency of the calculations.

There are different flavours of the pseudopotentials available based on the criteria used for making them: norm-conserving, ultra soft potential and projector augmented wave (PAW) method. Details of these can be found in the book [80]. VASP has implemented PAW based pseudopotentials and they are used for most of the calculations done in this thesis.

Augmented plane wave method

Although pseudopotential methods are widely used because of their computational efficiency, certain applications need the knowledge of both core states and valence states wavefunction at nucleus. In those scenarios all electron calculations need to be done. As already discussed near to the nucleus a very large number of plane waves will be required to represent the oscillations of the valence electron wave function near the nucleus but far from nucleus, the wavefunctions are rather flat (slowly varying) as potential is smooth there. Augmented plane wave (APW) method uses different types of basis functions in these two environments, near to nucleus and far from nucleus. The unit cell is divided into non-overlapping atomic spheres (centered at the atomic sites) and an interstitial region as shown in figure.

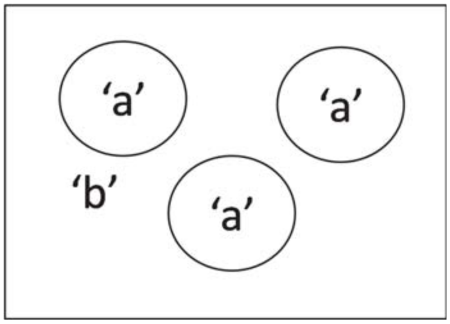

Figure 2.1 – Division of the unit cell in two regions. Atomic spheres represented as region 'a' and interstitial region represented as region 'b'.

Inside the atomic spheres the potential is similar to the potential of the atom and the wavefunction is represented as a linear combination of radial functions times spherical harmonics and in the interstitial region a plane wave expansion is used [80].

$$\psi_{i,\mathbf{k}}(\mathbf{r}) = \sum_{G=0}^{\infty} C_{i\mathbf{k}}(G)\chi^{APW}_{\mathbf{k+G}}(\mathbf{r}) \tag{2.28}$$

where

$$\chi^{APW}_{\mathbf{k+G}}(\mathbf{r}) = \begin{cases} exp(i(\mathbf{k}+\mathbf{G}).\mathbf{r}) & r > S \\ \sum_{lm,s} c_{lm,s}(\mathbf{k}+\mathbf{G})Y_{lm}(\hat{r})u_{l,s}(\epsilon, r) & r < S \end{cases} \tag{2.29}$$

$Y_{lm}(\hat{r})$ are spherical harmonics and $u_{lm,s}(\epsilon, r)$ is a solution of the radial Schrodinger equation regular at the origin at energy ϵ. The coefficients $c_{lm,s}(\mathbf{k}+\mathbf{G})$ are obtained by requiring waves to match at the surface of the spheres. In general for an accurate description of wave function $\psi_{i,k}(r)$, energy parameter ϵ should be equal to the eigenvalue of that state. For each eigen value basis functions are need to be calculated self-consistently which is very time consuming.

In linear augmented plane wave (LAPW) method $u_{lm,s}(\epsilon, r)$ in equation 2.29 is calculated at some value of energy E_0 and a Taylor expansion is made to find its value at eigenvalues $\epsilon_{i,\mathbf{k}}$ as

$$u_{lm,s}(\epsilon_{i,\mathbf{k}}, r) = u_{lm,s}(E_0, r) + (E_0 - \epsilon_{i,\mathbf{k}}) \left. \frac{\partial u_{lm,s}(\epsilon, r)}{\partial E} \right|_{E=E_0} + O(E_0 - \epsilon_{i,\mathbf{k}})^2 \tag{2.30}$$

and last term $O(E_0 - \epsilon_{i,k})^2$ is ignored. Thus the definition of LAPW becomes

$$\chi_{\mathbf{k+G}}^{LAPW}(\mathbf{r}) = \begin{cases} exp(i(\mathbf{k}+\mathbf{G}).\mathbf{r}) & r > S \\ \sum_{lm,s} \left[A_{lm,s}(\mathbf{k}+\mathbf{G}) u_{l,s}(\epsilon, r) + B_{lm,s}(\mathbf{k}+\mathbf{G}) \dot{u}_{l,s}(\epsilon, r)\right] Y_{lm}(\hat{r}) & r < S \end{cases} \tag{2.31}$$

where coefficients $A_{lm,s}(\mathbf{k}+\mathbf{G})$ and $B_{lm,s}(\mathbf{k}+\mathbf{G})$ are determined by requiring that the function inside the sphere matches the plane wave both in value and in slope at sphere boundary. Last term in the equation 2.30 is small if $E_0$is close to $\epsilon_{i,k}$. This can be realized if we do not take a different value of E_0 for each physically important l. For $l \geq 4$ a fixed value can be kept. Therefore LAPW basis function can be written as

$$\chi_{\mathbf{k+G}}^{LAPW}(\mathbf{r}) = \begin{cases} exp(i(\mathbf{k}+\mathbf{G}).r) & r > S \\ \sum_{lm,s} \left[A_{lm,s}(\mathbf{k}+\mathbf{G}) u_{l,s}(E_{i,l}, r) + B_{lm,s}(\mathbf{k}+\mathbf{G}) \dot{u}_{l,s}(E_{i,l}, r)\right] Y_{lm}(\hat{r}) & r < S \end{cases} \tag{2.32}$$

Here to choose a finite number of basis set in equation 2.28, only those G's are selected which satisfy the condition $|(\mathbf{k}+\mathbf{G})| \leq K_{max}$. In practice one specifies the value of $R_{MT}K_{max}$, where R_{MT} is the radius of the smallest muffin-tin sphere of the cell. LAPW method is implemented in Wien2K code which is used in this thesis to verify some results where different pseudopotentials were giving qualitative by different results.

2.3 Linear response calculations

In section 2.2 we discussed various approximations to calculate the total energy of the system using DFT. Once we get a way to get the total energy of the system for a given external potential (nuclei positions), we can calculate many different properties of the system (force constants, phonon, elastic constants, etc.) by calculating the derivatives of energy with respect to some perturbations. One way is by carrying out full self consistent calculations for various values of the perturbation and extracting derivatives from finite difference formulas. Other more efficient way is given by Density Functional Perturbation Theory (DFPT) [13] which is briefly explained in the following section.

2.3.1 Density functional perturbation theory

In DFPT, the response of the system to perturbations (nuclei displacement for phonon and unit cell distortions for elastic constants) are calculated using perturbation method without explicitly calculating the density or wave function for the perturbed state. The first order correction to energy can be calculated using Hellman-Feynman theorem [98, 99] as the expectation value of the derivative of the Hamiltonian with respect to unperturbed wave function.

$$\frac{\partial E}{\partial \lambda} = \int \frac{\partial V^{\lambda}(\mathbf{r})}{\partial \lambda} n^{\lambda}(\mathbf{r}) d\mathbf{r} \tag{2.33}$$

here λ is a continuously varying parameter that is perturbed. (atomic position, stain etc).

The second order correction to energy will be

$$\frac{\partial^2 E}{\partial \lambda^2} = \int \frac{\partial^2 V^{\lambda}(\mathbf{r})}{\partial \lambda^2} n^{\lambda}(\mathbf{r}) d\mathbf{r} + \int \frac{\partial n^{\lambda}(\mathbf{r})}{\partial \lambda} \frac{\partial V^{\lambda}(\mathbf{r})}{\partial \lambda} d\mathbf{r} \tag{2.34}$$

Electron charge density distribution, n^{λ} is given by

$$n^{\lambda}(\mathbf{r}) = 2\sum_{n=1}^{N/2} \left|\psi_n^{\lambda}(\mathbf{r})\right|^2 \tag{2.35}$$

where N is number of electrons in the system, the single-particle orbitals, $\psi_n^{\lambda}(r)$, satisfy the Kohn-Sham equation 2.17. The electron density response in equation 2.34 can be evaluated by linearising equations 2.17, 2.35 and 2.18 with respect to wave function, density and potential variations respectively which leads to:

$$n'(\mathbf{r}) = 4Re\sum_{n=1}^{N/2} \psi_n^{*}(\mathbf{r})\psi_n'(\mathbf{r}) \tag{2.36}$$

where prime symbol indicates differentiation with respect to one λ. The variation of Kohn-Sham orbitals, $\psi_n^{'}(r)$, is obtained by standard first order perturbation theory:

$$(H^0 - \epsilon_n^0)\left|\psi_n'\right\rangle = -(V_{eff}' - \epsilon_n')\left|\psi_n'\right\rangle \tag{2.37}$$

Here H^0 is unperturbed KS Hamiltonian, (label λ is omitted for simplification). $V_{eff}^{'}(\mathbf{r})$ is first order perturbation to Kohn-Sham effective potential and is given by

$$V_{eff}'(\mathbf{r}) = V_{ext}'(\mathbf{r}) + \int \frac{n'(\mathbf{r}')}{|\mathbf{r}-\mathbf{r}'|}d\mathbf{r}' + V_{xc}(\mathbf{r}) \tag{2.38}$$

The first order variation of KS eigenvalue, ϵ_n, is

$$\epsilon_n' = \left\langle \psi_n' \left| V_{eff}' \right| \psi_n^0 \right\rangle \tag{2.39}$$

Equations 2.37, 2.38 and 2.39 form a set of self consistent linear equations for perturbed system. The computational cost of determination of the density response to single perturbation is of same order as that needed for the calculation of the unperturbed ground state[100].

2.3.2 Phonon calculations

For phonon frequency calculations, perturbation is the displacement of atoms from their equilibrium positions. Equilibrium geometry of the system is determined by the condition that the forces acting on the individual atom vanish:

$$F_I = -\frac{\partial E(\{\mathbf{R}\})}{\partial \mathbf{R}_I} = 0 \tag{2.40}$$

E({R}) which is the eigenvalue of equation 2.6. The vibrational frequencies (ω) are determined by the eigenvalues of the Hessian of the total energy E({R}) scaled by the nuclear masses:

$$det \left| \frac{1}{\sqrt{M_I M_J}} \frac{\partial^2 E(\{\mathbf{R}\})}{\partial \mathbf{R}_I \partial \mathbf{R}_J} - \omega^2 \right| = 0 \tag{2.41}$$

Hessian Matrix is usually called the matrix of inter-atomic force constants (IFC). For crystal we can write

$$C_{ss'}^{\alpha\alpha'}(\mathbf{R} - \mathbf{R}') = \frac{\partial^2 E(\{\mathbf{R}\})}{\partial u_s^\alpha(\mathbf{R}) \partial u_{s'}^{\alpha'}(\mathbf{R}')} \tag{2.42}$$

where $u_s^\alpha(\mathbf{R})$ is the α^{th} Cartesian components of the displacement of the s^{th} atom of the crystal unit cell located at lattice site **R** and translational invariance shows manifestly in the dependence of the IFC matrix on **R** and **R**' through their difference only. IFC are calculated using the DFPT as explained in previous section. The Fourier transform of of the IFC matrix is called Dynamical matrix:

$$C_{st}^{\alpha\beta}(\mathbf{k}) = \sum_R C_{st}^{\alpha\beta}(\mathbf{R}) e^{i\mathbf{k}.\mathbf{R}} \tag{2.43}$$

and the vibrational frequencies $\omega(\mathbf{k}, \nu)$, are the square root of the eigenvalues of $3n \times 3n$ dynamical matrix, where n is the number of atoms in unit cell.

2.3.3 Non-analytical term correction

In case of polar semiconductors, a macroscopic electric field is associated with the longitudinal optic phonon modes in the limit $q \to 0$ because of the long range nature of Coulomb forces. The electronic potential corresponding to this macroscopic electric field associated with lattice distortion in the limit $q \to 0$ is not lattice periodic. The effect of this macroscopic electric field is not incorporated in supercell based phonon dispersion calculations. This is usually done by incorporating a non- analytical contribution to the dynamical matrix that involve the Born effective charges of the constituent atoms [101, 102] as

$$C_{ij}^{na^{\alpha\beta}} = \frac{4\pi e^2}{\mathit{\Omega}} \frac{\left(\mathbf{q}.\mathbf{Z}_i^*\right)_\alpha \left(\mathbf{q}.\mathbf{Z}_j^*\right)_\beta}{\mathbf{q}.\epsilon^\infty.\mathbf{q}} \tag{2.44}$$

where ϵ^∞ is the high frequency static dielectric tensor and $\mathbf{Z_i^*}$ is the Born effective charge tensor for the ith atom in unit cell.

2.3.4 Quasi harmonic approximation

Density functional theory is for 0 K, so Kohn-Sham equation gives energy at 0 K. Phonon calculations are done within harmonic approximation. In harmonic approximation lattice volume, bulk modulus and phonon frequencies does not depend on temperature. But the real solids are not harmonic and many of the thermal properties like thermal expansion and temperature dependence of bulk modulus etc are an outcome of the anharmonicity of the system. In quasi harmonic approximation, anharmonicity or the effects of temperature are indirectly incorporated by the phonon frequency dependence on volume. The Phonon spectra are calculated for various volumes around equilibrium volume at zero Kelvin from which the temperature and the volume dependent free energy can be computed. For a given temperature T and volume V, the crystal free energy F (T, V) is

$$F(T,V) = E(V) + F_{ph}(T,V) + F_{el}(T,V) \tag{2.45}$$

Here, E(V) is the electron-ion ground state energy, $\mathrm{F_{ph}}$ (T, V) is the lattice vibration energy and $\mathrm{F_{el}}$ (T, V) is the contribution to the free energy from electronic excitations. The electronic contribution $\mathrm{F_{el}}$ (T, V) will be negligible for insulators. The Helmholtz free energy F (T, V) is calculated with in QHA as

$$F(T,V) = E(V) + \frac{k_B T}{N_{\mathbf{q}}} \sum_{\mathbf{q},\nu} \ln\left(2\sinh\left(\frac{\hbar\omega_{\mathbf{q},\nu}}{2k_B T}\right)\right) \tag{2.46}$$

$\omega_{\mathbf{q}\nu}$ is the frequency of the ν^{th} phonon mode at wave vector q in the first Brillouin zone and $N_{\mathbf{q}}$ is the total number of wave vectors considered in the first Brillouin zone. Fitting the $F(T,V)$ vs volume data at a given temperature T to the Birch-Murnaghan equation of state[103], gives the equilibrium volume and bulk modulus at that particular temperature. After obtaining the equilibrium volume at different temperatures, the thermal expansion coefficient can be calculated as

$$\alpha = \frac{1}{V}\frac{\partial V}{\partial T} \tag{2.47}$$

The specific heat at constant volume, which goes to the classical limit at high temperature, can be estimated from the phonon frequencies $\omega_{q\nu}$ as

$$C_V(T,V) = \frac{1}{VN_{\mathbf{q}}} \sum_{\mathbf{q},\nu} C_{V\mathbf{q},\nu}(T,V) \tag{2.48}$$

where

$$C_{V\mathbf{q},\nu}(T,V) = \hbar\omega_{\mathbf{q},\nu}(V)\frac{d}{dT}\left(\frac{1}{\exp\left(\frac{\hbar\omega_{\mathbf{q},\nu}}{k_B T}\right) - 1}\right) \tag{2.49}$$

is the contribution to the specific heat at constant volume from the $(\mathbf{q}\nu)^{th}$ mode.

When anharmonicity is taken into account, the specific heat at constant pressure C_p will no longer be the same as the specific heat at constant volume C_V and is estimated as

$$2C_p(T) = C_V(T,V) + TB_T\alpha_T^2 \tag{2.50}$$

where, B_T is the isothermal bulk modulus and α_T is the thermal expansion coefficient.

2.3.5 Elastic constants

The elastic properties of a lattice are described by its matrix of second-order elastic constants (Voigt notation) defined as

$$C_{ij} = \frac{1}{V_0}\left(\frac{\partial^2 E}{\partial e_i \partial e_j}\right) \tag{2.51}$$

where E is the energy of the crystal, V_0 its equilibrium volume and e denotes a strain [104, 105]. This elastic matrix has size 6 × 6 and is symmetric: it is thus composed of 21 independent components.

The elastic energy change associated with a arbitrary deformation is given by

$$U_{elastic} = \frac{1}{2}V_0\sum_{i,j}^{6} C_{ij}e_ie_j + O(e^3) \tag{2.52}$$

where e_i and e_j are elastic strains and $O(e^3)$ denote terms of order e^3 and higher. For small strains term $O(e^3)$ can be ignored (harmonic approximation).

A lattice is stable is if $U_{elastic}$ is positive for arbitrary small deformations [105]. This imposes a condition on C_{ij}, that the matrix C_{ij} should be positive definite or all the principle minors of the determinant of C_{ij} should be positive. The symmetry of the lattice reduces the number of independent elastic constants and it simplifies the condition of being positive definite of elastic constant matrix into simpler expressions. For cubic crystal lattice it reduces to

$C_{11} > |C_{12}|$, $C_{11} + 2C_{12} > 0$, and $C_{44} > 0$

For a hexagonal lattice, the condition for stability is given by

$C_{11} > |C_{12}|$, $2C_{13}^2 < C_{33}(C_{11} + C_{12})$, $C_{44} > 0$ and $C_{66} > 0$

These are called Born stability criteria.

A crystalline structure is stable if and only if meets both dynamical and elastic stability criteria [104]. While the elastic stability is governed by Born stability criteria, the dynamical stability means that all the phonon modes should have real frequencies corresponding to all wavevectors.

Elastic constants of a single crystal can be calculated using first principles by two routes: energy-strain approach and the stress-strain approach. In the energy-strain approach, the total energies are calculated for different strained states of the crystal. Whereas in the stress-strain approach elastic constants are determined by the stress calculated for different finite distortions of the crystal. In this thesis, stress-strain approach is used combined with finite difference method and symmetry generalized least square method [106]. In this method the elastic tensor is determined by performing six finite distortions of the lattice and deriving the elastic constants from the strain-stress relationship. The elastic tensor is calculated both, for rigid ions, as well, as allowing for relaxation of the ions.

Chapter 3

Electron correlations and thermal properties of UO_2

UO_2 *is known to be a Mott insulator where strong electron correlations in 5f electrons of uranium split the partially filled band to give anti-ferromagnetic insulating property of the system. This chapter discusses the reproduction of antiferromagnetic insulating ground state within DFT+U formalism that account for the strong Coulomb correlations in uranium 5f electrons. The effect of these strong correlations in other structural and thermal properties like bulk modulus, phonon, thermal expansion coefficient are computed and the results obtained are compared with the corresponding experimental data.*

3.1 Introduction

UO_2 is a material that has attracted significant interest due to its interesting properties as well as its use as a nuclear fuel material. Even though several experimental and theoretical studies exist for UO_2, the understanding of the properties of this system is far from complete. DFT calculations with LDA or GGA, which has been quite successful in predicting the ground state structure and properties of a wide range materials, has failed to give a proper description of the properties of UO_2. It predicted a ferromagnetic metallic [47] ground state for UO_2 where as it is well known that UO_2 is an anti-ferromagnetic insulator [48]. Further, in this compound the ground state magnetic order is crucially dependent on the strength of the on-site Coulomb repulsions. UO_2 also show the interesting phenomena of super-ionic conduction at higher temperatures, in which oxygen sublattice becomes unstable whereas the material retains its identity because the uranium sublattice continues to be stable.

UO_2 belongs to the class of strongly correlated materials where some of the f and d electrons are partially delocalized. The strong on-site Coulomb repulsion experienced by these electrons cannot be satisfactorily described by mean field based theories. Various experimental studies like X-ray photoemission spectroscopy [107, 108] , resonant photoemission spectroscopy [109], optical spectroscopy [110] , bremsstrahlung isochromat spectroscopy [107] and X-ray absorption studies [111, 112] have shown that UO_2 is a Mott insulator. Recently Yu et al [60] by X-ray absorption spectroscopy have demonstrated that it is a f-f Mott Hubbard insulator.

Approaches to describe the electronic structure of strongly correlated systems include DFT+U formalism, dynamical mean field theory (DMFT), self-interaction correction (SIC) and hybrid functionals, which are described in chapter 1. Hybrid functionals [16], DMFT [17] and DFT+U based [18–20] studies, which are reported in literature, have been able to predict the anti-ferromagnetic insulating ground state of UO_2. These studies have shown that including the strong correlation is a must for reproducing the insulating state of UO_2, but there are no studies on the effect of incorporation of strong electron correlations on the other properties like phonons and thermal properties. The aim in the present study is to systematically obtain the structure, electronic and mechanical properties for the insulating ground state of UO_2 and then compute the thermal properties from the first principles calculations. We have used the DFT+U technique as hybrid functionals, DMFT and SIC techniques are computationally very expensive.

Further, the influence of U_{eff} on the band gap, equilibrium volume, magnetic moment and bulk modulus are also studied. The anti-ferromagnetic insulating ground state obtained from these studies is subsequently used to calculate the thermal properties through the computation of the phonon spectrum in the harmonic approximation using the DFPT [13, 113] in conjunction with DFT. The anharmonicity is then indirectly incorporated through the volume dependence of phonon frequencies using QHA. Non analytic term correction for the macroscopic electric field associated with the longitudinal optic modes in insulating UO_2 is also applied. The role of strong correlation on the phonon spectrum, bulk modulus and thermal expansion is studied. Further the effect of spin orbit coupling on the above mentioned properties is also investigated.

3.2 Computational details

In order to perform the computations, we have used the fluorite structure of UO_2 whose space group is $Fm\bar{3}m$ (#225). In order to account for the strong correlations of the 5f electrons of uranium atom, the on-site Coulomb repulsion is incorporated using the rotationally invariant DFT + U approach of Dudarev et al [18, 19]. The calculations were done for different values of the Hubbard parameter U_{eff} ranging from 0 to 7 eV and the value of 4 eV is found to reproduce the band gap of 2 eV [61] in this system. UO_2 is known to undergo a magnetic transition from the anti-ferromagnetic state to the paramagnetic state at 30.8 K [61]. The temperature range of interest for thermal property calculation is above this temperature. Thus, the paramagnetic phase should be used for thermal properties calculation. Meaningfully simulating a paramagnetic system having magnetic moments oriented in random directions, requires a large cell and hence is computationally very expensive. An alternative way is to do non-spin-polarized calculations. However, the spin polarization is necessary for incorporating on-site Coulomb repulsion within the DFT + U formalism. We have used an anti ferromagnetic tetragonal cell having two U atoms: $(\frac{1}{\sqrt{2}} \times \frac{1}{\sqrt{2}} \times 1)$ of the conventional cubic unit cell, as shown in figure 3.1.

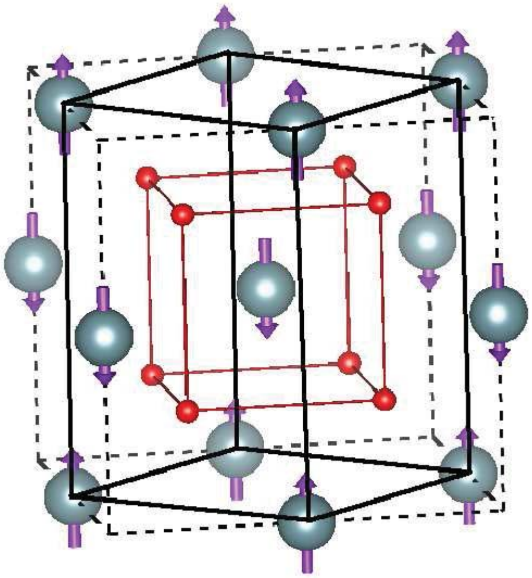

Figure 3.1 – Antiferromagnetic tetragonal unit cell of UO_2. The larger grey spheres are uranium atoms and the smaller red ones are oxygen atoms. The arrows indicate the directions of the magnetic moments.

The calculations were carried out using the Vienna Ab-initio Simulation Package (VASP) [81, 82, 114] which is a plane wave pseudopotential implementation of DFT. The interaction between the valence electrons and the ionic core is described by projector augmented wave (PAW) based pseudo-potential [115, 116]. For the exchange-correlation functional, GGA as parametrized by Perdew, Burke and Ernzerhof (PBE)

[88] is used. Fully relativistic calculations were done to incorporate the effect of spin-orbit (SO) coupling. A Monkhorst–Pack (MP) k-point mesh of (8 × 8 × 6) for sampling the Brillouin zone (BZ) and a plane wave cut-off energy of 450 eV are found to render the energy convergence better than 1 meV/atom. The structure optimization was carried out for a fixed volume with relaxation of the atomic positions until the forces on each ion is less than 0.001 eV/Å. The calculations were repeated for several volumes to obtain the total energies at different values of the cell volume. The equilibrium volume and the bulk modulus of UO_2 were obtained using a fit with 3^{rd} order Birch-Murnaghan equation of state [103].

In order to compute the thermal properties, the force constant matrix was calculated using DFPT as implemented in VASP. The dynamical matrix is then obtained from the force constant matrix in the standard way [117, 118] and the eigenvalues of the dynamical matrix correspond to the square of the phonon frequencies. The calculations were performed for a (2 × 2 × 2) 48 atom supercell consisting of eight primitive cells with a (4 × 4 × 3) **k**-point sampling of the Brillouin zone. The Phonopy package [119] was used to extract the necessary data from the VASP calculations to set up the dynamical matrix and to obtain the phonon spectra. Fourier interpolation is done to get the dynamical matrix on a fine (31 × 31 × 31) **k**-point mesh. The phonon spectra were calculated for various volumes around the equilibrium volume at zero Kelvin from which the temperature and the volume dependent free energy were computed. Minimizing the free energy with respect to volume at different temperatures gives the equilibrium volume at different temperatures. Thermal expansion, bulk modulus and specific heat were calculated as explained in Chapter 2.

3.3 Results and Discussion

3.3.1 Ground state properties

Ground state properties were first calculated with GGA approach for both ferromagnetic (FM) and anti-ferromagnetic (AFM) ordering in the system. The total energy is computed for different volumes and fitted to the Birch-Murnaghan equation of state to get the equilibrium volume, energy and bulk modulus. Ferromagnetic state is found to be energetically most stable.

Type of calculation	Energy (eV)	a(Å)	B (GPa)	B'	Magnetic moment (μ_B)
FM	-31.059	5.423	198.7	4.39	1.99
AFM	-30.882	5.411	179.0	4.06	1.52
FM+SO	-34.045	5.433	185.4	5.43	1.56
AFM+SO	-34.001	5.425	181.4	4.13	0.94
Expt.		5.47 [120]	207 [121]		1.8 [122]

Table 3.1 – Equation of state fitting for ferromagnetic and anti-ferromagnetic ordering with and without including spin-orbit (SO) coupling using GGA calculations compared with experimental data.

The equilibrium lattice parameters turn out to be 5.423 Å and 5.411 Å for the ferromagnetic and anti-ferromagnetic states. Comparing with the experimental lattice parameter of 5.47 Å [120] , the calculated values lattice parameters are underestimated by 0.8% and 1.0% for ferromagnetic and anti-ferromagnetic states respectively. Other ground state properties are given in table 3.1 along with the corresponding available experimental results. For both the ferromagnetic and anti-ferromagnetic states, even though the lattice parameter is under predicted, bulk modulus is also under predicted which is contradictory to the general argument of over binding or under binding of a system where under prediction of lattice parameter corresponds to overestimation of the bulk modulus and over prediction of lattice parameter corresponds to under-

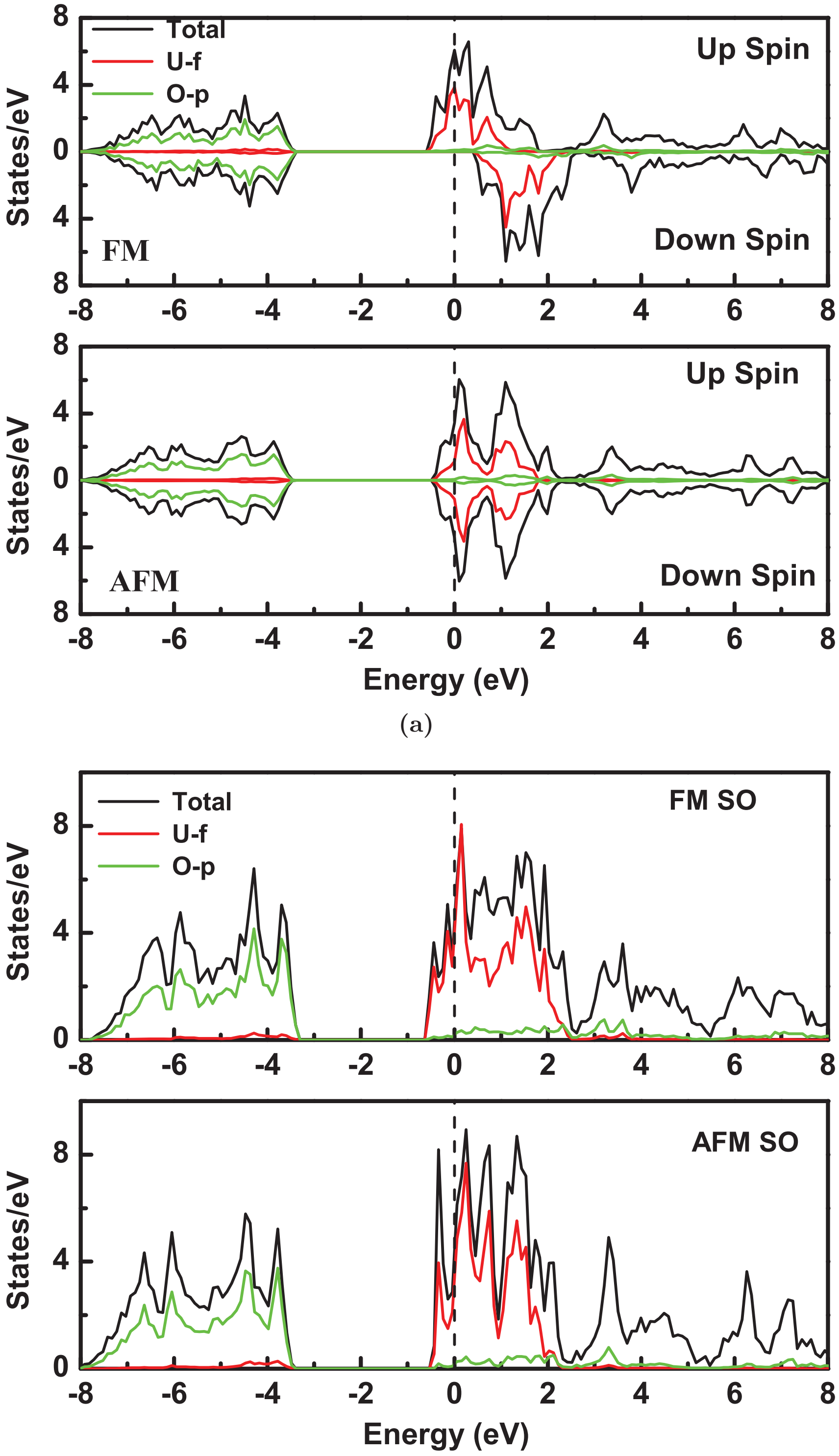

(a)

(b)

Figure 3.2 – Electronic Density of states for ferromagnetic (FM) and anti-ferromagnetic (AFM) ordering (a) without SO coupling and (b) with SO coupling. Different colours denote different orbitals, Black: total density of states; Green: oxygen p orbitals (O-p) and Red: uranium f orbitals (U-f). Fermi level in each case is represented by vertical dashed line.

estimation of bulk modulus. The magnetic moments obtained are respectively 1.99 μ_B and 1.52 μ_B for ferromagnetic and anti-ferromagnetic states, which are above and below the experimental magnetic moment of 1.8 μ_B [122]. With the inclusion of spin-orbit coupling, magnetic moment is found to decrease from 1.99 μ_B to 1.56 μ_B for ferromagnetic state and from 1.52 μ_B to 0.94 μ_B for anti-ferromagnetic state. As can be seen from table 3.1 bulk modulus also decreases with the inclusion of SO coupling in both the ferromagnetic and anti-ferromagnetic states. Further the electron density of states for both the ferromagnetic and anti-ferromagnetic states (as plotted in figure 3.2) shows both to be metallic with partially filled f band of uranium lying on the Fermi level. The density of states at Fermi level is mostly from uranium f orbitals with marginal contribution from oxygen p orbitals. Anti-ferromagnetic state with SO coupling shows a dip in density of states at Fermi level but it remains metallic.

GGA based calculations have given a ferromagnetic metallic state as the ground state of UO_2 which is contradictory to the experimentally known fact of it being an insulator with anti-ferromagnetic alignment below the Neel's temperature of 30.8 K [61]. From the electron density of states plot, we can see that the partially filled uranium f bands lie on the Fermi level. These are sharp bands so the electron correlations are known to be strong among the electron in these bands. DFT is not able to describe these strong correlations properly because of the approximate exchange correlation functionals used in the calculations. The DFT+U method can incorporate the effect of these strong correlations by using Hubbard on-site repulsion.

3.3.2 DFT+U and Band Gap

DFT+U method is used to describe the strong on-site Coulomb correlations in 5f electrons of U atom. As the exchange-correlation functional used is GGA, the DFT+U calculations in the present study are referred as GGA+U. Effect of the incorporation of Coulomb correlations on electron density of states can be seen in figure 3.3. The states near to Fermi level start splitting as U_{eff} is increased and at U_{eff} of 2 eV we can see a gap appears at the Fermi level and the system is no more a metal. As U_{eff} is increased above 2 eV, the gap at the Fermi level also increases and reaches a value of approximately 2 eV for U_{eff} of 4 eV. Based on the band gap values, U_{eff} is chosen to be 4 eV and all further calculations were done using $U_{\text{eff}} = 4$ eV.

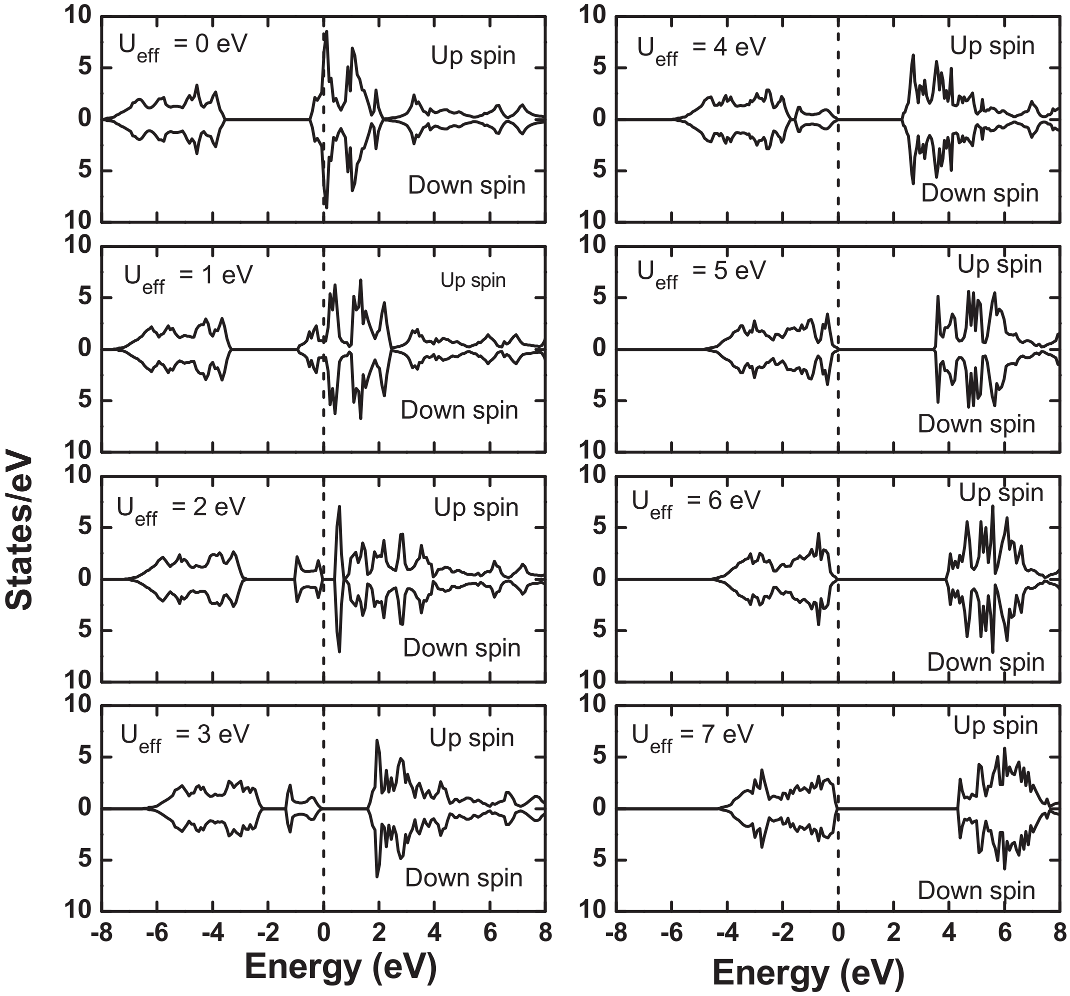

Figure 3.3 – Electronic density of states of anti-ferromagnetic state for different values of U_{eff}. Fermi level in each case is represented by vertical dashed line. States near to Fermi level start splitting as U_{eff} is increased and at U_{eff} of 2 eV a gap appears at the Fermi level and system is no more a metal.

U_{eff}	Energy (eV)	$'a'$(Å)	B (GPa)	B'	Magnetic moment (μ_B)	Band Gap (eV)
0.0	-30.880	5.4114	187.0	4.01	1.51	0.0
1.0	-30.185	5.4953	186.52	4.04	1.82	0.0
2.0	-29.812	5.5185	189.65	4.00	1.97	0.4
3.0	-29.490	5.5356	191.47	4.32	2.00	1.2
4.0	-29.206	5.5500	192.03	4.31	2.00	2.0
5.0	-28.953	5.5620	192.33	4.29	2.01	3.4
6.0	-28.728	5.5742	192.46	4.28	2.04	3.9
7.0	-28.526	5.5846	192.43	4.26	2.05	4.3

Table 3.2 – Variation of equation of state parameters obtained from the Birch-Murnaghan state fit, magnetic moment and band gap with U_{eff}. Band gap appears and increases with increase in U_{eff} whereas bulk modulus shows initial increase followed by almost saturation above 4 eV. Lattice constant first increases sharply and then slowly with U_{eff}.

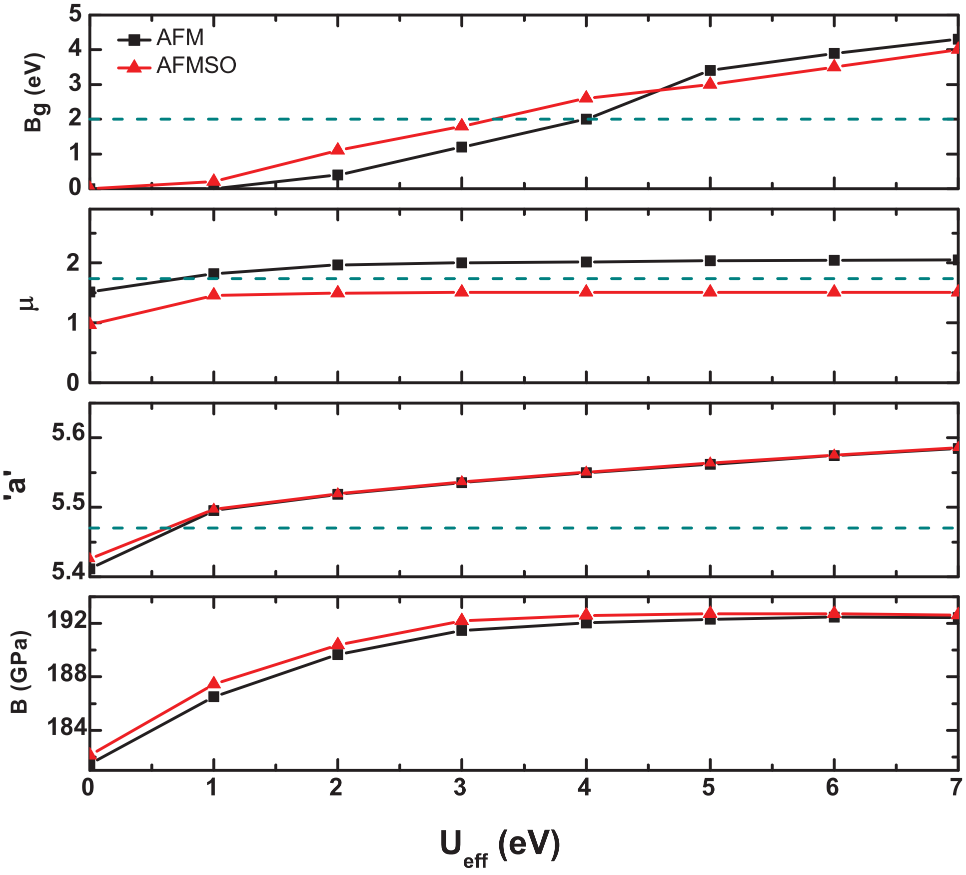

Figure 3.4 – Variation of band gap (B_g), magnetic moment (μ), lattice parameter (a) and bulk modulus (B) with U_{eff} for AFM ordering with and without including SO coupling. Horizontal dash line shows the experimental values of corresponding physical quantities. There is almost negligible effect of SO coupling on bulk modulus and lattice parameter. Magnetic moment deceases with inclusion of SO coupling. Band gap also shows a slight increase for a range of U_{eff} values.

Lattice parameter and bulk modulus obtained by fitting the 3rd order Birch-Murnaghan equation of state fitting for the anti-ferromagnetically ordered system for different values of U_{eff} are given in table 3.2. It can be seen that equilibrium energy increases with increase in U_{eff} and there is also an expansion in equilibrium lattice parameter. Bulk modulus initially increase with increase in U_{eff} and then almost saturates above a value of 4 eV for U_{eff} . The magnetic moment saturates above a value of 3 eV for U_{eff} . Variations of lattice parameter 'a', bulk modulus, band gap and magnetic moment with U_{eff} are shown in figure 3.4 along with the effect of SO coupling.

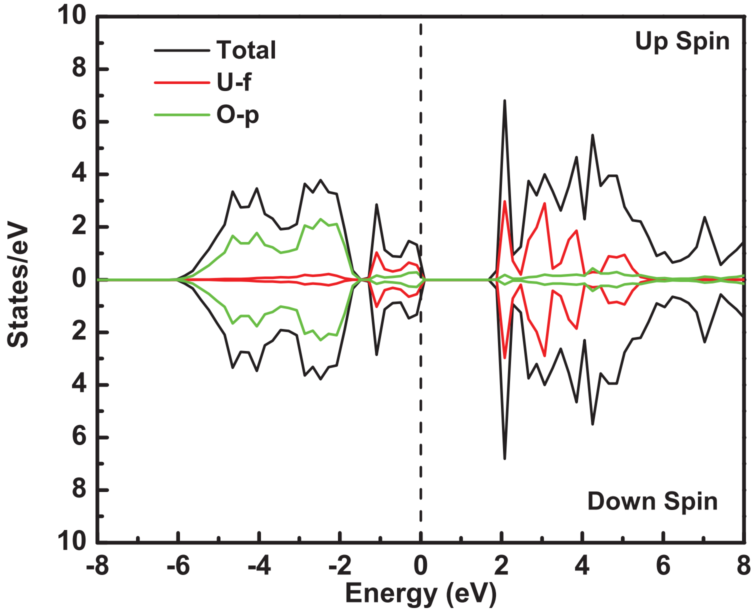

Figure 3.5 – Projected electron density of states from GGA+U calculations. (Up spin is plotted along positive Y-axis and down spin is plotted along negative Y-axis.) There is small overlap between uranium f states and oxygen p states showing small hybridization between these states but the band gap is predominantly between uranium f bands with a very small contribution from oxygen p bands establishing the Mott-Hubbard insulating behaviour.

The calculations are also carried out by including spin-orbit (SO) coupling for different values of U_{eff} and the values are plotted in figure 3.4 along with the results of without SO coupling. It can be seen from the figure 3.4 that there is negligibly small effect of SO coupling on bulk modulus and lattice parameter. Whereas the saturated magnetic

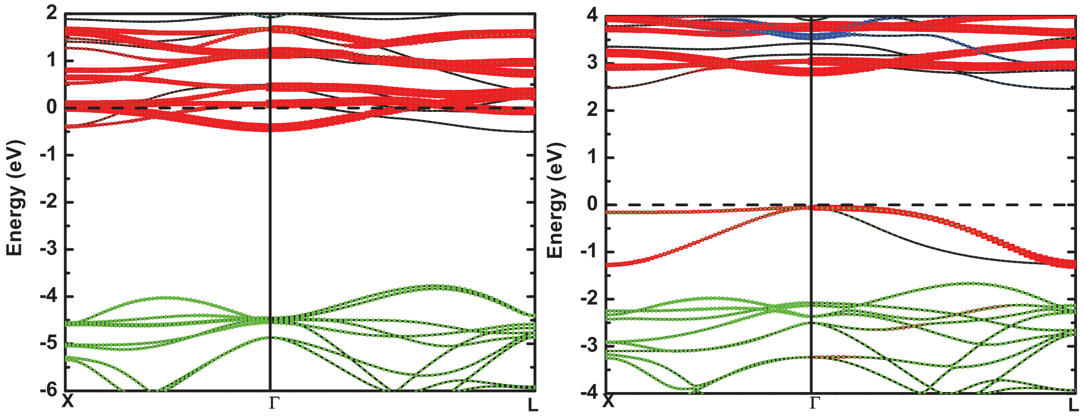

(a) **(b)**

Figure 3.6 – Electronic band structure of UO_2 calculated using GGA and GGA+U. Fermi level is shown by black dashed horizontal line corresponding to zero energy in Y axis. Different colours represents projected bands, red: uranium f bands, blue: uranium d bands and green: oxygen p bands.

moment decreases from 1.99 μ_B (when SO coupling is not included) to 1.51 μ_B (when SO coupling is included). SO coupling has given a little higher value of band gap for the energies of U_{eff} from 2 eV to 4eV.

3.3.3 Projected electron density of states and band structure

Projected electronic density of states for GGA+U calculations ($U_{eff} = 4$ eV) with anti-ferromagnetic ordering is plotted in figure 3.5. A band gap can be clearly seen between the filled states below Fermi level and empty states above Fermi level. Projected density of states shows the split of filled and empty uranium f-orbitals. There is a small overlap between uranium f bands and oxygen p bands showing small hybridization between these bands. The band gap is predominantly between uranium f bands with a very small contribution from oxygen p bands verifying the Mott-Hubbard insulating behaviour of UO_2[123].

Band structure calculated using GGA and GGA+U is plotted in figure 3.6. Different colours represent the contribution from different orbitals. At the Fermi level, in GGA calculated band structure, mainly uranium f-orbitals are present. With GGA+U the uranium f orbitals split and a gap appears in the band structure. Filled uranium f-bands shifts down in energy with Fermi level lying just above them.

3.3.4 Phonon dispersion

Phonon dispersion of UO_2 calculated using GGA and GGA+U are plotted in figure 3.7 along with experimental data available from neutron scattering experiments [124]. Phonon dispersion consists of 9 modes (3 acoustic and 6 optic modes) corresponding to 3 atoms in the primitive cell. In three acoustic modes (one LA and two TA) one U and two O atoms in primitive cell vibrates in phase having zero frequency corresponding to gamma point. Next three modes around 8 THz (one LO1 and two TO1) corresponds to U and O atoms moving out of phase with respect to each other. Three remaining modes around 14 THz (one LO2 and two TO2) corresponds to predominantly two O atoms only which vibrate out of phase with respect to each other. These designations are given according to vibration near gamma point.

As can be seen from figure 3.7, the phonon dispersion calculated using GGA fails to reproduce the highest optical mode observed in experimental measurements whereas the phonon dispersion calculated using GGA+U shows a good agreement with the experimental values except for the highest optical mode near gamma point. UO_2 being an ionic insulator, the longitudinal optical (LO) mode should be affected by the macroscopic electric field associated with that mode which is absent in supercell based approaches. But this effect can be incorporated using a non-analytical term correction to the dynamical matrix that involve Born effective charges of constituent atoms [101, 102]. The Born effective charges calculated using VASP with GGA+U are 5.56 and -2.78 for U and O atoms respectively. Incorporating the non analytical term

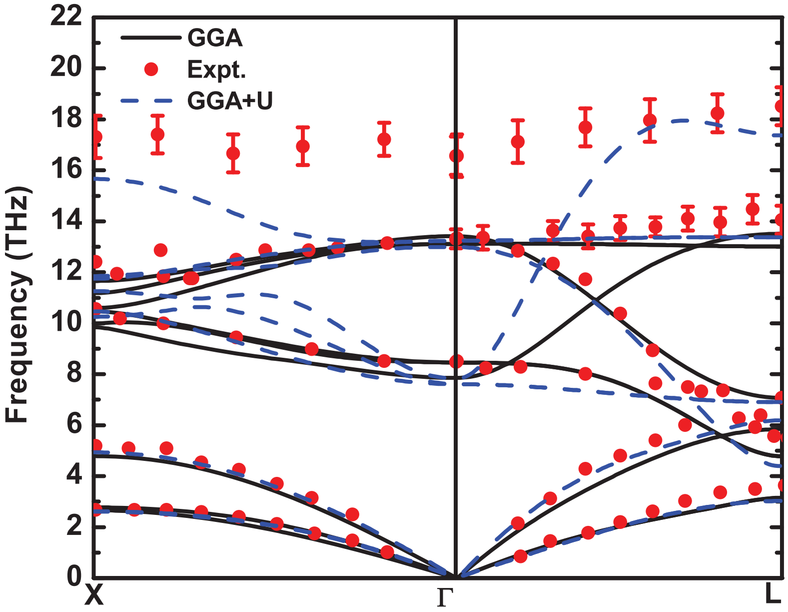

Figure 3.7 – Phonon spectrum of UO_2 calculated using GGA and GGA+U methods. Experimental data available from neutron scattering [124] are also shown.

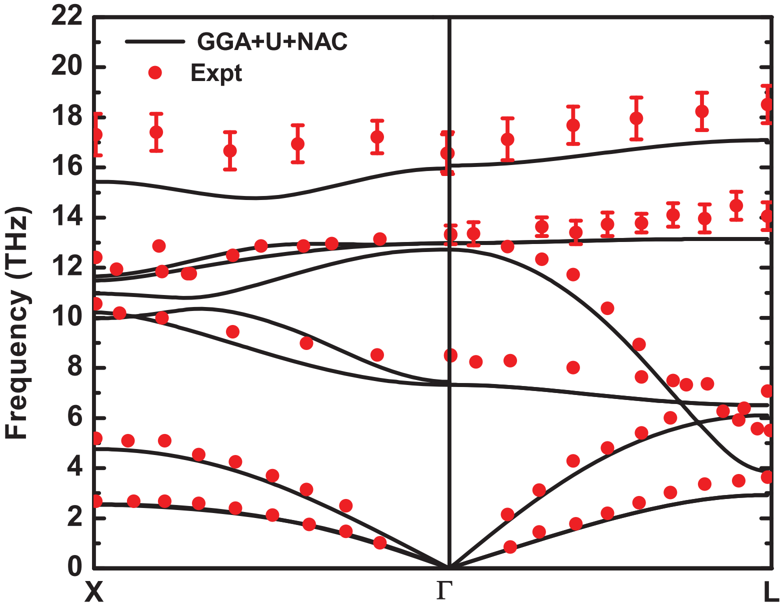

Figure 3.8 – Phonon dispersion calculated using GGA+U with non analytic term correction. Experimental data is from neutron scattering experiments [124]. Applying non analytic term correction has resulted in splitting of the highest frequency modes at gamma point, which has resulted in better matching with the experimental data.

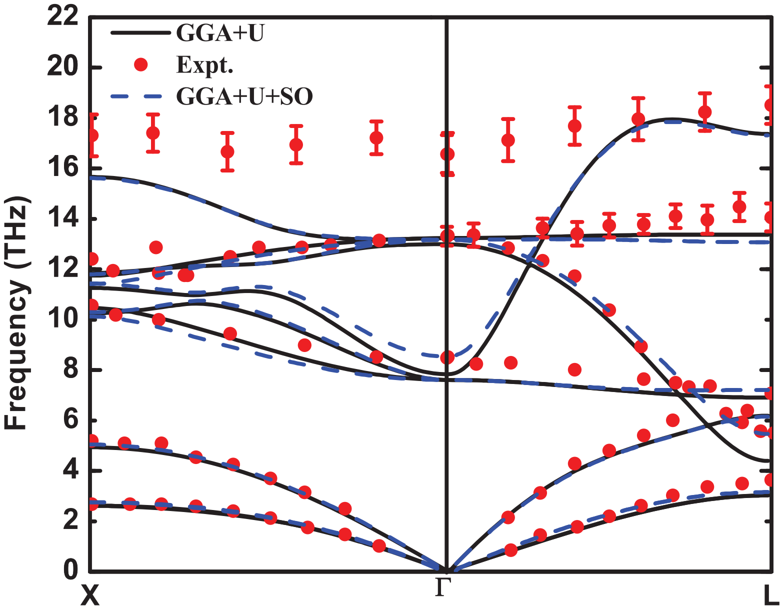

Figure 3.9 – Phonon dispersion calculated using GGA+U with and without the incorporation of SO coupling. Experimental data is from neutron scattering experiments [124].

correction to dynamical matrix has lifted the discrepancy for the highest frequency mode near gamma point which can be seen in figure 3.8. The highest LO mode in the phonon dispersion calculated using GGA+U with non analytical term correction is close to experimental values, however still lying below experimental values. Also there is small discrepancy at gamma point around 8 THz frequency and near L point for frequencies around 6 THz. However, the overall agreement with the experimental data on the whole is quite good.

In order to further understand the effect of spin-orbit coupling on the phonons, we have calculated the phonon dispersion using the fully relativistic non collinear calculations. Figure 3.9 shows the phonon dispersion corresponding to GGA+U calculations for both the cases with and without incorporation of SO coupling. It can be seen that incorporation of SO coupling has weak effect on the middle frequency modes which involves movement of both O and U atoms and has marginally improved the agreement with the experiments. But because of the difficulty in calculating the Born effective charges with SO coupling, non analytical term correction is not applied for calculations with SO coupling. Further the fully relativistic calculations which incorporate SO coupling are computationally very demanding. The phonon dispersion obtained with GGA+U and non-analytical term correction is in reasonable agreement with the experimental data. The GGA+U results are then used for further calculations of the thermal properties without including SO coupling.

3.3.5 Calculations of the thermal properties

Effect of temperature on the phonon spectrum is included using quasi harmonic approximation. The phonon spectra are calculated for various values of volume around the equilibrium volume and the Helmholtz free energy F(V,T) is computed for these volumes at different temperatures from 0 K to 1000 K. Figure 3.10 shows the Helmholtz free energy as a function of volume for various temperatures as calculated using GGA and GGA+U. The equilibrium volume, bulk modulus and Gibbs free energy are obtained as a function of the temperature by fitting the F(V,T) vs V data for various temperatures to Birch-Murnaghan equation of state. Using the temperature dependant volume data, the thermal expansion coefficient is calculated as explained in chapter 2. The computed bulk modulus and thermal expansion as a function of temperature for both the GGA and GGA+U are plotted in figure 3.11.

The computed thermal expansion coefficient is over predicted for both GGA and GGA+U with respect to experimental values [125] and bulk modulus is under predicted with respect to experimental data [121]. The over prediction of thermal expansion coefficient and under prediction of bulk modulus within the GGA+U can be seen as a consequence of the over prediction of the equilibrium lattice parameter by

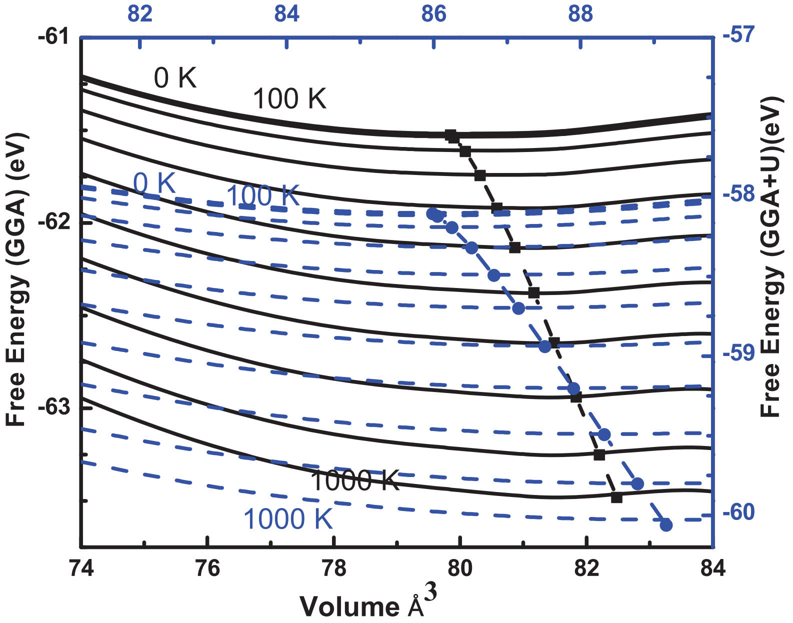

Figure 3.10 – Equation of state fit at different temperatures (0 K to 1000 K) for GGA and GGA+U. Solid black line represents free energy for GGA whereas dashed blue line represents free energy for GGA+U. The black square marks represent the equilibrium volume at different temperatures for GGA and the blue spheres represent the equilibrium volume for different temperatures for GGA+U.

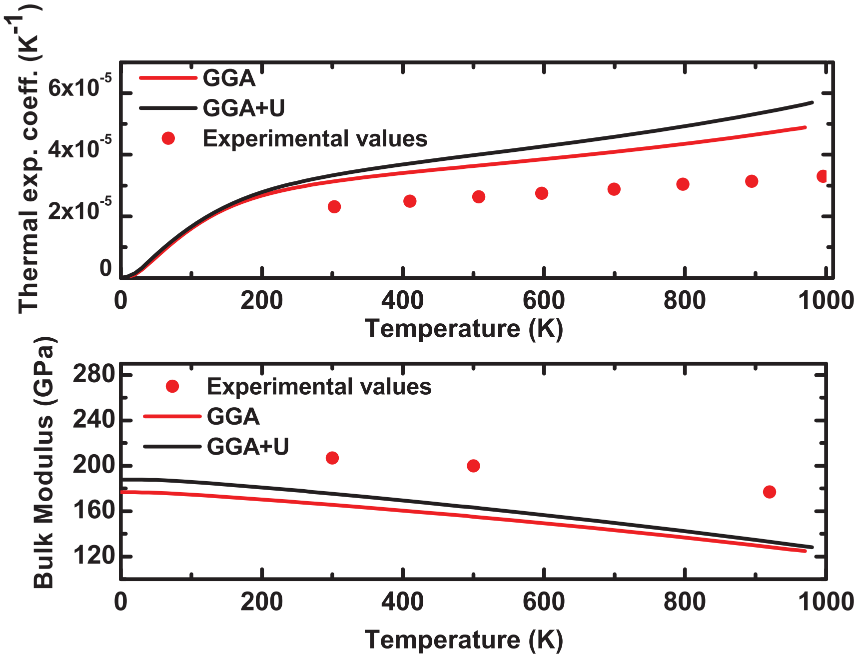

Figure 3.11 – Thermal expansion coefficient and bulk modulus calculated using GGA (red curve) and GGA + U (black curve) ; The filled red circles are experimental data [121, 125].

GGA+U, on the other hand, the GGA is already found to under predict the equilibrium lattice parameter. So the over prediction of thermal expansion coefficient in case of GGA can not be simply related to under prediction of lattice parameter. The discrepancies in bulk modulus and thermal expansion coefficient obtained using the GGA+U can be ascribed to the over-prediction of the lattice parameter and under-prediction of the bulk modulus in the ground state. A non local exchange-correlation pressure correction was applied to correct the over prediction of lattice parameter and under-prediction of the bulk modulus in the ground state for the calculations using GGA+U and its effects on other properties with respect to the temperature is explained in the next section.

3.3.5.1 Non local exchange-correlation pressure correction

The huge discrepancies in bulk modulus and thermal expansion coefficient in GGA+U were removed by applying a uniform pressure of 7 GPa on the system to bring both lattice parameter and bulk modulus of the ground state close to experimental values. This correction helps in reducing both the discrepancies of over prediction of thermal expansion coefficient and under prediction of bulk modulus drastically. This uniform pressure applied to correct for the shortcomings of the approximations used for the generation of the exchange correlation functional is named as non-local exchange correlation pressure correction by Van de Walle and Ceder [126] who explored the applicability of the non local exchange correlation pressure correction to calculate the ground state of transition metals and their alloys. They computed the values of the exchange correlation pressure correction by calculating the pressure of the system at the equilibrium volume. It should be mentioned that there exist no ab-initio prescription to calculate the value of this correction pressure for the cases where experimental data are not available. For our computations it is found that an exchange correlation pressure correction of 7 GPa gives both bulk modulus and thermal expansion coefficient very close to experimental values over the entire range of temperature for which we have done the calculations and they are discussed below. The Birch-Murnaghan equation of state at different temperatures for the GGA+U with pressure correction is given in figure 3.12 along with that of without pressure correction. The calculated thermal expansion coefficient and bulk modulus obtained using GGA+U for both the cases of with and without pressure correction are plotted in figure 3.13. It can be seen from the figure that the pressure correction of 7 GPa has resulted in the correction of both the over prediction of thermal expansion coefficient as well as the under prediction of bulk modulus and a very good agreement of these quantities with the corresponding experimental data is also obtained. Further the effect of this non local exchange-correlation pressure correction on phonons and specific heat is also studied. The effect of this non local pressure correction on phonon dispersion can be seen from figure 3.14 There is a slight hardening of the optic modes after applying the pressure correction. The discrepancies of the phonon dispersion obtained from GGA+U calculations at gamma point around 8 THz and at L point around 6 THz which were pointed out earlier in section 3.3.4 are also almost removed by applying the pressure correction giving a very good agreement with the experimental data.

The computed phonon contribution to the specific heat at constant volume is plotted in figure 3.15. Both the results obtained with and without pressure correction lie close by. It may appear in the first glance that the specific heat computed without pressure correction is closer to the experimental data [127]. However it has to be remembered that the experimentally measured specific heat also has the electronic contribution

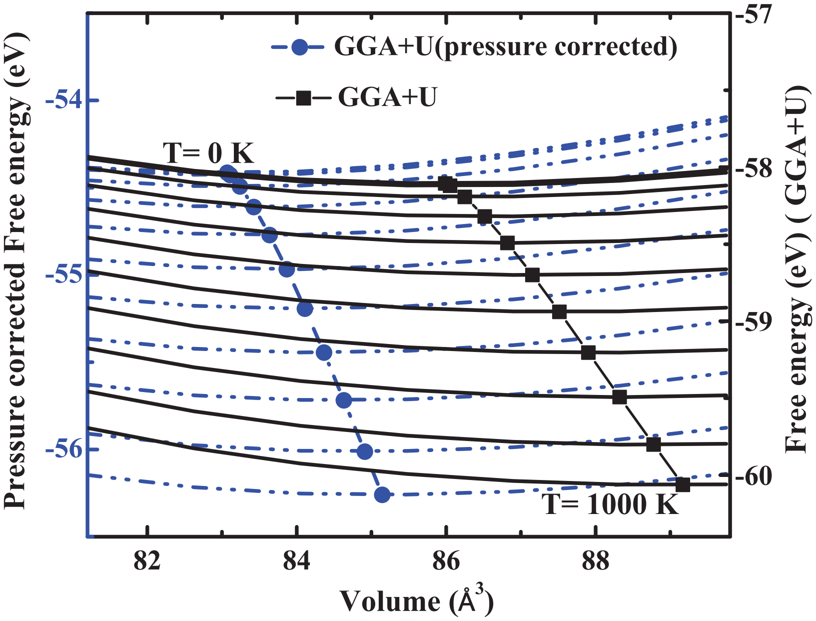

Figure 3.12 – Equation of state fit at different temperatures (0 K to 1000 K) for GGA+U with and without pressure correction. Solid black line represents the free energy for GGA+U whereas dashed blue line represents the free energy for GGA+U with pressure correction. The black square marks represent the equilibrium volume at different temperatures for GGA+U and the blue spheres represent the equilibrium volume for different temperatures for GGA+U with pressure correction.

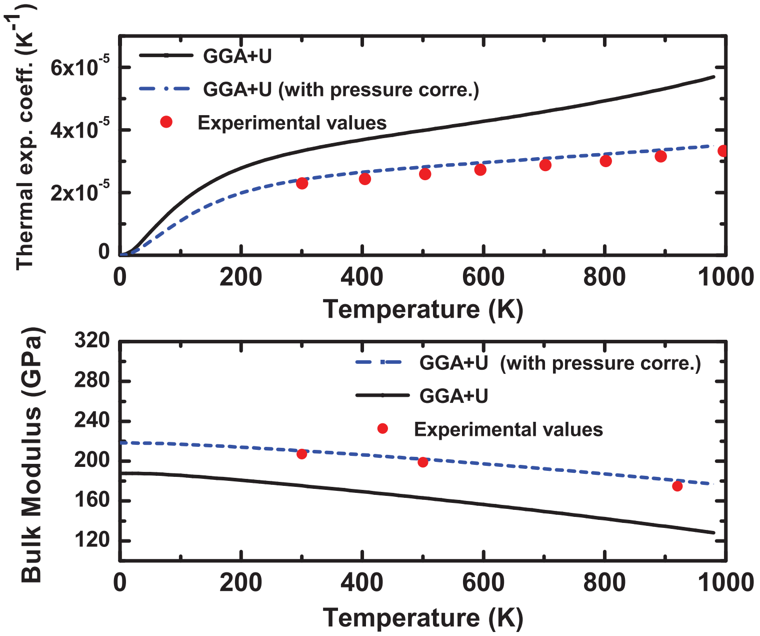

Figure 3.13 – Thermal expansion coefficient and bulk modulus calculated using the GGA + U formalism with and without pressure correction along with available experimental data [121, 125].

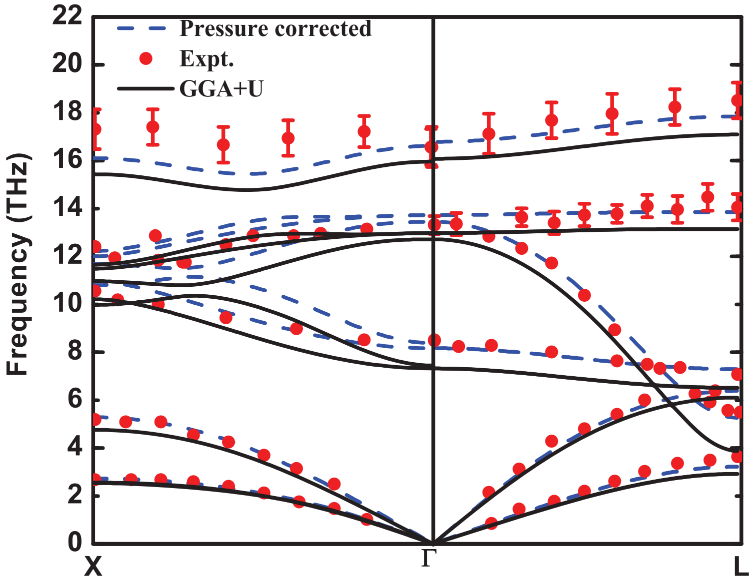

Figure 3.14 – Calculated phonon dispersion with GGA+U formalism including non-analytical term correction for LO mode with (dashed blue line) and without pressure correction (solid black line) and filled red circles are experimental data at room temperature [124].

and contribution due to defects etc. If all the contributions to the specific heat are also taken into account it can lead to a better understanding of the pressure corrected phonon contribution to the specific heat.

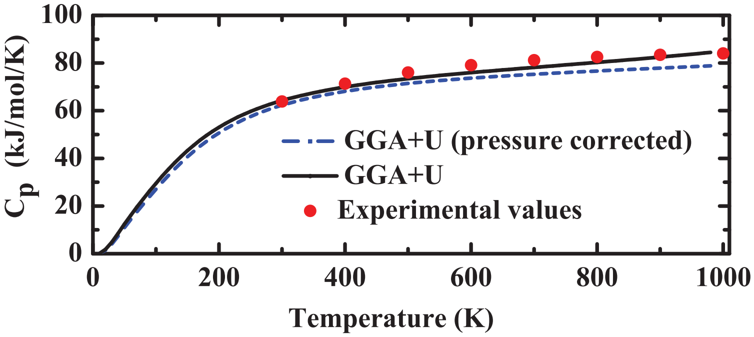

Figure 3.15 – Calculated specific heat with and without pressure correction along with experimental data [127].

3.4 Summary

In this chapter the reproduction of the antiferromagnetic insulating ground state of UO_2 within DFT+U formalism, to account for the strong Coulomb correlations in uranium 5f electrons, is discussed. The effect of these strong correlations in other structural and thermal properties like bulk modulus, phonon, elastic constant, thermal expansion coefficient are computed and the results obtained are compared with experiments.

- DFT calculations with GGA gives a ferromagnetic metallic state whereas the GGA+U calculations with a Hubbard parameter U_{eff} of 4 eV reproduces the correct Mott-insulating anti-ferromagnetic ground state of UO_2.

- The phonon dispersion is well described by GGA+U with a non-analytical term correction to the dynamical matrix, where as GGA fails to do so, corroborating the effect of strong Coulomb correlations on the phonon dispersion.

- The calculated thermal properties (bulk modulus and thermal expansion) using both GGA and GGA+U shows a significant discrepancy with the corresponding experimental data. These discrepancies are systematically corrected in case of GGA+U by applying a non local exchange correlation pressure correction of 7 GPa.

- The correction of over predicted equilibrium lattice parameter in GGA+U calculations, by non local exchange correlation pressure correction, also improved the agreement of calculated phonon dispersion with the corresponding experimental data.

Chapter 4

Structural stability and disorder in UZr_2

This chapter presents the studies on the electronic structure, elastic and dynamical properties of UZr_2 *. The role played by site occupancy disorder in providing the dynamical stability is discussed in this chapter.*

4.1 Introduction

U-Zr based metallic fuel are material for future fast reactors. They have better thermal conductivity and higher fissile atom density. Their harder neutron spectrum combined with higher density gives higher breeding ratio [69]. In the optimally designed alloy composition, Zr content varies from 6 to 10 percent [70]. Uranium with 6-10% zirconium at normal temperature and pressure conditions have an orthorhombic structure but in reactor conditions of high temperature, pressure and irradiation, the U-Zr alloy fuel has different phases in different region of fuel pin, central high temperature region in bcc phase and peripheral lower temperature zone is a mixture of orthorhombic phase and delta phase. Delta phase usually represented as $\delta - UZr_2$ or simply UZr_2 has a hexagonal structure with the stoichiometry range varying over

Zr concentration [70].

The crystal structure and stability of the $\delta - UZr_2$ phase have been studied by Akabori et al using electron probe microanalysis, X-ray diffraction and differential thermal analysis [45, 46]. This study establishes that the $\delta - UZr_2$ phase forms below 885 K in a modified AlB_2-type structure with a homogeneity range of 63 to 82 at.% Zr. Landa et al have computed the formation enthalpy of the bcc (U, Zr) and $\delta - UZr_2$ phases, estimated the decomposition temperature of the γ-(U, Zr) and established the partial ordering in $\delta - UZr_2$ using Korringa-Kohn-Rostoker (KKR), exact muffin-tin orbital (EMTO) and full potential linear muffin-tin orbital (FPLMTO) methods of density functional theory (DFT) calculations [72, 73]. Recently, Xiong et al have reviewed the thermodynamic modelling of the U-Zr system assessing the existing phase stability data combined with fresh first principles thermochemical calculations [128]. Xie et al have examined the effects of electron correlation and relativity on the ground state properties of all the known solid phases of the U-Zr system using projector augmented wave (PAW) method of DFT calculations [29]. They have shown that computed f-electron bands of uranium using the DFT+U technique results in better agreement with the ultraviolet photo emission spectroscopy (UPS) measurement than conventional PAW+PBE method. Based on the calculations of the formation energy they have suggested to use DFT+U technique for UZr_2 . But the formation energy calculations involve different phases and the parameter U_{eff} in DFT+U particularly depends on the bonding environment and is different for the same atom in different compounds. Considering this fact, the formation energy calculation using same U_{eff} in different environment of reference phase is not reliable. Further, Soderlind et al [129] have also shown that how DFT+U is not suitable for uranium as it artificially induces magnetism in bcc uranium and the improvement in the description of alpha uranium with DFT+U is a consequence of the volume increase which was under predicted by DFT. Soderlind et al [129] find that DFT+U is inappropriate for uranium and U-Zr alloys and suggested the inconsistencies in using DFT+U for other metallic actinide fuel systems.

Ab initio calculations of phonon spectrum and thermal properties such as specific heat and thermal expansion coefficients are not found in the literature. Further, the role of disorder in site occupancy as observed experimentally [46] has not been addressed in the literature. This chapter discuses the electronic structure, bonding and stability of UZr_2 . DFT based calculations were performed taking into account the recommendations suggested by Soderlind et al [129]. The phonon dispersion and dynamical stability for both ordered and partially ordered structures are presented. Role played by site disorder in stability of the structure is discussed. The thermal properties such as specific heat, thermal expansion and bulk modulus are also calculated as a function of temperature.

4.2 Computational details

UZr_2 has a modified AlB_2-type structure with space group P6/mmm (#191) [46] where zirconium atoms occupying the Al sites and B sites are randomly occupied by uranium and zirconium atoms. The disorder in the B sites are represented with Special Quasi Random structures (SQSs) generated using the Monte Carlo generator of special quasi random structure method [130] implemented in Alloy Theoretic Automated Toolkit (ATAT) [131].

The calculations are performed using the Vienna ab-initio Simulation Package (VASP)

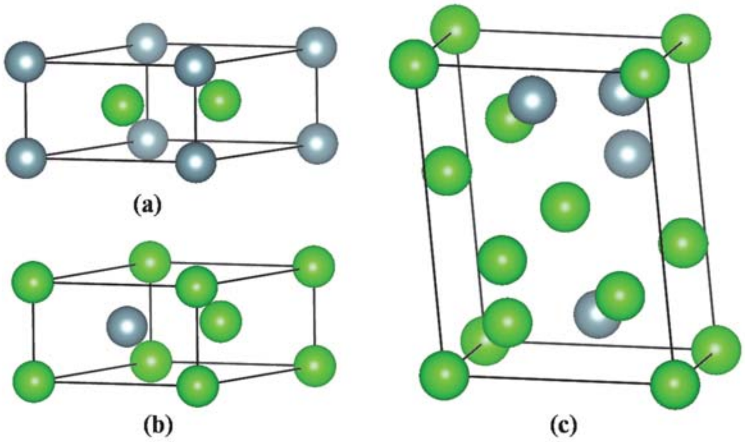

Figure 4.1 – Unit cells for different structures of UZr_2. (a) Ideal AlB_2 type, (b) Modified AlB_2 type and (c) Special quasi random structure. (Green balls represent Zr and grey balls represent U)

[81, 82, 114]. Interaction between the valence electrons and the ionic core is described by Projector Augmented Wave (PAW) based pseudopotentials [115, 116]. The pseudopotentials used for U and Zr treat $6s^2 6p^6 7s^2 5f^3 6d^1$ and $4s^2 4p^6 5s^2 4d^2$ respectively as valence electrons. Generalized gradient approximation as parametrized by Perdew, Burke and Ernzerhof (PBE) [88] is used for exchange correlation functional. A plane wave energy cut-off of 450 eV and Brillouin zone sampling using a 9×9×15 gamma centred mesh are used to ensure a convergence of better than 1 meV/atom in the energies. Structural relaxation is carried out by allowing the cell shape and ionic positions to relax so that the force on each ion becomes less than 0.001 eV/Å. Calculations are done for several values of volumes which were fitted to Birch-Murnaghan equation of state [103] to obtain equilibrium volume , bulk modulus and pressure derivative of bulk modulus. All the calculations are scalar relativistic and non spin polarized. For comparison some fully relativistic calculations are done including both spin polarization and spin-orbit coupling. The incorporation of spin orbit (SO) coupling in fully relativistic calculations have shown no effect on the relative energetics of different structures. SO coupling has a very small effect on volume and bulk modulus and no magnetic moment appear on U and Zr atoms. Hence the non magnetic calculations are done for all studies ignoring the effect of SO coupling except for the cases where it is mentioned.

To compute the elastic constants VASP implementation of the finite difference combined with symmetry general least-square method [106] is used. Phonon dispersion is calculated using Density Functional Perturbation Theory (DFPT) [13, 113] as implemented in VASP using a 81 atom (3×3×3 of unit cell) supercell for ordered structure. The Phonopy package [119] is used to extract the necessary data from VASP calculations to set up the Dynamical matrix and then calculate the phonon spectra. Fourier interpolation is done to get the dynamical matrix on a fine grid of 21×21×21 **k**-point mesh.

Structure	Volume ($\mathring{A}^3$/atom)	Energy (eV/UZr_2)	Bulk Modulus (GPa)	Pressure Derivative of Bulk Modulus
Ideal AlB_2	23.14	-27.327	86.3	3.70
Modified AlB_2	22.51	-27.705	97.2	3.36
SQS	22.63	-28.218	99.6	3.82
Expt.	22.49			

Table 4.1 – Equation of state for the ordered structures ideal AlB_2 and modified AlB_2 , and the disordered structure, SQS.

4.3 Results and discussion

4.3.1 Structural parameters

The calculations are done for three structures respectively: ideal AlB_2 structure with the Al site occupied by uranium atom and two B sites occupied by zirconium atoms, modified AlB_2 structure with Al site occupied by one zirconium atom and two B sites occupied by uranium and zirconium atoms, and a 12 atom SQS structure based on modified AlB_2 structure where Al site is occupied by zirconium atom and two B

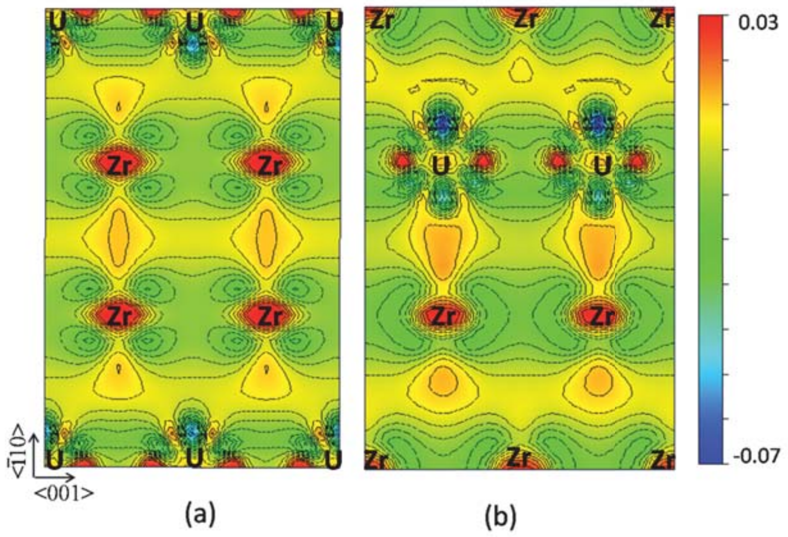

Figure 4.2 – Charge density difference plot for ordered structures in [110] plane. (a) Perfect AlB_2 structure (b) Modified AlB_2 structure . For clarity two unit cells are shown along the <001> direction.

sites occupied randomly by uranium and zirconium atoms. The unit cell for these structures is given in figure 4.1. Equation of state is calculated for these structures by relaxing the shape and ion position at a fixed volume and repeating the calculations for different values of volumes and the results are given in table 4.1.

From the table 4.1, we can see that the SQS structure is energetically more stable than both ordered structures signifying that random occupation of B sites or site occupation disorder on B sites is energetically favourable as seen in experiments [45]. Partial disorder is mainly driven by entropy effects and is stable at higher temperatures. But in case of UZr_2, partially disordered structure is found to be more stable than the ordered structure as obtained using 0 K DFT calculations where there is no entropy effects. This suggests that d and f-electron of Zr and U atoms may be playing a key role in stabilizing the partial disorder.

To study the bonding characteristics, charge density difference is plotted for different ordered structures as shown in figure 4.2. The contour plots show the bonding type to be predominantly metallic for both perfect AlB_2 and modified AlB_2 structures. For the modified AlB_2 structure which is found to be energetically more favourable, there is accumulation of charge along the bonding direction between U and Zr atoms on the 2b (1/3 2/3 1/2) sites in unit cell showing the covalent interaction between uranium and zirconium atom. Whereas there is no covalent interaction between U and Zr atoms in perfect AlB_2 structure.

SQS size convergence

As SQS representing the partial order in the 2d (1/3 2/3 1/2) sites occupancy is found to be energetically most favourable, we analysed the convergence with respect to the size of SQS. Calculations are done for different sizes of SQS and the total energy obtained from the calculations is plotted as a function of SQS size in terms of number of atoms in figure 4.3. It shows a convergence of energy with respect to SQS size and 12 atom SQS is chosen for all further calculations (except for verification some calculations are done using 24 atom SQS also).

Even though the SQS structure is more stable than ordered structures, to study the role played by disorder, all results are computed for both modified AlB_2 and SQS structures which are the ordered and partially ordered structures. SQS possesses disorder only in B sites and Al sites is uniformly occupied by zirconium atoms.

4.3.2 Electronic structure

The electron density of states for both the ordered and SQS structure are shown in figure 4.4. It may be inferred from the figure that both structures are metallic as there is non zero density of states at Fermi level. In both the structures uranium f and zirconium d states are dominating near the Fermi level along with contribution from uranium d and zirconium p states. Uranium f orbitals are seem to be hybridising

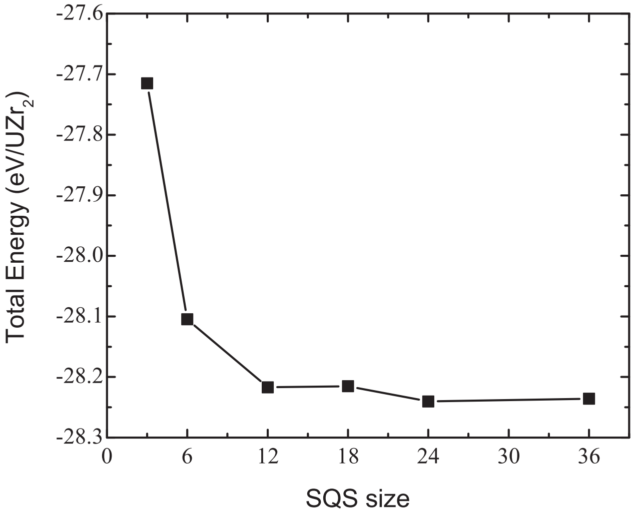

Figure 4.3 – Total energy for various special quasi random structures (SQS) as a function of the size of SQS. Total energy per formula unit (i. e. per UZr $_2$) is shown in the figure and SQS size is the number of atoms in the SQS cell.

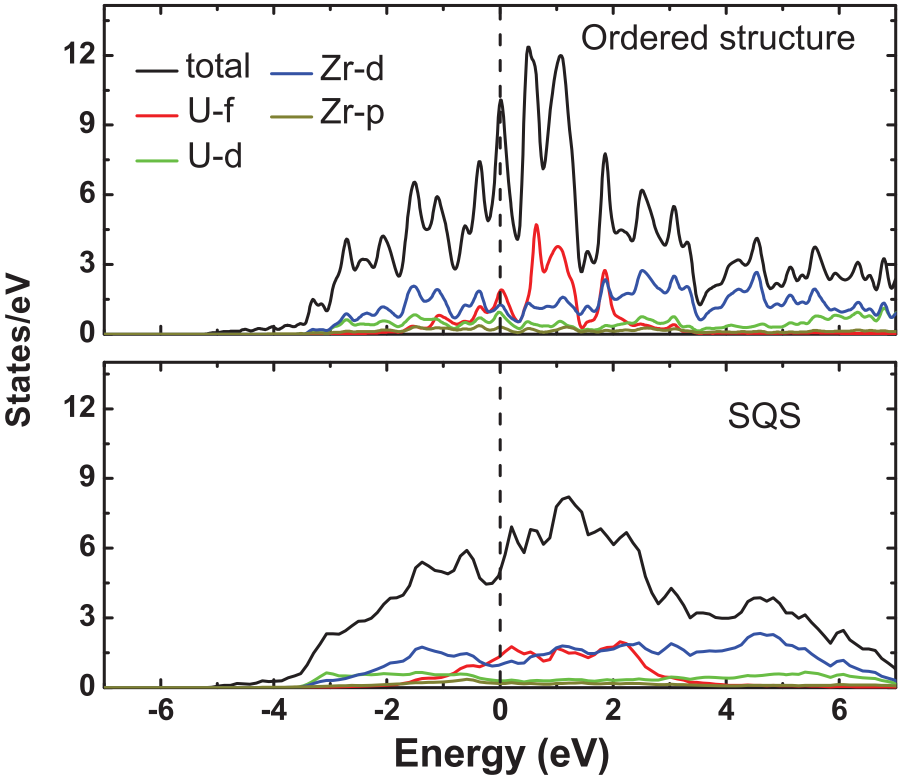

Figure 4.4 – Projected electron density of states for ordered structure (modified AlB$_2$) and SQS. In both structures main contribution at Fermi level is from uranium f-orbitals and zirconium d-orbitals. In ordered structure Fermi level lies on a peak.

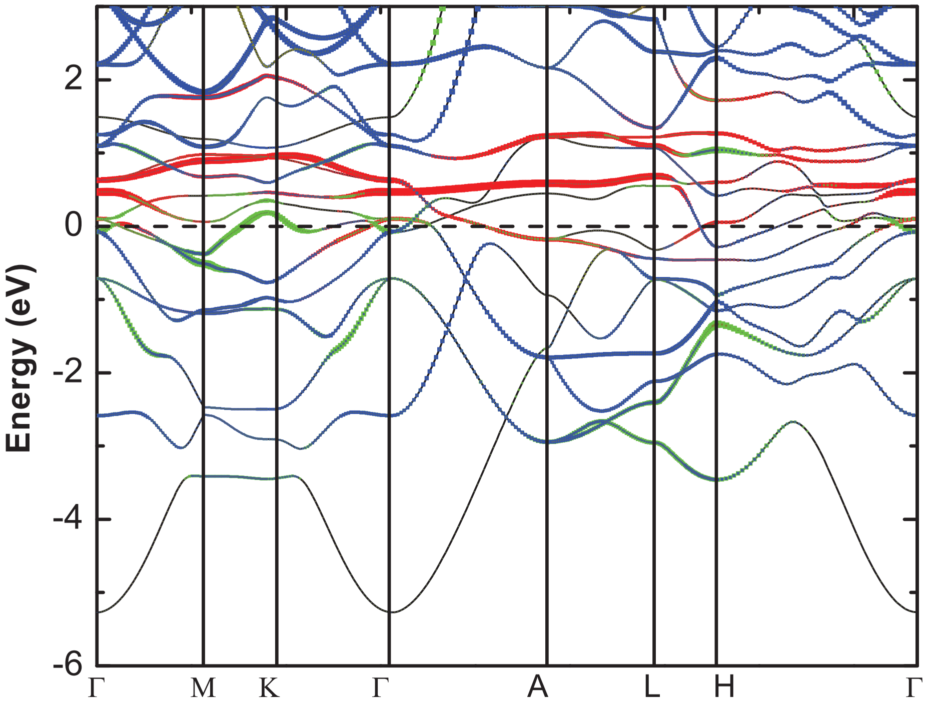

Figure 4.5 – Fat bands plotted for ordered UZr_2 (modified AlB_2). Different colours show different orbitals, red colour: U-f orbitals, green: U-d orbitals, blue: Zr-d orbitals and dark yellow: Zr-p orbitals. Thickness denotes the relative weights of different orbitals.

with other orbitals to participate in bonding in both structures. The band structure for ordered structure of UZr_2 as shown in figure 4.5 also shows the hybridisation of uranium f orbitals. Further, the electron density of states looks more smooth in case of SQS than ordered structure. Also density of states show a peak at Fermi level in ordered structure suggesting the less stability of ordered structure, where as in SQS Fermi level is near a small dip in density of states.

We have further investigated the elastic and dynamical stability of ordered and SQS structures by calculating elastic constants and phonon spectrum.

4.3.3 Elastic constants and phonon spectrum

Calculated elastic constants for the ordered and SQS structures are given in table 4.2. The SQS structure as a consequence of symmetry reduction due to disorder, have small

Structure	C11	C12	C13	C22	C23	C33	C44	C55	C66
Ordered	175.8	92.4	44.5	175.8	44.5	186.9	43.1	43.1	41.6
SQS	151.0	99.3	52.0	163.9	48.4	197.0	40.5	40.4	37.1

Table 4.2 – Calculated elastic constants for ordered and SQS structures of UZr_2 . The other 12 elastic constants which are not mentioned here and are zero for the hexagonal ordered structure, have small non zero values for the SQS because of symmetry reduction by disorder

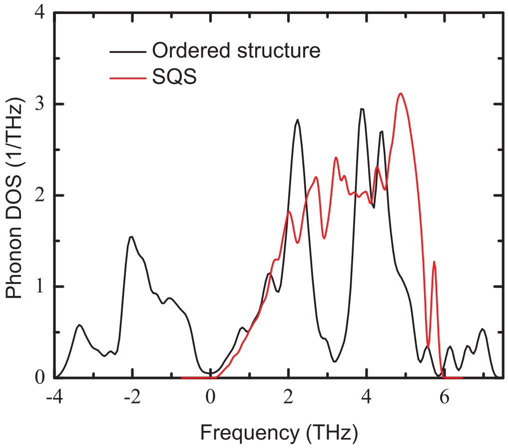

Figure 4.6 – Phonon density of states for ordered structure and SQS. Imaginary frequencies are shown on the negative frequency axis. Ordered structure have imaginary or unstable phonon whereas the SQS structure has all positive phonon frequencies and hence no phonon instability.

non zero values for the remaining elastic constants (not given in the table) which are zero for the hexagonal structure of the ordered UZr_2. For the determination of Born stability criteria these small non zero values are also considered to check the positive definiteness of the matrix of elastic constants for meeting Born stability criteria. It is found that both ordered structure and SQS meet the Born stability criteria.

In order to investigate the dynamical stability of both structures, phonon spectra are calculated. The phonon density of states are given in figure 4.6 for both the structures. The phonon density of states for the ordered structure shows imaginary frequencies plotted on the negative frequency axis, which shows that there are phonon instabilities in this structure, whereas SQS has no imaginary frequencies and has all stable phonons. Thus ordered structure is dynamically unstable and disordered

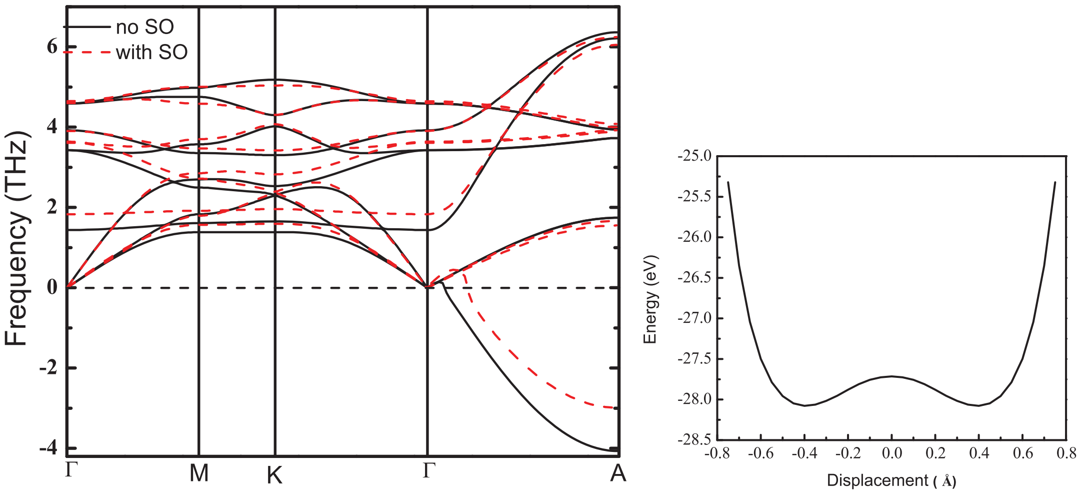

(a) **(b)**

Figure 4.7 – (a) Phonon dispersion for ordered structure with and without spin-orbit coupling.(Imaginary frequencies are plotted along the negative frequency axis.) Both with and without spin-orbit coupling phonon dispersion show an imaginary mode corresponding to A (0 0 1/2) point in Brillouin zone. (b) Potential energy curve for the unstable phonon mode. The double well potential energy curve suggested a distortion.

structure (SQS) is dynamically stable. This shows that the disorder provide the dynamical stability to UZr_2.

4.3.4 Phonon instability and structural distortion

To investigate the details of phonon instability in the ordered structure, phonon dispersion is plotted along the high symmetry directions (Γ-M-K-Γ-A) in figure 4.7a. Corresponding to 3 atoms in unit cell there are total nine phonon modes: three acoustic and six optic modes. In three acoustic modes (one LA and two TA) one U and two Zr atoms in primitive cell vibrate in phase having zero frequency corresponding to gamma point. Next modes at gamma point near 1.4 THz and 3.4 THz are the LO and TO modes corresponding to out of phase vibration of U and Zr atoms at 2d sites. Modes corresponding to 3.9 THz and 4.5 THz are LO and TO modes corresponding to Zr atoms vibrating out of phase with each other. In order to have a comparison, phonon dispersion calculations incorporating SO coupling are also done and plotted

Structure	C11	C12	C13	C22	C23	C33	C44	C55	C66
Ordered	175.8	92.4	44.5	175.8	44.5	186.9	43.1	43.1	41.6
SQS	151.0	99.3	52.0	163.9	48.4	197.0	40.5	40.4	37.1
Distorted ordered	180.4	82.1	42.4	180.4	42.4	206.7	38.6	38.6	49.1

Table 4.3 – Calculated elastic constants for the distorted structure of UZr_2. Elastic constants for ordered and SQS structures are also given for comparison.

in figure 4.7a. It is seen that the unstable phonon mode is along Γ-A direction and the potential energy curve for the phonon corresponding to the A point in Brillouin zone is plotted in figure 4.7b. The potential energy curve shows a double well structure and when the atoms are given small displacement along this mode (and are allowed to relax) , it eventually goes to a distorted structure where the U atoms along the Z direction ('c' axis) dimerize. The distance between alternative U atoms along Z direction decreases. The unitcell corresponding to the new structure is double of the unitcell of the original structure as shown in figure 4.8a and the relaxed lattice parameters 'a' and 'c' of the new distorted structure are 5.0329 Å and 6.2543 Å respectively. Cell volume is found to increase by 1.9% with slight contraction of 0.06% along a and b axis and an expansion of 2.27% along c axis. To evaluate the mechanical stability of new structure, its elastic and dynamical properties were studied. The calculated elastic constants are given in table 4.3 and they are found to meet Born stability criteria. The phonon dispersion for the distorted dimerized structure is plotted in figure 4.8b. In contrary to the original ordered structure which has unstable phonon mode, the phonon spectrum of the distorted structure does not posses any imaginary frequency. It may be noted that this structure has 18 modes corresponding to 6 atoms in unitcell. Thus new distorted structure is both elastically and dynamically stable.

The charge density difference plot for both ordered structure and distorted structure is given in figure 4.9. The dimerization of alternative uranium atoms along <001>

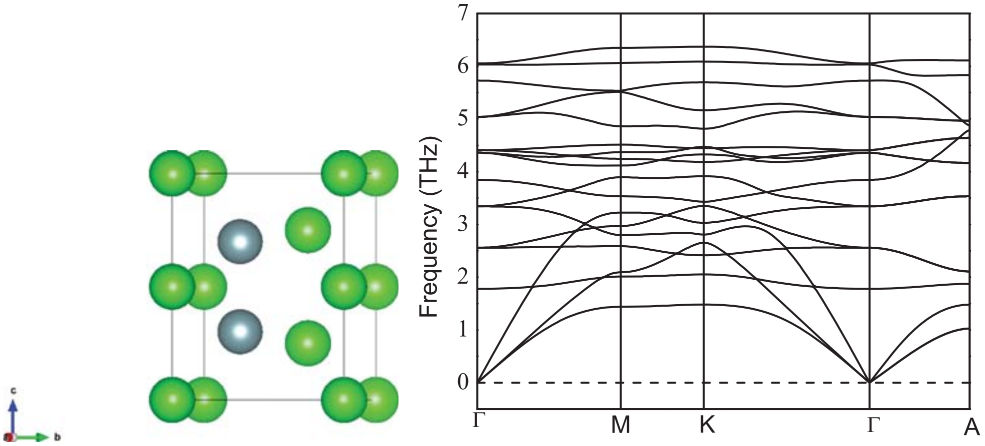

(a) **(b)**

Figure 4.8 – (a) The unit cell of distorted structure (dimerized ordered structure). Green sphere represent Zr and grey sphere represent U. (b) Phonon dispersion for the distorted structure.

direction is clearly visible in the charge density plot. As can be seen from the plot, the distortion or dimerization of uranium atoms alters the bonding characteristics significantly. The covalent character in U-Zr bonding diminishes and strong bonding between uranium atoms appear as is clear from the charge accumulation between two uranium atoms seen in the figure 4.9.

Thus the ordered UZr_2 would undergo a distortion to dimerized structure which is similar to the Peierl's transition known to occur in alpha-U at 43 K, below which a charge density wave (CDW) appears in alpha-U [3, 132, 133]. A similar uranium intermetallic compound U_2Mo is also predicted to show such transition [40].

The ground state energy difference between the original structure and new distorted structure is 0.405 eV/UZr_2. The variation of the energy difference with pressure is plotted in figure 4.10. There is a small increase in energy difference between the two structures as the pressure is increased and even upto a pressure of 20 GPa the distorted structure remains more stable than the ordered structure. Generally the CDW transition get suppressed by applying pressure e.g. in alpha-U no CDW exist

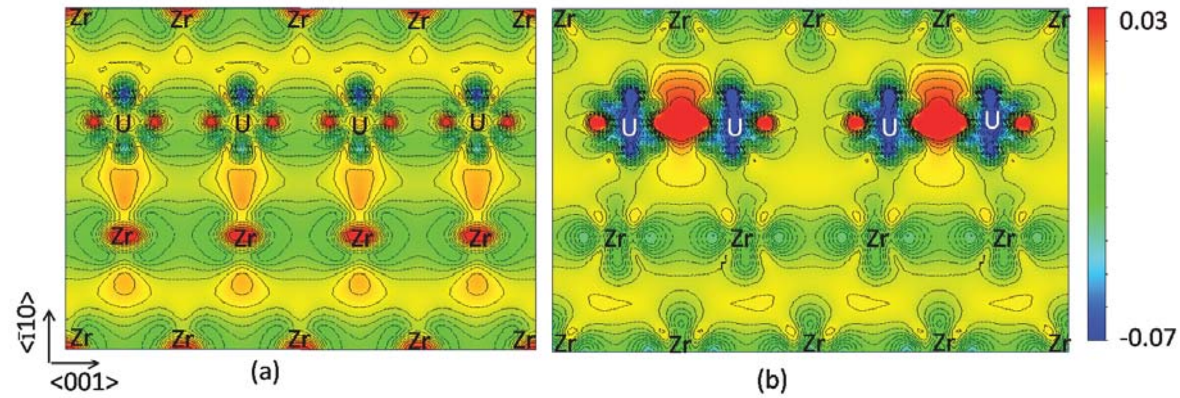

Figure 4.9 – Charge density difference distribution in [110] plane for (a) original structure (b) distorted structure. Dimerization of uranium atoms in the distorted structure can be clearly seen with charge accumulation in between alternative uranium atom pairs.

at a pressure of 1 GPa. But in present case of ordered UZr_2, the CDW transition remains stable even upto 20 GPa.

Both SQS and dimerized ordered structure are elastically and dynamically stable but energetically the SQS is more favourable than the ordered dimerized structure. In the absence of disorder, UZr_2 would have shown the dimerization transition but disorder become more energetically favourable and hence suppresses the charge density wave transition.

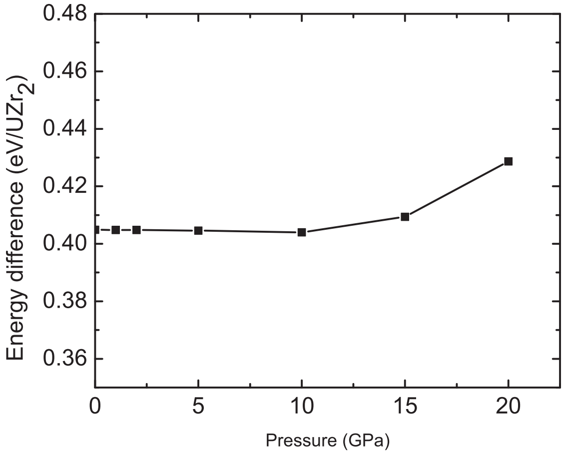

Figure 4.10 – The ground state energy difference between the original structure and the distorted structure as a function of pressure. This energy difference slightly increases with pressure suggesting that the distortion will not be suppressed by pressure.

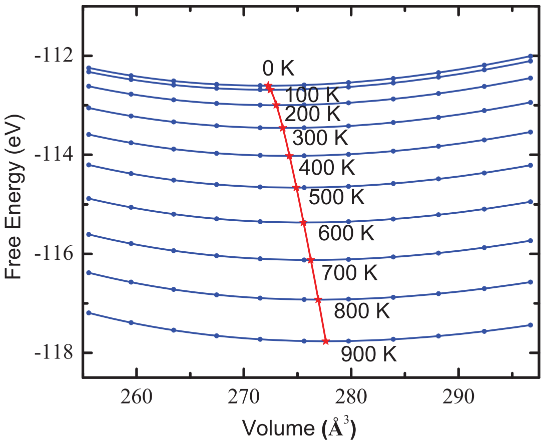

Figure 4.11 – Birch-Murnaghan equation of state fitting to free energy vs volume at different temperatures (0 K to 900 K). Red stars are the minima of different curves and shows the equilibrium volumes at different temperatures.

4.3.5 Thermal properties

SQS structure representing the partial disorder in site occupancy in UZr_2 is elastically and dynamically stable and also energetically favourable over the dimerized ordered structure. Hence, the SQS is used for the calculation of thermal properties. Quasi harmonic approximation is used to calculate the thermal properties as a function of temperature. Phonon spectrum is calculated for different volumes of SQS and Helmholtz free energy is calculated for different temperatures at each volume. Birch-Murnaghan Equation of state fit for different temperatures is plotted in figure 4.11. Equilibrium volume at each temperature from Birch-Murnaghan Equation of state fit give the volume variation with temperature, from which volume expansion and thermal expansion can be calculated.

The calculated thermal expansion coefficient and volume expansion are plotted in figure 4.12 along with the available experimental data for delta-UZr_2. The experimental data is available for an alloy having mixture of delta-UZr_2 phase and alpha-Zr. For comparison we have also plotted the experimental data for alpha-U and alpha-Zr.

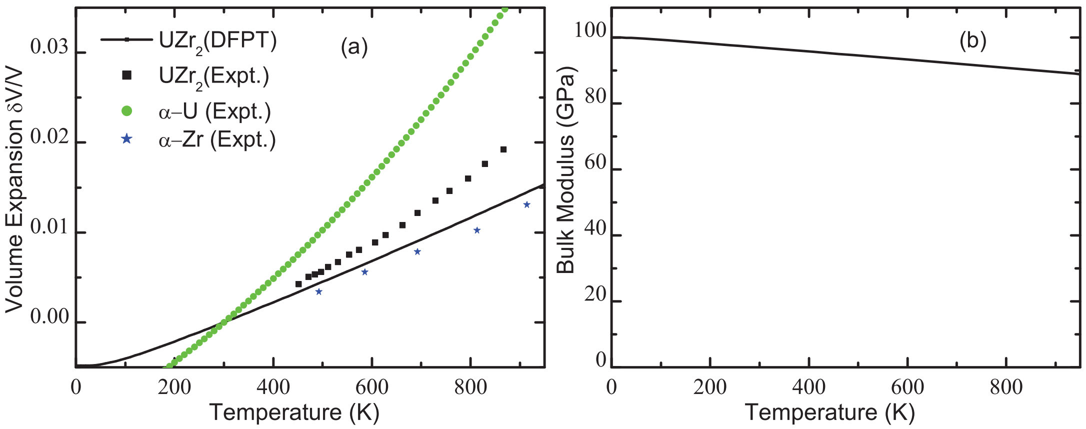

Figure 4.12 – Volume expansion and bulk modulus for SQS compared with available experimental data [70]. Calculated volume expansion lies in between volume expansion of alpha-U [70] and alpha-Zr [134] but lies below the experimental volume expansion for delta-UZr$_2$.

The calculated volume expansion is under predicted in comparison to the experimental data for UZr$_2$.

The equilibrium volume of SQS structure of UZr$_2$ is in very good agreement with the experimental volume of UZr$_2$ but the volume expansion is under predicted. To check for the SQS size convergence for thermal properties, the quasi harmonic approximation calculations are repeated with 24 atom SQS and the corresponding volume expansion and bulk modulus obtained from the calculations are shown in figure 4.13.

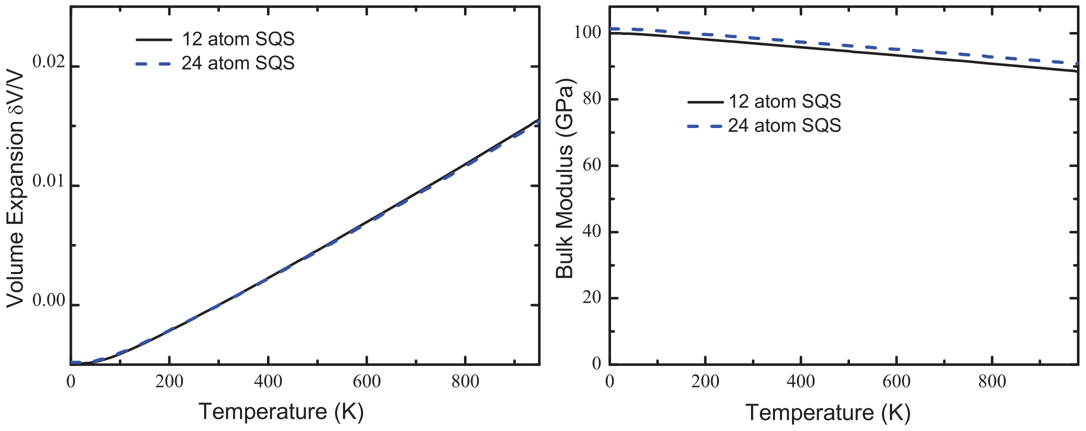

Figure 4.13 – Volume expansion and bulk modulus comparison for 12 atom and 24 atom SQSs. No significant difference between the volume expansion calculated using 12 atom SQS and 24 atom SQS.

There is no significant difference between the volume expansion calculated using 12 atom SQS and 24 atom SQS. The other possible reason for the under prediction of volume expansion can be presence of strong anharmonicity in the system which is taken care by QHA only in an approximate way. Further, the experimental data is not for pure UZr_2 and the present calculations does not incorporate the electronic contribution.

4.4 Summary

The density functional theory based first principles calculations are performed for three different structures of UZr_2 ideal AlB_2 , modified AlB_2 and disordered structure represented by SQS. These calculations have given the following insights.

- The modified AlB_2 structure is energetically favourable for UZr_2 over ideal AlB_2. In the modified AlB_2 structure, the site occupancy disorder is energetically favourable making partially ordered structure more stable than the perfectly ordered structure. This is different from the structural disorder stabilized by entropy. Partially ordered structure in UZr_2 is stable even without entropy contribution.

- In the modified AlB_2 structures, the electron density of states for ordered structure shows a peak corresponding to the Fermi level whereas for the disordered SQS structure, Fermi level lies near a dip in electron density of states.

- Both the ordered and the partially disordered structure are elastically stable as they meet the Born stability criteria but the ordered structure is dynamically unstable and has unstable phonon modes whereas, the partially ordered structure is dynamically stable.

- The phonon instability in the ordered structure leads to the distortion of U atoms causing the doubling of unit cell along 'c' axis (Z direction). The distorted structure with doubled unit cell is found to be both elastically and dynamically stable.

- The distorted or dimerized structure remains energetically more favourable than the ordered structure even after applying pressure up to 20 GPa.

- Both the distorted structure and the partially disordered structure are elastically and dynamically stable but partially disordered structure is the one which is energetically more favourable.

- The thermal properties calculated using QHA for energetically favourable partially disordered structure shows the discrepancy in the calculated volume expansion and available experimental data which suggests the presence of strong anharmonicity in the system.

Chapter 5

Structural stability and evidence of charge density wave in U_2Ti

---

This chapter discusses the structural, electronic, elastic and dynamical properties of U_2Ti*. U-Ti system is isoelectronic with U-Zr system but the intermetallic phase in this system is* U_2Ti *which is a line compound as opposite to* UZr_2 *which has a stoichiometry range. The relation between phonon instability, periodic lattice distortion and charge density wave in* U_2Ti *is also established.*

5.1 Introduction

Studies on the uranium compounds and alloys have continued to attract attention for many years due to their application as nuclear fuel material. From practical application point of view uranium is not only important as a nuclear fuel in fission reactor but also seen as a potential candidate for tritium storage in fusion reactor [135] because of its higher absorption capacity and wide plateau in pressure-composition isotherms. For safe storage of radioactive tritium in uranium, its storage capability and stability against powdering on hydrogenation, sudden explosion and environmental pollution are improved by alloying with other elements [1, 2, 74] (e.g. Ti, Zr, Al, Ni etc). In particular, U_2Ti has acquired growing attention because of its potential application as a safe and heavy metal based storage material for radioactive tritium in fusion reactor. The primary reason for this interest is due to the high durability of its hydride against powdering. The CALPHAD thermodynamic description and the phase boundaries of different phases present in U-Ti alloy are studied by Berche et al [136] and Bajaj et al [137]. First principles studies of the properties of U_2Ti available in the literature are rather limited. Chattaraj et al [77] have studied the structural and electronic properties of U_2Ti using DFT calculations. They inferred that electronic density of states at Fermi level is mostly due to the uranium f electrons and titanium atoms contribution is at higher energies. They also showed that the spin-orbit coupling exhibit a small effect on the bands below Fermi level and predominant on the states above Fermi level. Hasan et al [78] calculated the thermodynamical and optical properties showing that the material is an excellent reflector between 8 eV to 12.45 eV. Elastic anisotropy, vibrational and thermal properties of U_2Ti are studied by Yang et al [79] who showed that this compound possess slight elastic anisotropy at zero pressure, however the anisotropy becomes more and more significant with the increasing pressure. They also showed that U_2Ti will be mechanically stable up to 100 GPa.

A detailed study of the structure and stability is important in understanding of the thermodynamic, elastic and cohesive properties of the system. In the present work, we have systematically investigated the electronic, structural, elastic and dynamical properties of U_2Ti using the DFT based ab-initio calculations which revealed the presence of dynamical instability in the known ground state structure of U_2Ti in contrary to the available DFT calculations [79]. Stability of the ground state or the knowledge of true ground state is also important for the phase diagram calculation. As discussed by Losada et al [40] for the case of U-Mo system the use of unstable compound for phase diagram calculations can lead to non-physical conclusions. So it is very important to know the proper ground state and the corresponding properties. The instability of U_2Ti found in present calculations reveals an interesting behaviour of the system. It distorts the original structure to a new ground state structure which is both elastically and dynamically stable. The new ground state structure shows the possible existence of Peierl's transition [138] leading to dimerization and charge density wave [139] in U_2Ti at low temperatures.

5.2 Computational details

U-Ti system is isoelectronic with U-Zr system and the intermetallic phase in this system is U_2Ti where as it is UZr_2 for U-Zr system. In contrast to UZr_2 which is having a stoichiometry range, U_2Ti is a line compound stable up to 1171 K (898 °C) above which it transforms to bcc gamma phase [76]. Its structure is AlB_2 type having space group P6/*mmm* (#191). The U atoms occupy 2d (1/3, 2/3, 1/2) sites and Ti atom occupies 1a (0, 0, 0) site [140].

The calculations are performed using the Vienna ab-initio Simulation Package (VASP) [81, 82, 114]. Interaction between the valence electrons and the ionic core is described by Projector Augmented Wave (PAW) based pseudopotential [115, 116]. The pseudopotentials used in the calculation treat $6s^2 6p^6 7s^2 5f^3 6d^1$ and $3s^2 3p^6 4s^2 3d^2$ of U and Ti respectively as valence electrons. Generalized Gradient Approximation as parametrized by Perdew, Burke and Ernzerhof (PBE) [88] is used for exchange correlation functional. All the calculations are scalar relativistic and non spin polarized.

For the purpose of comparison some fully relativistic calculations were also done including both the spin polarization and spin-orbit coupling. A plane wave energy cut-off of 450 eV and the Brillouin zone sampling using a 11×11×17 gamma centred mesh were used to ensure a convergence of better than 1 meV/atom in the energies. Structural relaxation is carried out by allowing the cell shape and ionic positions to relax so that the force on each ion becomes less than 0.001 eV/Å. Calculations were done for several values of volumes which were fitted to Birch-Murnaghan equation of state [103] to obtain equilibrium volume, bulk modulus and pressure derivative of bulk modulus.

In order to compute the elastic constants, VASP implementation of the finite difference combined with symmetry general least-square method [106] was used. In this method the elastic tensor is determined from the strain-stress relationships for six different finite distortions of the lattice. Phonon dispersions were calculated using Density Functional Perturbation Theory (DFPT) [13, 113] as implemented in VASP using an 81 atom (3×3×3 of unit cell) supercell. The Phonopy package [119] was used to extract the necessary data from VASP calculations to set up the Dynamical matrix and then calculate the phonon spectra. Fourier interpolation is done to get the dynamical matrix on a fine grid of 21×21×21 **k**-point mesh.

To ensure the reliability of the calculations and to verify the results, the phonon spectrum of U_2Ti was calculated using the full potential linear augmented plane wave (LAPW) based method implemented in WIEN2k code [83] too. The cut-off parameter $\mathrm{RMT}\times\mathrm{K}_{\mathrm{max}}$=10.0 is used along with RMT values of 2.3 a.u. for both U and Ti atoms. Brillouin zone integration were performed using a 1000 **k**-points mesh. For the Fermi surface calculations, self consistent charge densities were calculated using a denser **k**-

point mesh having 3000 points and Fermi surface was obtained on a 10,000 **k**-points mesh.

5.3 Results and Discussion

5.3.1 Structural parameters

Total energy calculations were carried out for known AlB_2 structure at different volumes and the results were fitted to the Birch Murnaghan equation of state to get the equilibrium volume, ground state (equilibrium) energy, bulk modulus and pressure derivative of bulk modulus. The computed values and comparison with earlier calculations and experimental results are given in Table 5.1. Our calculated values of lattice parameters 'a' and 'c' are respectively 4.7725 Å and 2.8045 Å which are close to experimental values and matches well with the earlier results obtained using PW91 and PBE except for the LDA results which are far less than experimental values. Inclusion of spin orbit coupling in our calculations has marginally improved the agreement with experimental values of the lattice parameters whereas a small decrease in bulk modulus compared to both the non spin polarized calculations and the values available in the literature was observed.

As explained in chapter 1, U-Ti system is isoelectronic to U-Zr system and both the U_2Ti and UZr_2 have AlB_2 type hexagonal crystal structure with space group P6/*mmm* (#191). In UZr_2, partial site occupancy disorder is known to exist at 2d (1/3 2/3 1/2) site as it is randomly occupied by U and Zr atoms. To explore the possibility of site occupancy disorder in U_2Ti, three special quasi random structures were generated for random configurations of U and Ti atoms on 2d (1/3 2/3 1/2) site and fixed occupation of 1a (0 0 0) site by U atom in AlB_2 hexagonal crystal structure.

Structure	'a' (in Å)	'c' (in Å)	Volume (in $Å^3$)	Energy (in eV)	Bulk modulus (in GPa)	B'
GGA(PBE) this work	4.7725	2.8045	55.372	-30.759	129.0	4.831
GGA(PBE)+SO this work	4.7759	2.8067	55.518	-36.810	125.7	4.889
LDA[79]	4.659	2.724	51.210			5.326
GGA (PW91)[79]	4.777	2.806	55.440			5.046
GGA(PW91)+SO[77]	4.773	2.815	55.54			
GGA(PBE)[78]	4.782	2.822	55.87			
Expt.[141]	4.8347	2.8442	57.574			

Table 5.1 – Relaxed lattice parameters 'a' and 'c' , equilibrium volume, energy , bulk modulus and pressure derivative of bulk modulus (B') of U_2Ti.

Configuration	Energy (eV/U_2Ti)	Volume ($Å^3$)
Perfect AlB_2	-30.759	55.372
Modified AlB_2	-29.816	58.263
SQS-6	-29.167	59.225
SQS-12	-30.169	59.377
SQS-24	-30.263	59.211

Table 5.2 – Energetics of AlB_2 based ordered structures and special quasi random structures (SQS) of U_2Ti. The SQS-6, SQS-12 and SQS-24 represent the site occupancy disorder and are same configurations as used in case UZr_2.

The total energies of these SQS along with the perfect ordered structure are given in table 5.2. In case of U_2Ti, the perfect AlB_2 structure is energetically more stable than modified AlB_2 structure as well as disordered structures represented by SQS, where as in the case of UZr_2 the disordered structure (SQS) is energetically more stable than ordered structures (perfect AlB_2 and modified AlB_2) as already seen in chapter 4. Thus the site occupancy disorder on the 2d (1/3 2/3 1/2) site of AlB_2 is energetically favourable in UZr_2 whereas perfect order is favourable in U_2Ti corroborating with the absence of site occupancy disorder in U_2Ti and its line compound nature [76].

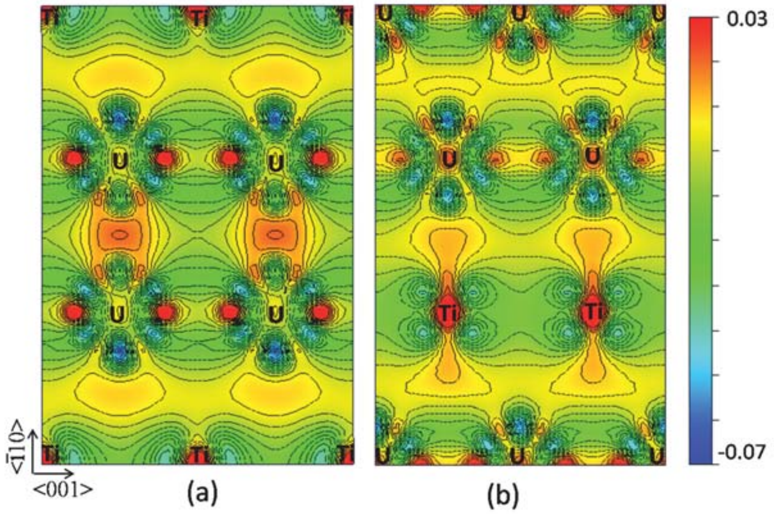

Figure 5.1 – Charge density difference plot for ordered structures of U_2Ti. (a) Perfect AlB_2 (b) modified AlB_2. For clarity two unit cells are shown along the <001> direction.

5.3.2 Charge density

To bring out the differences in the bonding characteristics, charge density difference in the [110] plane for both the perfect AlB_2 and modified AlB_2 structures of U_2Ti are plotted in figure 5.1. In both structures, the spread out of charge shows metallic bonding. In perfect AlB_2 structure, there is an accumulation of charge in between two uranium atoms at 2d (1/3 2/3 1/2) sites in the unitcell showing the covalent character of bonding interaction whereas in case of modified AlB_2 structure, because of smaller size and higher electronegativity of Ti atom the covalent bonding is missing among the U and Ti atoms present as 2d (1/3 2/3 1/2) sites in the unitcell and there is weak ionic character too visible in the nearest pair of U and Ti atoms. Further in case of modified AlB_2 structure, the U-U bonding is possible only along 'c' direction which is also metallic.

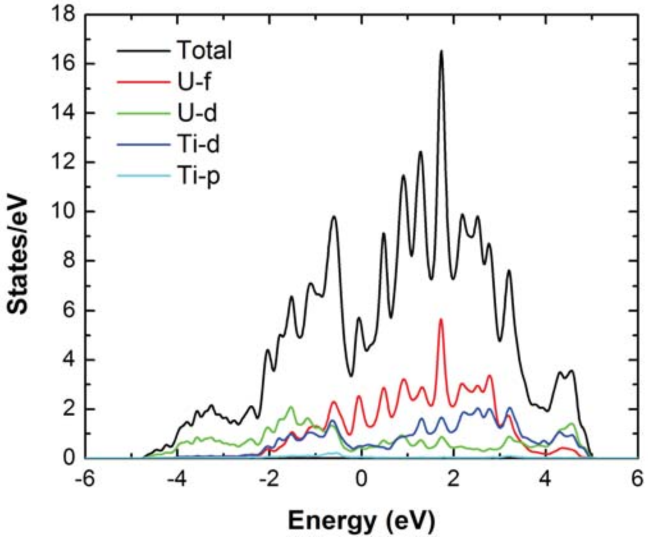

Figure 5.2 – Projected electron density of states of U_2Ti. Fermi level at 0 eV is shown by vertical black dashed line. The main contribution to density of states at Fermi level is from U-f, U-d and Ti-d orbitals.

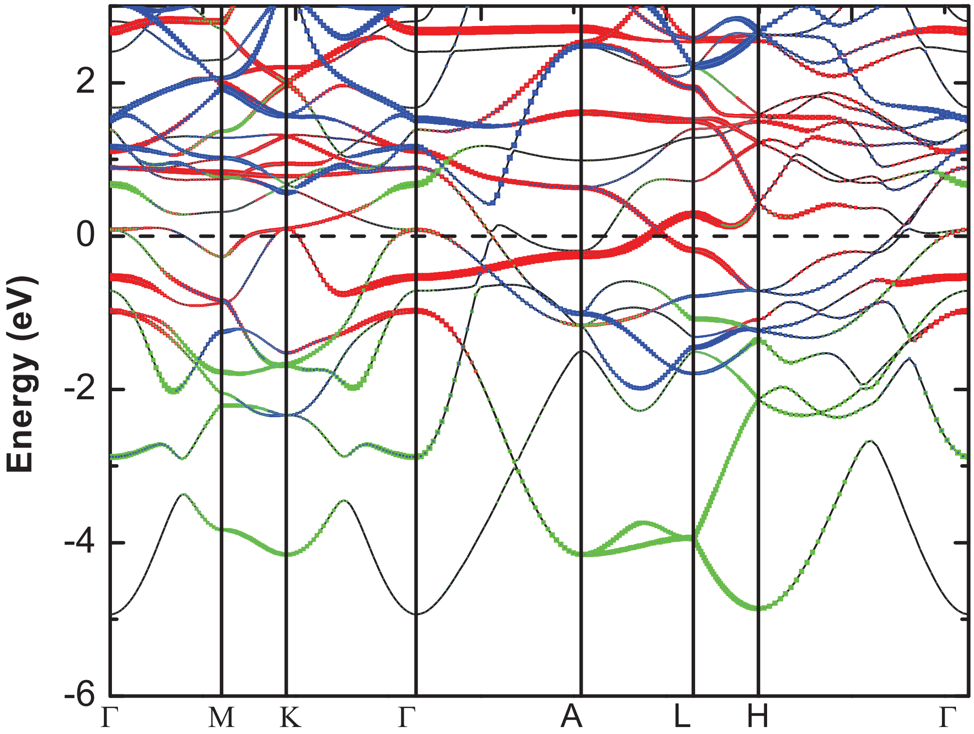

Figure 5.3 – Band structure of U_2Ti. Different colours show different orbitals, red colour: U-f orbitals, green: U-d orbitals, blue: Ti-d orbitals and cyan: Ti-p orbitals. Thickness denotes the relative weights of different orbitals. Mixing of U-f with U-d and Ti-d bands can be seen which shows that U-f bands are participating in bonding.

5.3.3 Electronic structure

Electronic density of states, plotted in figure 5.2, shows that at the Fermi level, main contribution to total electron density of states comes from uranium f states, uranium d states and titanium d states. Band structure of U_2Ti plotted in figure 5.3 shows the hybridization (mixing) of uranium f, uranium d and titanium d bands which indicates that the uranium f bands are participating in bonding and are not localized. This suggests that the correlations will not be that important and DFT will be able to describe the properties of U_2Ti.

5.3.4 Elastic constants and phonons

In order to study the phase stability of U_2Ti, phonon spectrum and elastic constants were calculated. The calculated phonon spectrum for the optimized structure is plotted along high symmetry directions (Γ-M-K-Γ-A) in the Brillouin zone is shown in figure 5.4. It may be noted that the dispersion curve around the A-point shows imaginary values which are plotted on the negative frequency axis. There are a total of 9 phonon modes (3 acoustic and 6 optic modes) originating from the 3 atoms in the unit cell. All phonon modes are stable except the one mode that shows negative frequency near A point in the Brillouin zone. Inclusion of spin orbit coupling in fully relativistic calculations has slightly softened some phonon modes but the overall effect of spin orbit coupling on phonon spectrum is rather weak as can be seen in Figure 5.4.

Earlier reported calculations by Yang et al [79] on the phonon spectrum of U_2Ti does not show any instability which is in contrast to our present results. The difference of our present calculations from that of Yang et al is that they have used the GGA based exchange correlation functional parametrized by Perdew and Wang (PW91)

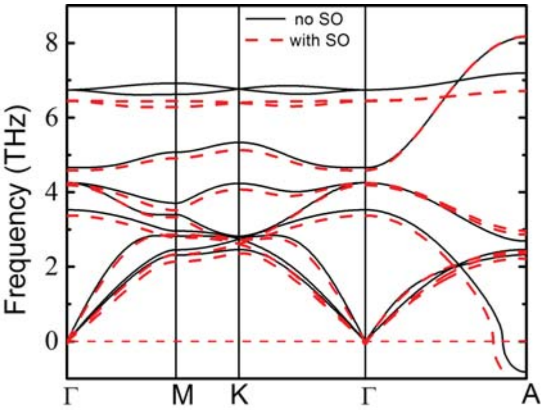

Figure 5.4 – Phonon dispersion of U_2Ti calculated with and without inclusion of spin orbit (SO) coupling. Imaginary phonon frequencies are plotted along negative frequency axis. One of the phonon modes has imaginary frequency around A-point which indicates the instability of that mode.

[87] whereas we have performed our calculations using the GGA based exchange correlation functional parametrized by Perdew, Burke and Ernzerhof (PBE) [88]. When we performed the calculations using PW91, we found that our results matches well with that of Yang et al and does not show any instability. However the inclusion of spin-orbit coupling along with PW91 showed an instability in the phonon dispersion. Moreover, our calculations of phonon spectrum using PW91 based pseudopotential corresponding to experimental volume, also showed this instability even without the inclusion of spin orbit coupling. This indicates that phonon instability is also present for the case of PW91 based calculations and it is absent only for the calculated equilibrium volume with PW91 and without the inclusion of spin orbit coupling.

As there was qualitative inconsistency in the results using different pseudopotentials, we have also performed full potential LAPW calculations using WIEN2k to verify the existence of the phonon instability. The phonon spectrum was calculated for 24 atom supercell (2×2×2 times of unitcell). The calculated phonon spectrum is similar to our PAW-PBE calculations and it is shown in Figure 5.5. It can be seen that WIEN2k calculated phonon spectrum also confirms the existence of instability of LO phonon

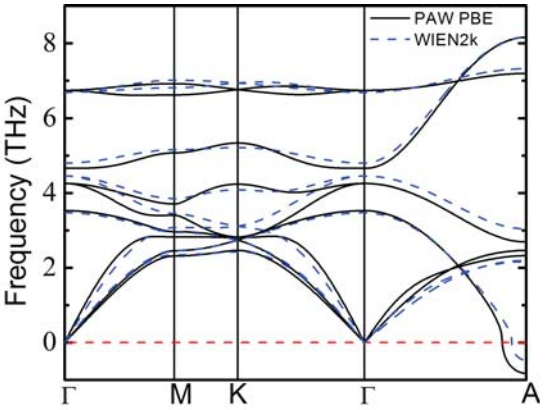

Figure 5.5 – Phonon dispersion calculated using VASP (PAW PBE) and WIEN2k. Phonon instability around A point is reproduced by WIEN2k calculations also.

mode around A (0 0 1/2) point in Brillouin zone.

5.3.5 Phonon instability and structural distortion

This unstable phonon mode is a longitudinal optical (LO) mode consisting of predominantly the movement of U atoms along the 'c' direction (Z direction) and can be represented using a six atom supercell (1×1×2 times of unitcell) as shown in figure 5.6a. The potential energy curve for this mode was calculated by giving displacement to the atoms according to this mode with increasing amplitude. Figure 5.6b shows the potential energy curve of this mode which is a double well with maxima at zero displacement. When the structure is relaxed after giving a small displacement corresponding to this mode the structure attains its minimum energy in one of the double wells which corresponds to the breaking of symmetry along Z direction thereby the distance between alternate pairs of U atoms decreased along the Z axis. The unitcell of the new structure is double of the unitcell of the original structure and the relaxed lattice parameters 'a' and 'c' of the new distorted structure are 4.7607 Å and 5.7664 Å respectively. Cell volume is found to increase by 2.2% with slight contraction of 0.025% along a and b axis with an expansion of 2.8 % along c direction. Unit cell of

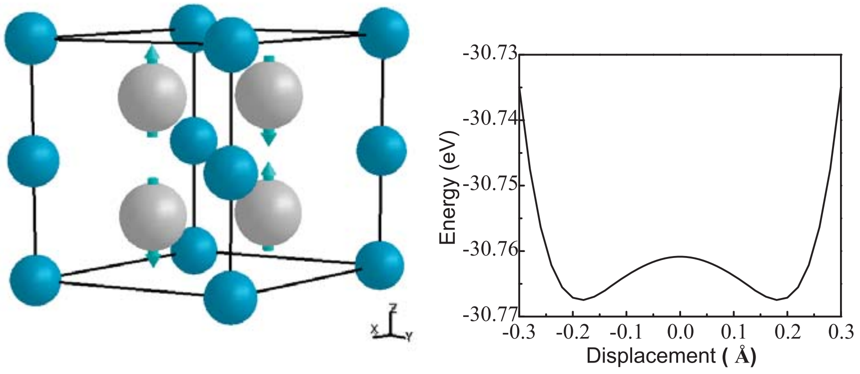

(a) (b)

Figure 5.6 – (a) Uranium atom movement corresponding to unstable phonon mode at A point. (b) Potential energy curve for displacement along the unstable mode.

	C_{11}	C_{12}	C_{13}	C_{33}	C_{44}	B
Original structure	288.7	80.0	29.5	313.1	134.6	129.0
New distorted structure	255.4	104.9	35.6	212.6	100.5	115.2
Earlier calculations[79]	285	74	28	300	129	125

Table 5.3 – Calculated elastic constants (in GPa) and bulk modulus (in GPa) of U_2Ti. Calculated elastic constants for both original structure and distorted structure meet Born stability criteria.

the new distorted structure along with the unitcell of the original structure are shown in figure 5.7. To investigate the stability of the new structure, we calculated its structural , elastic and dynamical properties. The phonon spectrum of the new structure is plotted in figure 5.8. In contrary to the original structure which has unstable phonon mode, the phonon spectrum of the distorted structure does not possess any imaginary frequency. It may be noted that this structure has 18 modes corresponding to 6 atoms in the unitcell. The calculated elastic constants of both the original structure and the new distorted structure are found to meet Born stability criteria. The values of elastic constants are given in table 5.3. The lattice distortion is found to affect the elastic constants. Increase of C12 and C13 and softening of C11, C33 and C44 can be seen.

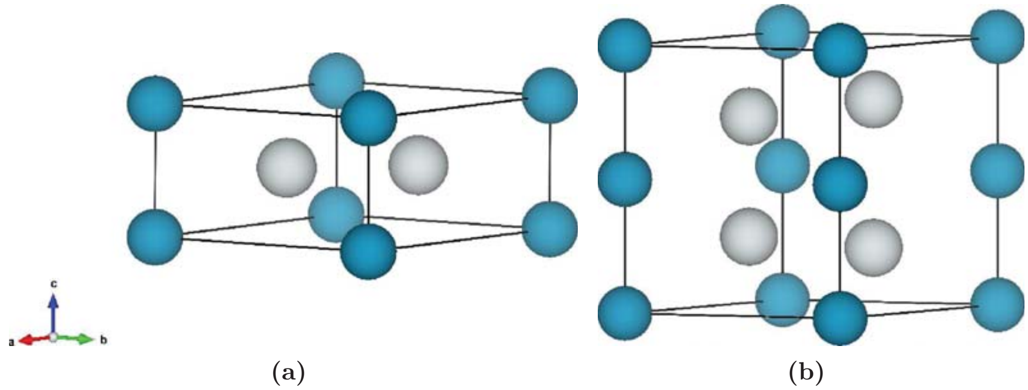

Figure 5.7 – Unitcell for (a) original structure and (b) new distorted structure. The unitcell for new distorted structure is double of the original cell along 'c' axis along with distortion of uranium atoms.

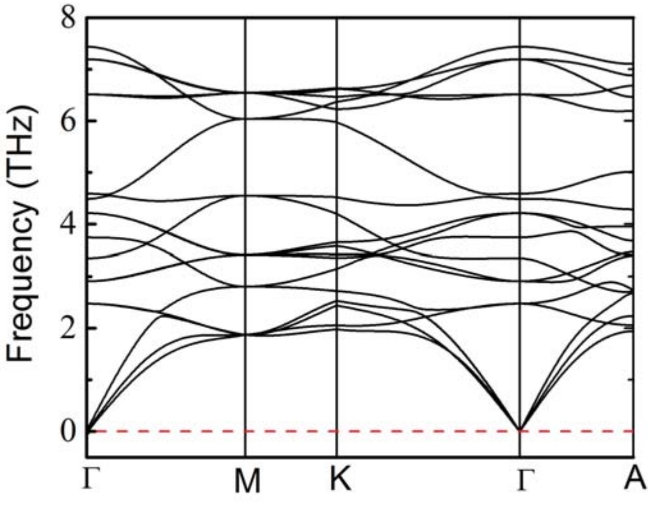

Figure 5.8 – Phonon dispersion for new distorted structure. No imaginary frequencies are found showing the absence of phonon instability.

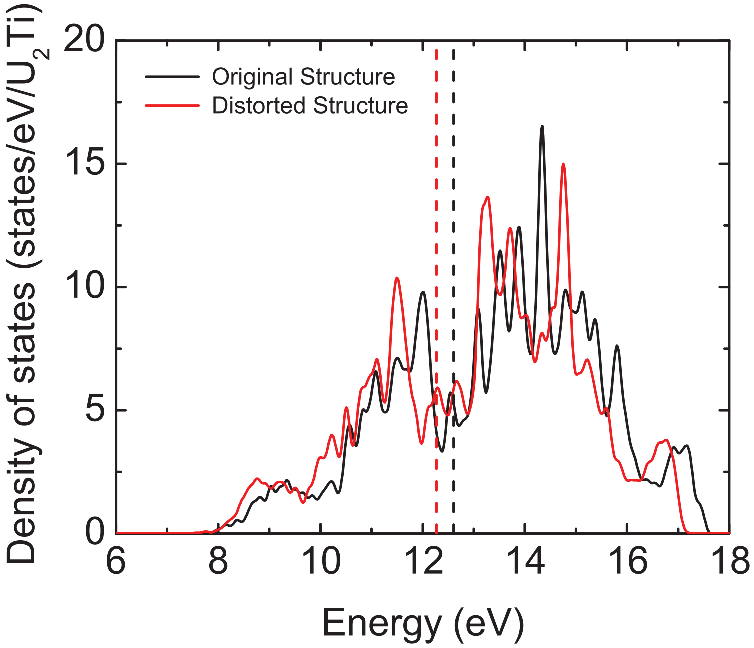

Figure 5.9 – The electronic density of states of the original structure and new distorted structure of U_2Ti. Fermi level for both structures are shown by horizontal dashed curves.

5.3.6 Electronic structure and Fermi surface

Figure 5.9 shows the electron density of states for the original structure and the new distorted structure. Fermi energy in both cases is represented by dashed line. Fermi energy decreases from 12.607 eV for original structure to 12.269 eV for distorted structure. There is also shift of bands to lower energy with distortion. But there is no significant change in the electronic density of states at the Fermi level with distortion. Fermi surface of the original structure is plotted in Figure 5.10a which is having contribution from four bands(band no. 19, 20 21 and 22). Fermi surface corresponding to band 21 is shown separately in figure 5.10b and it shows nesting. The nesting vector is (0 0 1/2). This vector corresponds to the wave vector of phonon instability which leads to the distortion of the structure.

The ground state energy difference between the original structure and that of the new distorted structure is 31.8 meV/U_2Ti. The variation of the energy difference with

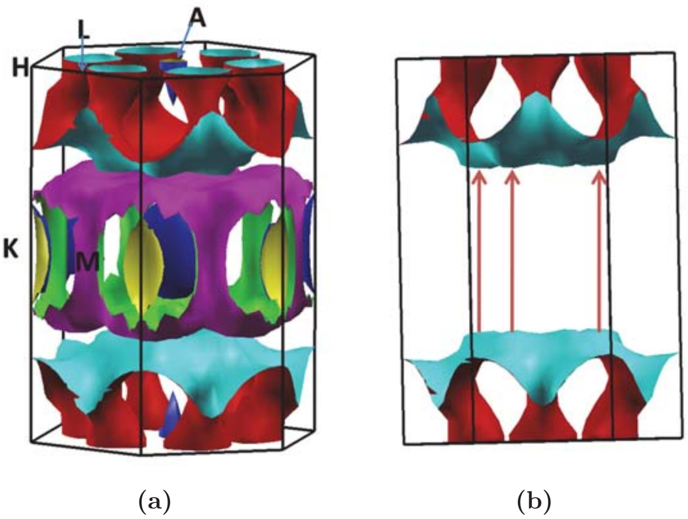

(a) **(b)**

Figure 5.10 – (a) Fermi surface of U_2Ti in original structure. (b) Band showing Fermi surface nesting. Fermi surface shows nesting and nesting vector (0 0 1/2) is same as wave vector corresponding to the instability in phonon dispersion.

pressure is plotted in figure 5.11. Upto 4 GPa the distorted structure is more stable after which the original structure becomes more stable.

5.3.7 Charge density variations

The charge density difference of the original structure and that of the distorted structure in the [110] plane are shown in figure 5.12. For the original structure, the electrons distribution around U atoms are equivalent along 'c' direction (<001>), whereas in distorted structure, the distribution is no longer equivalent and the charges concentrate between two neighbouring U atoms. This non-uniform charge density distribution is similar to the charge density wave in alpha-U as observed by Qiu et al [133]. Thus the phonon anomaly leading to a periodic lattice distortion of U atom chains along the <001> direction in C32 structure of U_2Ti suggests the possibility of existence of charge density wave (CDW) at lower temperatures. Losada et al [40] have earlier predicted the Peierl's type distortion and CDW in U_2Mo. The CDW is known to exist in alpha-U below 43 K as observed from experiments. In alpha U, sev-

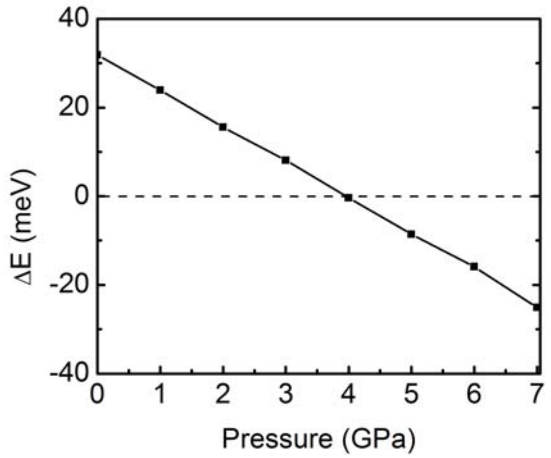

Figure 5.11 – The ground state energy difference between the original structure and the distorted structure as a function of pressure.

eral physical properties such as elastic constants, Hall coefficient, electrical resistivity, thermal conductivity, specific heat, magnetic susceptibility and thermal expansion show anomalous behaviour at this temperature [3, 132, 142]. Hence, if CDW exist in U_2Ti, similar anomalous behaviour should be seen in the above stated properties of U_2Ti for temperature at which CDW exist in the system. However, the resistivity data is available for temperatures ranging from 2K to 300K that shows U_2Ti becomes superconductor at 0.4 K and there is a cusp in resistivity-temperature plot around 80 K [143]. This cusp in the resistivity may correspond to CDW formation in U_2Ti at that temperature which can be verified by other experimental measurements. Present calculations have predicted the existence of CDW in U_2Ti that requires further experiments for confirmation.

5.4 Summary

In summary, DFT based first principles calculations are done to investigate the structure, electronic structure, elastic and dynamical properties of U_2Ti which have given following insights

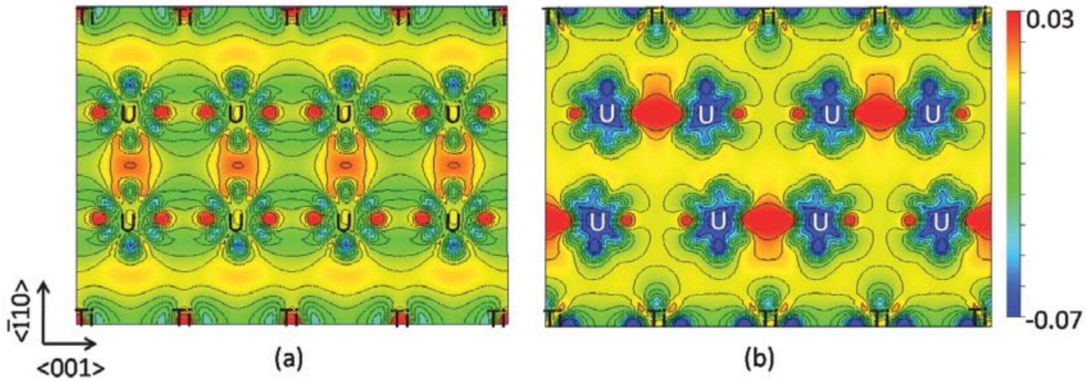

Figure 5.12 – Charge density difference distribution in [110] plane for (a) original structure (b) distorted structure. The electrons distribution around U atoms is equivalent along 'c' direction (<001>) in the original structure whereas in distorted structure, the distribution is no longer equivalent and the charges concentrate between two neighbouring U atoms.

- The ideal AlB_2 structure is more stable than modified AlB_2 structure and site occupancy disorder is not energetically favourable in case of U_2Ti.
- The electron density of states of ideal AlB_2 structure shows that Fermi level lies close to a peak in density of states and there is strong mixing of f-orbitals of uranium atom with d-orbitals of uranium and d-orbital of titanium atoms.
- The calculated elastic constants are found to meet the Born stability criteria whereas the phonon spectrum showed an instability in an LO mode near A (0,0,1/2) point in the Brillouin zone which was not seen in earlier calculations. The existence of this phonon instability is alternatively verified by all electron calculations using WIEN2k.
- This unstable phonon mode have a double well type potential energy curve and it displaces the U atoms along Z-direction and displacement of U atoms along this mode leads to dimerization of uranium atoms along 'c' axis (Z direction). This is a Peierl's type of transition and suggests the possibility of existence of

CDW in U_2Ti.

- A pressure of 4 GPa is found to suppress this phonon instability and hence the transition to charge density wave in U_2Ti.

Chapter 6

Conclusions and future outlook

In this chapter, the main results and conclusions of the thesis are given followed by discussion of the scope for future work.

6.1 Conclusions

In this thesis, the density functional theory based calculations are done for U based compounds (UO_2 , UZr_2 and U_2Ti) and the role played by electron correlations and site occupancy disorder in the structural, electronic, vibrational, elastic and thermal properties are investigated. Density functional theory with GGA exchange correlation functional has successfully described the structural and cohesive properties of UZr_2 and U_2Ti whereas it fails to give the structural, cohesive and magnetic properties of UO_2. For UO_2, DFT+U technique with non local exchange correlation pressure correction is applied to get a correct description of structural, cohesive and magnetic properties. The important outcomes of this study are as detailed below:

- DFT calculations with GGA gives a ferromagnetic metallic ground state for UO_2 whereas the GGA+U calculations with a Hubbard parameter U_{eff} of 4 eV reproduces the correct Mott-insulating anti-ferromagnetic ground state of UO_2.

- The phonon dispersion of UO_2 is well described by GGA+U with a non-analytical term correction to the dynamical matrix, where as GGA fails to do so, corroborating the effect of strong Coulomb correlations on the phonon dispersion.
- The calculated thermal properties (bulk modulus and thermal expansion) using both GGA and GGA+U shows a significant discrepancy with the corresponding experimental data. These discrepancies are systematically corrected in case of GGA+U by applying a pressure correction of 7 GPa.
- The correction of over predicted equilibrium lattice parameter in GGA+U calculations by non local pressure correction, also improved the agreement of calculated phonon dispersion with the corresponding experimental data.
- Both UZr_2 and U_2Ti are found to be metallic and DFT calculations within PBE exchange correlation functional gives a good description for these systems. The electronic structure in both these compounds show that there is a strong mixing of uranium f-orbitals with d-orbitals of other element atoms.
- In case of UZr_2, modified AlB_2 structure is more stable than ideal AlB_2 whereas in U_2Ti, ideal AlB_2 structure is more stable than modified AlB_2.
- Site occupancy disorder is energetically favourable in case of UZr_2 whereas in case of U_2Ti, disorder is not favourable. In case of UZr_2, disordered structure is not only energetically more stable than ordered structure, but also elastically and dynamically stable as oppose to ordered structure which is dynamically unstable.
- In case of U_2Ti, a phonon instability is observed corresponding to 'A' point in Brillouin zone which was not seen in earlier calculations. The potential energy

curve for the unstable phonon is a double well curve and this phonon instability leads to the dimerization of uranium atoms along 'c' axis and predicts the possibility of a charge density wave in U_2Ti. In ordered UZr_2 also a similar phonon instability is observed which lead to dimerization of U atoms along 'c' axis. But in this case, the phonon instability is removed by site occupancy disorder which is energetically more stable than ordered structure for UZr_2.

- The charge density wave in U_2Ti is found to be stable up to a pressure of 4 GPa, whereas in ordered UZr_2 the charge density wave will be stable even beyond 20 GPa.

6.2 Scope for future work

The work presented in this thesis can be advanced by carrying out further studies along the following directions:

- The present study has found phonon instability leading to Peierl's transition or charge density wave in U_2Ti and ordered UZr_2. Peierl's transition is observed experimentally in alpha-U [143] and calculations predicted a Peierl's transition in U_2Mo [40]. A comparative study of these systems (alpha-U, U_2Ti, ordered UZr_2 and U_2Mo) will provide a relation between U-U spacing and phonon instability.

- The known room temperature ground state structures of these systems (alpha-U, U_2Ti, ordered UZr_2 and U_2Mo) are found to be unstable at 0 K and they undergo Peierl's transition. But as they are found to be stable at room temperatures, the phonon instability seen at 0 K should vanish at the room temperature where they are known ground states. The study of the high temperature phonon spectrum in these compounds using the self consistent ab-initio lattice dynamical (SCALID) method [144] will give insight to their stability.

- The phonon instability and structural distortion predicted in U_2Ti by the present calculations calls for the experiments to find the true ground state of the system at low temperatures.
- The strong correlations in UO_2 will be studied using dynamical mean field theory. Dynamical mean field theory maps the actual many body lattice problem to many body local problem, called impurity model, which is solved by different methods. It will be interesting to know that how the results differ if dynamical mean field theory is used in place of DFT+U for UO_2.

References

[1] K. Asada, K. Ono, K. Yamaguchi, T. Yamamoto, A. Maekawa, S. Oe, and M. Yamawaki, Journal of Alloys and Compounds **231**, 780 (1995).

[2] T. Yamamoto, T. Yoneoka, S. Kokubo, and M. Yamawaki, Fusion Engineering and Design **7**, 363 (1988).

[3] G. Lander, E. Fisher, and S. Bader, Advances in Physics **43**, 1 (1994).

[4] W. N. Miner, *Plutonium 1970 and Other Actinides: Proceedings* (Metallurgical Society of the American Institute of Mining, Metallurgical, and Petroleum Engineers, 1970).

[5] A. Arko, J. J. Joyce, and L. Havela, in *The Chemistry of the Actinide and Transactinide Elements* (Springer, 2010), pp. 2307–2379.

[6] D. R. Bowler, Journal of Physics: Condensed Matter **28**, 421001 (2016).

[7] A. D. Becke, The Journal of Chemical Physics **140**, 18A301 (2014).

[8] M. Stan, J. Ramirez, P. Cristea, S. Hu, C. Deo, B. Uberuaga, S. Srivilliputhur, S. Rudin, and J. Wills, Journal of Alloys and Compounds **444**, 415 (2007).

[9] M. Stan, Nuclear Engineering and Technology **41**, 39 (2009).

[10] D. A. Vega, T. Watanabe, S. B. Sinnott, S. R. Phillpot, and J. S. Tulenko, Nuclear Technology **165**, 308 (2009).

[11] A. Marino, IAEA TECDOC series **26**, 17 (2013).

[12] P. Hohenberg and W. Kohn, Physical Review **136**, B864 (1964).

[13] S. Baroni, S. de Gironcoli, A. Dal Corso, and P. Giannozzi, Reviews of Modern Physics **73**, 515 (2001).

[14] Y. Yun and P. M. Oppeneer, MRS Bulletin **36**, 178 (2011).

[15] X. Y. Liu and B. P. Andersson, D. A.and Uberuaga, Journal of Materials Science **47**, 7367 (2012).

[16] I. D. Prodan, G. E. Scuseria, and R. L. Martin, Physical Review B **73**, 045104 (2006).

[17] Q. Yin and S. Y. Savrasov, Physical Review Letters **100**, 225504 (2008).

[18] S. L. Dudarev, G. A. Botton, S. Y. Savrasov, Z. Szotek, W. M. Temmerman, and A. P. Sutton, physica status solidi (a) **166**, 429 (1998).

[19] S. L. Dudarev, D. N. Manh, and A. P. Sutton, Philosophical Magazine Part B **75**, 613 (1997).

[20] S. Dudarev, M. Castell, G. Botton, S. Savrasov, C. Muggelberg, G. Briggs, A. Sutton, and D. Goddard, Micron **31**, 363 (2000).

[21] Y. Yun, P. M. Oppeneer, H. Kim, and K. Park, Acta Materialia **57**, 1655 (2009).

[22] H. Kim, K. Park, B. G. Kim, Y. S. Choo, K. S. Kim, K. W. Song, K. P. Hong, Y. H. Kang, and K. Ho, Nuclear technology **147**, 149 (2004).

[23] Y. Yun, D. Legut, and P. M. Oppeneer, Journal of Nuclear Materials **426**, 109 (2012).

[24] M. Sanati, R. Albers, T. Lookman, and A. Saxena, Physical Review B **84**, 014116 (2011).

[25] M. Freyss, Physical Review B **81**, 014101 (2010).

[26] Q. Yin, A. Kutepov, K. Haule, G. Kotliar, S. Y. Savrasov, and W. E. Pickett, Physical Review B **84**, 195111 (2011).

[27] A. Landa, P. Söderlind, B. Grabowski, P. E. Turchi, A. V. Ruban, and L. Vitos, MRS Proceedings **1444**, 67 (2012).

[28] G. Y. Huang and B. Wirth, Journal of Physics: Condensed Matter **24**, 415404 (2012).

[29] W. Xie, W. Xiong, C. A. Marianetti, D. Morgan, et al., Physical Review B **88**, 235128 (2013).

[30] C. Booth, Y. Jiang, D. Wang, J. Mitchell, P. Tobash, E. Bauer, M. Wall, P. Allen, D. Sokaras, D. Nordlund, et al., Proceedings of the National Academy of Sciences **109**, 10205 (2012).

[31] T. Petit, B. Morel, C. Lemaignan, A. Pasturel, and B. Bigot, Philosophical Magazine Part B **73**, 893 (1996).

[32] Z. Fisk, D. W. Hess, C. J. Pethick, D. Pines, J. L. Smith, J. D. Thompson, and J. O. Willis, Science **239**, 33 (1988).

[33] T. Oguchi and A. Freeman, Journal of Magnetism and Magnetic materials **61**, 233 (1986).

[34] F. Hillebrecht, D. Sarma, and N. Mrtensson, Physical Review B **33**, 4376 (1986).

[35] J. Hubbard, Proceedings of the Royal Society A **276**, 238 (1963).

[36] G. R. Stewart, Reviews of Modern Physics **56**, 755 (1984).

[37] G. Lander, Journal of Magnetism and Magnetic Materials **29**, 271 (1982).

[38] X. Zhu, Y. Cao, J. Zhang, E. Plummer, and J. Guo, Proceedings of the National Academy of Sciences **112**, 2367 (2015).

[39] S. Raymond, J. Bouchet, G. Lander, M. Le Tacon, G. Garbarino, M. Hoesch, J. P. Rueff, M. Krisch, J. Lashley, R. Schulze, et al., Physical Review Letters **107**, 136401 (2011).

[40] E. Losada and J. Garces, Journal of Nuclear Materials **466**, 638 (2015).

[41] S. Süllow, M. Maple, D. Tomuta, G. Nieuwenhuys, A. Menovsky, J. Mydosh, and R. Chau, Journal of Magnetism and Magnetic Materials **226**, 35 (2001).

[42] S. Süllow, G. J. Nieuwenhuys, A. A. Menovsky, J. A. Mydosh, S. A. M. Mentink, T. E. Mason, and W. J. L. Buyers, Physical Review Letters **78**, 354 (1997).

[43] C. Booth, D. MacLaughlin, R. Heffner, R. Chau, M. Maple, and G. Kwei, Physical Review Letters **81**, 3960 (1998).

[44] L. Shlyk and J. Stepien-Damm, Journal of Magnetism and Magnetic Materials **195**, 37 (1999).

[45] M. Akabori, T. Ogawa, A. Itoh, and Y. Morii, Journal of Physics: Condensed Matter **7**, 8249 (1995).

[46] M. Akabori, A. Itoh, T. Ogawa, F. Kobayashi, and Y. Suzuki, Journal of Nuclear Materials **188**, 249 (1992).

[47] T. Petit, B. Morel, C. Lemaignan, A. Pasturel, and B. Bigot, Philosophical Magazine B **73**, 893 (1996).

[48] M. R. Castell, C. Muggelberg, G. A. D. Briggs, and D. T. Goddard, Journal of Vacuum Science & Technology B: Microelectronics and Nanometer Structures Processing, Measurement, and Phenomena **14**, 966 (1996).

[49] A. J. Cohen, P. Mori-Sánchez, and W. Yang, Science **321**, 792 (2008).

[50] J. P. Perdew and A. Zunger, Physical Review B **23**, 5048 (1981).

[51] V. I. Anisimov, J. Zaanen, and O. K. Andersen, Physical Review B **44**, 943 (1991).

[52] J. P. Perdew, M. Ernzerhof, and K. Burke, The Journal of Chemical Physics **105**, 9982 (1996).

[53] A. I. Lichtenstein and M. I. Katsnelson, Physical Review B **57**, 6884 (1998).

[54] G. Kotliar, S. Y. Savrasov, K. Haule, V. S. Oudovenko, O. Parcollet, and C. Marianetti, Reviews of Modern Physics **78**, 865 (2006).

[55] A. G. Petukhov, I. I. Mazin, L. Chioncel, and A. I. Lichtenstein, Physical Review B **67**, 153106 (2003).

[56] A. D. Becke, The Journal of Chemical Physics **98**, 1372 (1993).

[57] J. Heyd, G. E. Scuseria, and M. Ernzerhof, The Journal of Chemical Physics **118**, 8207 (2003).

[58] J. Heyd, G. E. Scuseria, and M. Ernzerhof, The Journal of Chemical Physics **124**, 219906 (2006).

[59] J. Heyd, J. E. Peralta, G. E. Scuseria, and R. L. Martin, The Journal of Chemical Physics **123**, 174101 (2005).

[60] S. Yu, J. G. Tobin, J. C. Crowhurst, S. Sharma, J. K. Dewhurst, P. Olalde-Velasco, W. L. Yang, and W. J. Siekhaus, Physical Review B **83**, 165102 (2011).

[61] J. Schoenes, Physics Reports **63**, 301 (1980).

[62] I. A. E. Agency, *Thermophysical properties database of materials for light water reactors and heavy water reactors* (International Atomic Energy Agency, 2006).

[63] E. Vathonne, J. Wiktor, M. Freyss, G. Jomard, and M. Bertolus, Journal of Physics: Condensed Matter **26**, 325501 (2014).

[64] T. Uchida, T. Sunaoshi, M. Kato, and K. Konashi, Progress in Nuclear Science and Technology **2**, 598 (2011).

[65] P. Goel, N. Choudhury, and S. Chaplot, Journal of Nuclear Materials **377**, 438 (2008).

[66] P. Lindan and M. Gillan, Journal of Physics: Condensed Matter **3**, 3929 (1991).

[67] K. Govers, S. Lemehov, M. Hou, and M. Verwerft, Journal of Nuclear Materials **366**, 161 (2007).

[68] H. Kim, M. H. Kim, and M. Kaviany, Journal of Applied Physics **115**, 123510 (2014).

[69] H. J. Ullrich, Crystal Research and Technology **30**, 1084 (1995).

[70] C. B. Basak, Journal of Nuclear Materials **416**, 280 (2011).

[71] S. Kaity, J. Banerjee, M. Nair, K. Ravi, S. Dash, T. Kutty, A. Kumar, and R. Singh, Journal of Nuclear Materials **427**, 1 (2012).

[72] A. Landa, P. Söderlind, and P. E. Turchi, Journal of Alloys and Compounds **478**, 103 (2009).

[73] A. Landa, P. Söderlind, P. E. Turchi, L. Vitos, and A. Ruban, Journal of Nuclear Materials **385**, 68 (2009).

[74] T. Yamamoto, Supardjo, T. Terai, F. Ono, S. Tanaka, and M. Yamawaki, Fusion Science and Technology **14**, 764 (1988).

[75] R. A. Chattaraj, D.and Jat, S. C. Parida, R. Agarwal, and S. Dash, Journal of Thermal Analysis and Calorimetry **112**, 141 (2013).

[76] T. B. Massalski, J. Murray, L. Bennett, and H. Baker, *Binary Alloy Phase Diagrams. Vol. I and II* (American Society for Metals, 1986).

[77] D. Chattaraj, S. Parida, and C. Majumder, Physica B: Condensed Matter **406**, 4317 (2011).

[78] M. Hasan, M. Hossain, M. Islam, F. Parvin, and A. Islam, Computational Materials Science **63**, 256 (2012).

[79] J. Yang, T. Gao, B. Liu, G. Sun, and B. Chen, Journal of Applied Physics **117**, 125903 (2015).

[80] R. M. Martin, *Electronic structure: basic theory and practical methods* (Cambridge university press, 2004).

[81] G. Kresse and J. Furthmüller, Physical Review B **54**, 11169 (1996).

[82] G. Kresse and J. Furthmüller, Computational Materials Science **6**, 15 (1996).

[83] P. Blaha, K. Schwarz, P. Sorantin, and S. Trickey, Computer Physics Communications **59**, 399 (1990).

[84] S. Baroni, P. Giannozzi, and E. Isaev, Reviews in Mineralogy and Geochemistry **71**, 39 (2010).

[85] M. Born and R. Oppenheimer, Annalen der Physik **389**, 457 (1927).

[86] W. Kohn and L. J. Sham, Physical Review **140**, A1133 (1965).

[87] J. P. Perdew and W. Yue, Physical Review B **33**, 8800 (1986).

[88] J. P. Perdew, K. Burke, and M. Ernzerhof, Physical Review Letters **77**, 3865 (1996).

[89] J. P. Perdew, M. Ernzerhof, and K. Burke, The Journal of Chemical Physics **105**, 9982 (1996).

[90] M. Ernzerhof and G. E. Scuseria, The Journal of Chemical Physics **110**, 5029 (1999).

[91] J. Heyd, G. E. Scuseria, and M. Ernzerhof, The Journal of Chemical Physics **118**, 8207 (2003).

[92] J. P. Perdew and A. Zunger, Physical Review B **23**, 5048 (1981).

[93] C. Kittel, *Introduction to solid state physics* (Wiley, 2005).

[94] H. J. Monkhorst and J. D. Pack, Physical Review B **13**, 5188 (1976).

[95] D. Chadi, Physical Review B **16**, 1746 (1977).

[96] J. C. Phillips, Physical Review **112**, 685 (1958).

[97] J. C. Phillips and L. Kleinman, Physical Review **116**, 287 (1959).

[98] R. P. Feynman, Physical Review **56**, 340 (1939).

[99] H. Hellmann, *Einführung in die Quantenchemie* (J.W. Edwards, 1944).

[100] S. Baroni, S. De Gironcoli, A. Dal Corso, and P. Giannozzi, Reviews of Modern Physics **73**, 515 (2001).

[101] X. Gonze, Physical Review B **55**, 10337 (1997).

[102] P. Giannozzi, S. de Gironcoli, P. Pavone, and S. Baroni, Physical Review B **43**, 7231 (1991).

[103] F. Birch, Physical Review **71**, 809 (1947).

[104] F. Mouhat and F.-X. Coudert, Physical Review B **90**, 224104 (2014).

[105] M. Born, K. Huang, and M. Lax, American Journal of Physics **23**, 474 (1955).

[106] Y. Le Page and P. Saxe, Physical Review B **65**, 104104 (2002).

[107] Y. Baer and J. Schoenes, Solid State Communications **33**, 885 (1980).

[108] B. Veal and D. Lam, Physics Letters A **49**, 466 (1974).

[109] L. E. Cox, W. Ellis, R. Cowan, J. Allen, S. J. Oh, I. Lindau, B. Pate, and A. Arko, Physical Review B **35**, 5761 (1987).

[110] J. Schoenes, Journal of Applied Physics **49**, 1463 (1978).

[111] G. Kalkowski, G. Kaindl, W. Brewer, and W. Krone, Physical Review B **35**, 2667 (1987).

[112] F. Jollet, T. Petit, S. Gota, N. Thromat, M. Gautier Soyer, and A. Pasturel, Journal of Physics: Condensed Matter **9**, 9393 (1997).

[113] X. Gonze and C. Lee, Physical Review B **55**, 10355 (1997).

[114] G. Kresse and J. Hafner, Physical Review B **47**, 558 (1993).

[115] P. E. Blöchl, Physical Review B **50**, 17953 (1994).

[116] G. Kresse and D. Joubert, Physical Review B **59**, 1758 (1999).

[117] G. A. de Wijs, C. M. Fang, G. Kresse, and G. de With, Physical Review B **65**, 094305 (2002).

[118] M. T. Dove, *Introduction to Lattice Dynamics*, Cambridge Topics in Mineral Physics and Chemistry (Cambridge University Press, 1993).

[119] A. Togo and I. Tanaka, Scripta Materialia **108**, 1 (2015).

[120] M. Idiri, T. Le Bihan, S. Heathman, and J. Rebizant, Physical Review B **70**, 014113 (2004).

[121] D. G. Martin, High Temperature High Pressure **21**, 13 (1989).

[122] B. Frazer, G. Shirane, D. Cox, and C. Olsen, Physical Review **140**, A1448 (1965).

[123] L. E. Roy, T. Durakiewicz, R. L. Martin, J. E. Peralta, G. E. Scuseria, C. G. Olson, J. J. Joyce, and E. Guziewicz, Journal of Computational Chemistry **29**, 2288 (2008).

[124] G. Dolling, R. A. Cowley, and A. D. B. Woods, Canadian Journal of Physics **43**, 1397 (1965).

[125] M. A and K. M, High Temperature Science **45**, 10 (1978).

[126] A. van de Walle and G. Ceder, Physical Review B **59**, 14992 (1999).

[127] J. K. Fink, International Journal of Thermophysics **3**, 165 (1982).

[128] W. Xiong, W. Xie, C. Shen, and D. Morgan, Journal of Nuclear Materials **443**, 331 (2013).

[129] P. Söderlind, A. Landa, and P. Turchi, Physical Review B **90**, 157101 (2014).

[130] A. Van de Walle, P. Tiwary, M. De Jong, D. Olmsted, M. Asta, A. Dick, D. Shin, Y. Wang, L.-Q. Chen, and Z.-K. Liu, Calphad **42**, 13 (2013).

[131] A. van de Walle, Calphad **33**, 266 (2009).

[132] E. S. Fisher, Journal of Alloys and Compounds **213**, 254 (1994).

[133] R. Qiu, H. Lu, B. Ao, T. Tang, and P. Chen, Modelling and Simulation in Materials Science and Engineering **24**, 055011 (2016).

[134] G. B. Skinner and H. L. Johnston, The Journal of Chemical Physics **21**, 1383 (1953).

[135] E. Cordfunke, *The chemistry of uranium*, vol. 1 (Elsevier Amsterdam, 1969).

[136] A. Berche, N. Dupin, C. Guéneau, C. Rado, B. Sundman, and J. Dumas, Journal of Nuclear Materials **411**, 131 (2011).

[137] S. Bajaj, A. Landa, P. Söderlind, P. E. Turchi, and R. Arróyave, Journal of Nuclear Materials **419**, 177 (2011).

[138] S. Kagoshima, Japanese Journal of Applied Physics **20**, 1617 (1981).

[139] G. Grüner, Reviews of Modern Physics **60**, 1129 (1988).

[140] A. G. Knapton, Acta Crystallographica **7**, 457 (1954).

[141] R. A. Jat, S. Sawant, M. Rajan, J. Dhanuskar, S. Kaity, and S. Parida, Journal of Nuclear Materials **443**, 316 (2013).

[142] E. S. Fisher and H. J. McSkimin, Physical Review **124**, 67 (1961).

[143] M. Maple, M. Torikachvili, C. Rossel, J. Chen, and R. Hake, Physica B+C **135**, 430 (1985).

[144] P. Souvatzis, O. Eriksson, M. I. Katsnelson, and S. P. Rudin, Phys. Rev. Lett. **100**, 095901 (2008).